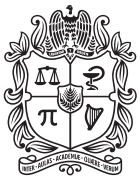

UNIVERSIDAD
NACIONAL
DE COLOMBIA

# Physics of Traffic Gridlock in a City:
## A Study of the Spreading of Traffic Jams on Urban Street Networks

**Luis Eduardo Olmos Sánchez**

Universidad Nacional de Colombia
Facultad de Ciencias, Departamento de Física
Bogotá D.C., Colombia
2016

# Physics of Traffic Gridlock in a City:
## A Study of the Spreading of Traffic Jams on Urban Street Networks

**Luis Eduardo Olmos Sánchez**

Tesis presentada como requisito parcial para optar al título de:
**Doctor en Ciencias Físicas**

Director:
José Daniel Muñoz Castaño

Línea de Investigación:
Física Computacional y Aplicada
Grupo de Investigación:
Simulación de Sistemas Físicos SSF

Universidad Nacional de Colombia
Facultad de Ciencias, Departamento de Física
Bogotá D.C., Colombia
2016

A mis padres,

A Luisa.

# Acknowledgements / Agradecimientos

En primer lugar quiero expresar mi gratitud a José Daniel Muñoz, jamás olvidaré su llamada para invitarme a hacer el PhD bajo su supervisión. Aprecio mucho la libertad que me dio para que yo explorara e investigara en los temas que llamaban mi atención, al igual que los consejos y ayuda para el desarrollo de las idea.

Son muchas las cosas por las que quisiera agradecer a Marta C. González, pero escojo el haberme confirmado de primera mano lo que siempre pensé y soñé acerca de lo que debería ser hacer ciencia, agradezco por todas las discusiones académicas en las reuniones privadas y en los group meetings.

A Simone simplemente por coincidir conmigo en Boston, no hubiese sido tan amena la pasantía y por cierto llevaba años sin hacer un nuevo gran amigo. Al mismo tiempo a Ana y Antonio, la comida, las conversaciones y su amabilidad de abrirme las puertas de sus vidas.

A Edwin Barrios, William Oquendo y Leonardo Gutiérrez por las discusiones y consejos sobre los algoritmos y herramientas que debía utilizar.

Al Centro de Estudios Interdisciplinarios Básicos y Aplicados en Complejidad (CeiBA), por el apoyo económico y nunca pedir nada a cambio.

Muchas gracias a Elizabeth Urrego, Herbert Vinck y Gerardo Lizcano, sin su ayuda jamás hubiera hecho mi pasantía doctoral.

A Juli, por convertirse en una gran compañera de café.

A la maravillosa estancia en París junto a Nan y Robin.

La última pero la más importante, Luisa. Vivir junto a un científico no es fácil, es la aceptación de una cama fría, ya que *él* ha huido al otro lado de la habitación para seguir trabajando. Espero algún día compensar todo ese tiempo robado.

# Resumen

La congestión vehicular tiene un impacto profundo y diverso en la sociedad actual. Sin embargo, caracterizar a nivel de ciudad la transición que da lugar a la congestión ha sido una tarea inalcanzable. El problema se centra en la dificultad para entender la interacción que existe entre la topología de la red y la dinámica espacial del flujo vehicular. En esta tesis se combina el modelamiento por autómatas celulares con herramientas de la física estadística para estudiar la formación de la congestión a escala de calle, de malla regular y de red real de calles. A nivel de calle, mostramos que para al menos dos modelos de autómata celular, una exploración por Monte Carlo de las reglas de manejo permite reproducir el diagrama fundamental de una calle. A nivel de mallas regulares, el modelo Biham-Middleton-Levine (BML) es el paradigma de los estudios de tráfico vehicular. Aplicando las herramientas de la Teoría de Percolación, logramos desentrañar los mecanismos de formación de atascos en este modelo, ya sea sobre mallas cuadradas o tipo panal. Logramos entonces resolver el misterio del origen los llamados *estados intermedios* en el BML en mallas cuadradas. Finalmente, usamos las matrices origen destino obtenidas a partir de datos de telefonía móvil para simular el tráfico vehicular de cinco ciudades alrededor del mundo: Rio de Janeiro, Boston, la bahía de San Francisco, Porto y Lisboa. A este nivel de red de ciudad, encontramos que el tiempo de recuperación característico de cada ciudad es proporcional a la fracción de infraestructura utilizada y el tiempo promedio de viaje. Adicionalmente, incrementando la demanda, estudiamos el colapso vehicular en redes de ciudad bajo el marco de transiciones de fase fuera del equilibrio. Nuestros resultados muestran características similares a las observados en los modelos dentro de la clase de universalidad de percolación dirigida (DP). Nuestro trabajo ilustra cómo una descripción computacional a nivel de vehículo junto con las herramientas de la física estadística permite analizar y comprender los orígenes y el comportamiento de la congestión vehicular.

**Keywords: Colapso vehicular, modelo de tráfico Biham-Middleton and Levine (BML), Teoría de Percolación y modelos de autómata celular para tráfico vehicular.**

# Abstract

Traffic congestion has profound and varied impacts on modern society, yet characterizing on a city scale the transition that gives rise to the congestion remains an elusive task. The challenge lies in understanding the role of the interplay between topology and spatial dynamics in this traffic phenomenon. In this thesis we combine cellular automata modelling with analysis tools from statistical physics to study the emergence of congestions at road (street), grid (neighbourhood) and network (city) levels. At street level, we shown for at least two traffic cellular automata that implementing a simple Monte Carlo exploration of the driving rules reproduces the fundamental diagram of a single road segment. Next, by applying tools of percolation theory, we unveiled the underlying mechanism of jamming process in the Biham-Middleton Levine model, i.e., a paradigmatic model for car traffic, both on square and honeycomb grids, solving a puzzle of more than a decade on the origin of the intermediate states of this model on square grids and pointing out the relevance of both asymmetry and the underlying grid on the model's behaviour. Finally, we used the origin-destination matrices obtained from mobile phone data to simulate car by car the traffic on the detailed road network of five large cities: Rio, Boston, San Francisco bay, Porto and Lisbon. We found at this network level that the characteristic recovery time the system takes to unload is proportional to the fraction of road infrastructure being used and the mean travel time on all trips. In addition, we study the emergence of congestion when the number of cars increases by keeping the trip distributions and street capacities unchanged. Our last findings strongly support the notion that the transitions to urban traffic gridlock resemble the direct percolation universality class and can be approached with the framework of non-equilibrium phase transitions. Our work illustrates the power of a computational description at the level of each car with the solid theoretical framework of statistical physics to analyze the origins and behaviour or vehicular traffic congestions.

**Keywords: Urban traffic gridlock, Biham-Middleton and Levine traffic model, Percolation Theory and Cellular automata models.**

# Publications

Most of the results and figures presented in this thesis have appeared or they will in the following publications:

[1] L. E. Olmos and J.D. Muñoz. A Simple Statistical Method for Reproducing the Highway Traffic. In *Proceedings of Traffic and Granular Flow '13, pp 407-414, (2014).* Springer. Included in the Appendix A.

[2] L. E. Olmos and J.D. Muñoz. Unraveling the puzzling intermediate states in the Biham-Middleton-Levine traffic model. *Physical Review E* **91**, *pp. 050801, (2015).* Rapid Communications. Included in the Appendix B.

[3] L. E. Olmos and J.D. Muñoz. Traffic gridlock on a honeycomb city. *Physical Review E* **95** *pp. 032320, (2017).* Included in the Appendix C.

[4] L. E. Olmos, S. Çolak and Marta C. González. Non-equilibrium dynamics in urban traffic networks. *Nature Communications, under review (2017).*

# Contents

# Figure List

# Table List

# 1. Introduction

Nowadays, the world is undergoing the largest wave of urban growth in history. This process is increasingly affecting our environment and our society. As city population rises, road infrastructure becomes increasingly constrained. As a result, congestion grows throughout the city and instances of gridlock are more frequent, especially during peak periods, where sometimes the true reality of traffic jams [5] becomes stranger than fiction [6]. Congestion not only brings an increase of the commuting times but also in fuel consumption [7] and air pollution [8]. In the most cases, the growing traffic volume cannot be compensated by the extension of infrastructure, due to financial, environmental, and social constraints. In this respect, a proper understanding of jamming processes is indispensable for developing strategies for congestion mitigation.

Traffic jams have been successfully studied through the lens of statistical physics. The availability of camera data have allowed to model the dynamics of jams in the freeways [9–12]. The relation between vehicular flow and density on the road is described via the well established fundamental diagram [13]. Cars traveling in free-flow phase, change to a jammed state that moves through the roadways [9,14]. Congestion in a road emerges as spontaneous transitions between these two phases [14, 15]. The fundamental diagram is strongly influenced by the driving rules adopted by the cars, and these rules also play a fundamental role in the modeling of car accidents. In turn, congestion at urban scale is the result of the interplay between the travel distribution of vehicles and the physical constraints of the roads, such as: network geometry, road lengths, road capacity and speed limits. This interplay leads to saturation of the most frequently used road segments spilling over into nearby streets, and large traffic jams emerge. In extreme cases these jams can sometimes collapse the entire system, and even last for days [5].

At street level, since the distinction between the two congested phases relay on their microscopic structure, the microscopic models have been more successful over the other models. Among those, cellular automata models (CA) have been very fruitful, due to its simplicity and flexibility. These models describe the drivers' driving (accelerating, bra-

king, lane-changing) depending on the surrounding traffic. Within this context, the Nagel-Schreckenberg (NaSch) model is the first model able to reproduce the basic phenomena of real traffic. Since then, many improved models has been developed. Today the more elaborated models (e.g. the KKW model [9]) are able to reproduce the spontaneous transitions and the detailed microscopic structure of vehicular traffic.

At grid level (comparable with the level of neighbourhoods), the Biham Middleton and Levine (BML) [16] model is the earliest CA attempting for modeling traffic in two dimensions. Defined on a square lattice, the BML model is the simplest traffic cellular automaton able to exhibit self-organization, pattern formation and dynamical phase transitions on a network scale [16–18]. Therefore, the BML model has become the paradigm for the study of jamming phenomena and congestion patterns on vehicular traffic research. The model exhibits three phases, namely, free flow, totally jammed phase and an intermediate phase [19–21] where jams and freely traffic coexist. However, for more than a decade, the origin of those intermediate states has remained a mystery, until now.

At the scale of city road networks, the transition to congestion has mainly been studied by simulations. Currently, there are two accepted approaches. The first [22, 23] consists in an agent-based model inspired by the traffic dynamics of the Internet traffic [16, 24, 25]. The increase of volume demand $R$ in the network beyond a threshold induces a transition to a congested state, where the number of vehicles in the network start increasing steadily in time, and the numbers of cars accumulating per unit time defines the order parameter. The aim of this approach consists of identifying the critical value $R_c$ at which vehicles start accumulating in the network and understanding how the various elements of the model (network topology, road capacity and routing strategy) affect the transition to a global congested state. The second approach relies on the existence of a well-defined relationship between network-wide average flow and the density of cars. The traffic dynamics is modeled via dynamic traffic assignment [26], as well as through macroscopic calculations based on car-following or cellular automata models [11,27–31]. In these cases, variations in flow and density can be measured at the road segment level. Considering the network density as the control parameter (similarly to the single road case), a congested state at the network level is defined as a drop in the cars outflow when density exceeds certain threshold value. More recently, a study based on taxi data revealed that changes in the state of the road network can be described by a percolation process [32] where the number of road links below a certain speed threshold form a giant component in the rush hour.

Until now, the lack of data for travel demand has prevented large-scale comparative studies of the relation between the empirical urban congestion and global traffic parameters such

as car volume, road network supply and travel times. Namely, there are two limitations in the simulation-based studies. One is the use of random origin-destination tables (ODs) that neglects the inherent spatial heterogeneity in the demand distribution. The other is the interpretation of transition to congestion as a loading process, where the order parameter is defined by the amount of accumulated vehicles. These limitations generate two main consequences. First it implies transition to congestion at unrealistic high density of vehicles. Second, it does not have relation to the empirical travel demand, which creates gridlocks in most used streets. Mahmassani et al. [26] characterize urban gridlock using descriptive measures from simulations of the Chicago road network. This work pioneered the concept of the recovery time as an important metric to diagnose urban congested states. The recovery time is the time vehicles take to reach to their destination after their maximum accumulation in the rush hour. Yet its connection with other global characteristics of urban travel remained missing. The recent availability of data on personal tracking devices allows us to overcome these limitations. Travel information can be extracted from the analysis of call detailed records (CDRs) [33–36] from mobile phones. Particularly, Çolak et al. [37] have estimated the home-based work ODs during the morning peak hour for five major cities around the world: Boston, San Francisco Bay, Rio de Janeiro, Lisbon and Porto. Using these ODs, along with road networks publicly available on OpenStreetMaps the congested travel time ($t_{ue}$) for each road was estimated and, at the network scale, the ratio of road supply to vehicles demand ($\Gamma$) explained the differences in the percentage of congestion reported in empirical GPS data from each of the five cities. This is a notable step forward in the urban traffic research, since these reliable OD tables are a essential input that was missing in the previous research.

The main objective of this dissertation is to use tools of statistical mechanics to investigate several aspects of car traffic at three main levels: the road, the grid and the network, which correspond to the ideas of street, neighbourhood and city, respectively. At road level, the goal is to determine how much of the fundamental diagram can be obtained by just analysing the driving rules, without running any dynamical evolution of the system. In addition, a novel model to study the accidents produced by distracted drivers will be introduced. At grid level, our efforts will focus on the Biham-Middleton-Levine model, first to establish the origin of the intermediate states described for the regional model on square grids and, next, to explore the effect of an hexagonal grid on the global model behaviour. At network level, the idea is to use data of mobile phones to simulate the recovery period after rush hours in five major cities around the world and to identify which variables determine the characteristic recovery time. All three aspects contain original and valuable contributions from the statistical mechanics to the understanding of this relevant and interesting phenomenon.

This thesis can be read in a normal fashion, but in a sense, this work consists in three paths which can be read independently.

**Part I**, dealing with roads, composed of Chap. 2 and 3, gives to the reader a brief overview of the empirical facts concerning traffic states and especially traffic jams at a highway level. The most common CA models are introduced and discussed by regarding to their jamming properties and, also, to their efforts to include accidents. Then we present two results: how a Monte Carlo exploration of the CA driving rules can reproduce the empirical fundamental diagram of a single road segment and, how the global system dynamics is affected when accidents can occur (not virtually) in the CA model.

**Part II**, dealing with grids, begins with Chap. 4, follows in Chapters 5- 6 and finishes with Chap. 7 . In Chapter 4, we start providing the fundamental concepts of both (isotropic) percolation theory and directed percolation (DP). In Chap. 5, we give an overview of the principles behind the city grid planning. We also present the most prominent cellular automaton models for traffic on lattice networks, namely the Biham Middleton and Levine model (BML). Then, in Chap. 6, we apply the tools from percolation theory to analyze the jamming transition on the BML. Within this framework, we show the relevance of the network isotropy on jamming processes. In the case of square lattices, we reveal that the anisotropy inherent to network is the origin of the intermediate states observed in the original model, a puzzle that remained unsolved for almost a decade. Finally, in Chapter 7 we also test the BML model on a honeycomb-like lattice. Unexpectedly, the system behaves isotropically in this case and thus, there are no intermediate states. More surprising is the fact that under some modifications, the BML on honeycomb lattices is more resilient than original BML model on square ones.

**Part III**, dealing with networks, addresses the simulation of whole cities at network level and, should be read in the sequence Chap. 2-4-8-9. Indeed, Chapter 2 presents the cellular automaton to be used at network level: the NaSch model. Similarly, Chapter 4 introduces the basic concepts of percolation, which will also be used for the network analysis. Next, after presenting in Chap. 8 an overview of the simulations models for traffic on realistic road networks, we propose in Chap. 9 a novel framework to characterize the transition to congestion at a city network level. From realistic simulations of the morning peak hours, we show that the congestion level of five cities around the world can be described by two observable quantities, namely: the car demand to road supply ratio and the median of the free travel time distribution. Our results offer quantitative insights on the interplay between the available capacity of road infrastructure and the travel demand, defined by both the traveled distances and the number of cars. Furthermore, we study the emergence of congestion by

increasing the number of cars and keeping the trip distributions and street capacities unchanged. In this case, our findings strongly support the notion that the transitions to urban traffic gridlock resemble the direct percolation universality class and can be approached with the framework of non-equilibrium phase transitions.

# 2. Empirical Findings and Model Approaches of Highway Traffic

Traffic jams have intrigued some of the most talented scientific minds of the 20th century, who see in them similarities to the freezing of water, the triggering of avalanches and even the onset of life itself. Among the most notable contributors are Montroll, Potts, Herman [38] and Prigogine. Last two names Nobel Laureates [39, 40]. At the scale of streets, traffic dynamics have been studied using many model types, ranging from macroscopic models based on kinetic gas theory or fluid dynamics to microscopic approaches where each vehicle is treated independently [12, 41, 42]. Recently, from the spatio-temporal analysis of extensive empirical data, it is widely accepted that traffic can flow in three sharply differing phases according to the car density (although some points remain controversial [43]): (1) free flow, in which each vehicle can move fast and on the desired lane; (2) synchronized flow, in which the high density prevents lane changes and passing; and (3) jammed flow, in which vehicles are immersed in a sequence of jams. Consequently, within the framework of the three-phase traffic theory [9], congestion is interpreted as spontaneous transitions between these phases, as described below.

In this chapter, we introduce briefly the most important aspects of the traffic flow, including empirical measurements, some microscopic features, fundamental diagrams and how it can be modeled by using cellular automata (CA).

## 2.1. Fundamental Diagrams and Three-Phase Traffic Theory

Experiments on traffic flow started in 1933, when Greenshields [44] filmed a section of highway to record how many cars passed along it (flow $q$), and how long it took them. By fitting

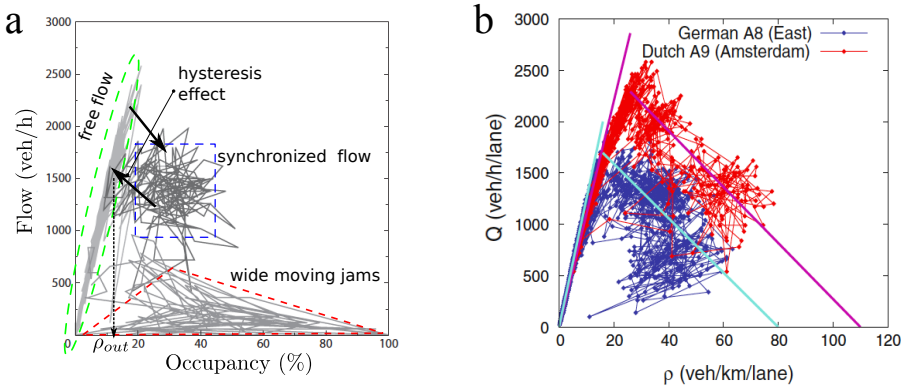


**Figure** 2.1.: **Empirical fundamental diagrams (4-min average data), where the three phases can be clearly distinguish. (a)** Two black arrows represents the hysteresis effect in the traffic breakdown and return transition from congested traffic to free flow. Occupancy can be given by $\rho \cdot \ell$, where $\ell$ is the effective vehicle length. Figure taken from [42]. Copyright (2002) by Elsevier Science B.V. **(b)** For comparison, figure shows the fundamental diagram (averaged over all lanes) for sections of the Dutch A9 (Haarlem to Amsterdam) and the German A8-East (Munich to the Austrian border). The difference between them is apparently due to the particular driving style in each country. Figure taken from [13]. Copyright (2013) by Springer-Verlag Berlin Heidelberg.

the empirical data with the relation $q(\rho)=\rho \cdot v(\rho)$, he found a linear relationship between speed and density. As the number of cars per km goes up, the speed of the traffic decreases until a particular density when it stops and traffic jam emerges. In other words, if flow is plotted against density on a graph, the curve looks like an inverted parabola. As the density of traffic increases, more cars per hour pass down the road and the flow rate goes up. But beyond a certain density, cars start to brake to avoid the vehicle in front. Fewer vehicles pass along per hour, so the flow decreases, resulting in congestion. Since then, those functional relationships between the flow $q$, the space-mean speed $v_s$ and the density of vehicles on a road $\rho$ were called fundamental diagrams.

Nevertheless, the fundamental diagram is more complex than just a well-defined function, see Fig. 2.1. It is usually discontinuous and, for high densities, the data are widely scattered, which is usually interpreted as an effect of fluctuations or unstable vehicle dynamics. Within the framework of the so called three-phases theory, supported by spatio-temporal analysis of empirical congested traffic patterns [10,45,46], B. Kerner [9,47] proposed that three different phases of traffic flow can be distinguished in the fundamental diagram:

- **Free flow**: For low densities, interactions between vehicles are negligible, and then, every vehicle has the opportunity to move at its speed limit; therefore, the flow increases linearly with car density. The slope of this line is the speed limit, averaged on all cars

via the hydrodynamical relation $q{=}\rho \cdot v$. The free flow branch can clearly be seen in Fig. 2.1. Regarding the formation of jams, two different regimes must be distinguished. Up to density $\rho_{out}$, small jams can emerge but dissolve quickly. Above $\rho_{out}$, the traffic state is metastable, i.e., local disturbances may lead to a breakdown of free flow traffic, so that a phase transition occurs.

All states that do not belong to the free flow line are called congested states. They are characterized by an average velocity that is smaller than the speed limit velocity. Two congested phases can be distinguished.

- **Wide Moving Jams:** Wide (moving) jams are regions with a very high density and negligible average velocity, and some street portions filled with stopped cars. Defining the front of the traffic jam as the first stopped car downstream, wide jams (the front downstream) move upstream (i.e., opposite to the driving direction) with a characteristic velocity $v_{jam}$ that seems to be a universal constant of traffic: $15km/h$ . In the empirical fundamental diagram in Fig. 2.1 (right), wide jam data are widely scattered within a two-dimensional area. This complexity is usually interpreted as an effect of fluctuations, jam formation, or instabilities in vehicle dynamics. The scattering reduces by increasing the sampling interval $\Delta t$ for the data averaging [48], until all data collapse on a line with almost no slope. This effect is due to the difficulty to obtain the spatial density from local measurements, which lead to the underestimation of the true density (as discussed before).

- **Synchronized Flow**[1]: A well known phenomenon in congested traffic on highways is the so-called *stop-and-go wave* or oscillation wave, i.e., a sequence of small jams. A car leaving one jam has to stop soon when it reaches the next one. The empirical properties of this pattern have been studied by many authors [49–51], but within the framework of three-phases theory, it is associated with the *synchronized flow* phase. In this phase, the average velocity is significantly lower than in free flow, but the flow can be much larger than in wide moving jams. This is a jam free phase in the sense that all vehicles move, but even so it is determinant in the formation of most traffic jams. Interestingly, in synchronized traffic no functional flow−density relation can be found, i.e., the corresponding data points spread irregularly over a wide area (see Fig. 2.1). Curiously, going back to 1990's, this wide spreading questioned the applicability of the fundamental diagrams and was the origin of the three-phase traffic theory.

[1]The notation *synchronized traffic* was chosen by Kerner and coworkers [9] because of the synchronization of the velocity and the flow among neighboring lanes. But, because this synchronization can also take place in other traffic states, this criterion is ambiguous.

## 2.2. Empirical Aggregated Data

Most empirical data are collected by stationary double-loop detectors composed of two or more induction loops separated by a fixed distance, usually 1 m. The time difference between passing the first and the second loop gives a direct measurement of the vehicle speed $v_i$. Quantities as the mean flow $q$ or the mean velocity $v$ can be derived and presented in aggregated values for a time period, for instance, 1 or 5 minutes, as follows: The flow $q$ is given by the number of vehicles $\Delta N$ passing the detector per time interval $\Delta t$,

$$q = \frac{\Delta N}{\Delta t} \ . \tag{2.1}$$

The time-mean speed, $v_t$, can be obtained either as the arithmetic average on all cars passing the detector in a fixed time interval $\Delta t$,

$$v_t = \frac{1}{\Delta N} \sum_{i=1}^{\Delta N} v_i \ , \tag{2.2}$$

or as a spatial average on the number $N$ of cars inside some fixed street length $L$,

$$v_s = \frac{1}{N} \sum_{i=1}^{N} v_i \ . \tag{2.3}$$

In contrast, determining the density is rather problematic. The difficulty arises from the fact the density is derived from the hydrodynamic relation $\rho = q/v$ and, when $v_t$ is used, standing or slow cars are not detected, so then density is underestimated. By assuming stationary conditions, some authors avoid this difficulty by computing the space-mean speed as the harmonic mean of the time measurements [10, 12, 52, 53],

$$v_s = \frac{1}{\frac{1}{N} \sum_{i=1}^{N} \frac{1}{v_i}} \ . \tag{2.4}$$

The harmonic mean value corrects the detection of slow cars, but it does not allow to account for standing cars. Even so, this relation is the mostly used in empirical data analysis. On respect to the differences between these two speed averages, Wardrop [54, 55] found that under homogeneous and stationary conditions,

$$v_t = \frac{\sigma_s^2}{v_s} + v_s \ , \tag{2.5}$$

where $\sigma_s^2$ is the variance of space mean speed. Nevertheless, Eq. 2.5 is not useful if one has just local measurements (real case).

### 2.2.1. Single-vehicle Data and Microscopic Structure

From double-loop detector measurements secondary microscopic quantities like vehicle length, vehicle type (motorcycle, car, truck, etc.), time and distance between consecutive cars can be derived. These quantities are also called *single-vehicle data*. As Kerner discussed in [56], rather than the fundamental diagram, spatio-temporal analysis of empirical congested traffic patterns is the key for the understanding of traffic flow characteristics as well as for the development of dynamic traffic management methods consistent with real traffic. Thus, single-vehicle data can provide important information about the microscopic structure of traffic flow that, of course, determines the macroscopic properties as well. For instance, when the distribution of time headways is studied for different densities, it shows a interesting property. It turns out that the distribution becomes sharply peaked around approximately $1s$ for densities close to congestion [53, 57, 58], but considerably broader for lower and higher densities (Fig. 2.2a). This suggests that congestion is an overcritical phenomenon [10, 12], occurring when the maximum efficiency in terms of time headways cannot be supported any longer.

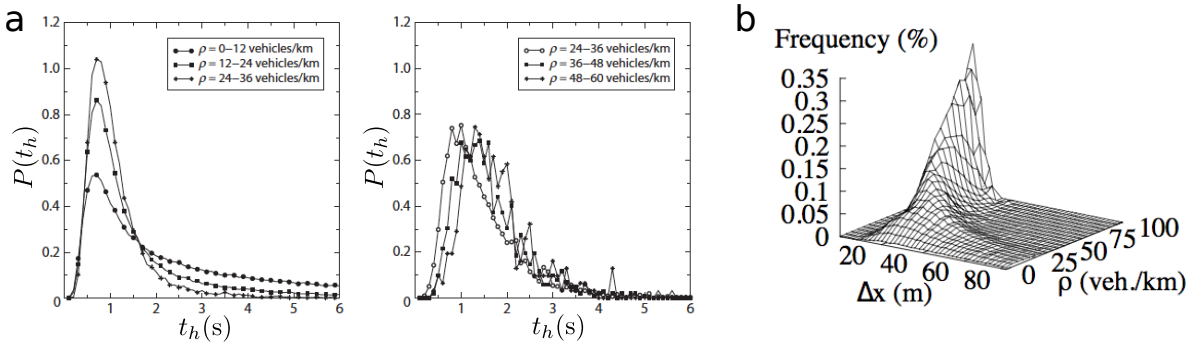


**Figure** 2.2.: **Single-vehicle data.** (a) Distribution of time-headways obtained empirically on German highways in both free flow (left) and synchronized regimes (right). Figures were taken from [59]. Copyright (2011) by Elsevier BV. (b) The broad distance headway distributions change rather smoothly with increasing density. Figure taken from [10]. Copyright (2000) by Springer-Verlag Berlin Heidelberg.

In the case of distance headways, a broad distribution can be observed for small density values (Fig. 2.2b). This reflects different driving styles. Despite all them can accelerate (there are few cars), some of them decide for maintaining a slower speed and then larger distance headways, e.g., there is a frustration effect. In other words, at the same highway density, drivers have different criteria for choosing their speeds.

### 2.2.2. Phase Transitions

Transitions between the three traffic phases have been empirically observed. Because they display a discontinuous change in a traffic observable (the velocity), they are considered as first order transitions [9,47,56]. Wide moving jams ($W$) do not emerge spontaneously in free flow ($F$)[2]; they can emerge spontaneously only in the synchronized flow phase ($S$). Then, jams emerge from the sequence of transitions $F \rightarrow S \rightarrow J$.

A transition from free flow to synchronized phase $F \rightarrow S$ (also named *traffic breakdown*) occurs due to a bottleneck, e.g. on- or off-ramps, accidents or constructions, or even without no apparent cause. Last case is known as a phantom jam, one of the more perplexing phenomenon in traffic which was demonstrated recently [60,61]. In reality, traffic flow is constantly exposed to tiny perturbations as imperfections on the asphalt or half-seconds of driver inattention that can decay or amplify. If they decay, the traffic flow is stable and there are no jams. But if they are amplified, the flow becomes unstable, with small perturbations growing into backwards-traveling waves called *jamitons*. This is what happens in the top of the free flow phase. Phantom traffic jams usually don't cause major delays, but they are hot spots for accidents, because they force unexpected braking.

Once in the synchronized phase, the emergence of a wide-moving jam ($S \rightarrow J$) is associated with the so-called pinch effect. The pinch effect [9, 47] describes a process of local self-compression in synchronized regions (called *pinch regions*) that can finally lead to the formation of small narrow jams. This small jams can evolve into a wide jam or simply dissolve after a while. The latter case is related to a reverse transition from congested traffic to the free flow at the bottleneck. Finally, traffic breakdown and the reverse transition are accompanied by a well-known hysteresis effect (loop) in the flow-density plane. As Fig. 2.1 shows, a congested pattern usually emerges at a greater flow rate downstream of the bottleneck than the flow rate at which the congested pattern dissolves (see references in [47]).

## 2.3. CA Models for Traffic Flow

Since the distinction between the two congested phases relay on their microscopic structure, the microscopic models have been more successful over the other models. Among those, CA

[2] At least they have not been observed in real traffic.

models have been very fruitful, not just because their simplicity and flexibility to implement, but also because of their fast computational performance. In a generic CA model, the road is represented by a finite lattice of length $\ell$ (see Fig. 2.3). Each lattice cell can either be empty or occupied by at most one car. The speed $v_n$ of each vehicle $n$=$1, 2, ..., N$ takes one of the $v_{max}$+1 allowed integer values $v_n$=$0, 1, ..., v_{max}$. The position of the $n^{th}$ vehicle is denoted by $x_n$, and $d_n$=$x_{n+1} - x_n$ is the distance ahead (gap) between the $n^{th}$ car and car $n + 1$ in front of it. At each time step $t + 1$, all vehicles update in parallel their speeds and positions according to some driving rule.

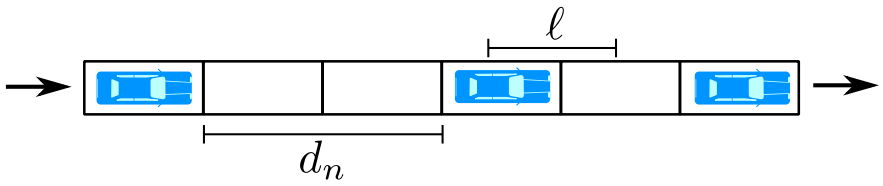


**Figure** 2.3.: **Typical road discretization used in CA models:** $\ell$ is the size of each cell, $d_n$ is the distance ahead and the arrows represent the periodic boundaries.

In the following we introduce some popular CA models for traffic flow.

### 2.3.1. Nagel-Schreckenberg Model, NaSch

In 1992, Nagel and Schreckenberg [62] proposed a model to describe the basic phenomena of real traffic flow on highways. In the NaSch model the road is divided into cells of length 7.5 m with periodic boundary conditions. Every car applies in parallel the following sequence:

- *Step 1: Acceleration*
  If $v_n$<$v_{max}$, velocity is increased by 1, i.e., $v_n^{(1)}$=$min(v_n + 1, v_{max})$.

- *Step 2: Deceleration*
  If $d_n$<$v_n^{(1)}$ velocity is reduced to $d_n$ , i.e., $v_n^{(2)}$=$min(v_n, d_n)$

- *Step 3: Randomization*
  If $v_n^{(2)} > 0$, velocity is decreased randomly by 1 with probability p, i.e.,

$$v_n^{(3)} = \begin{cases} max(v_n^{(2)} - 1, 0) & \text{with probability } p, \\ v_n^{(2)} & \text{with probability } 1-p \end{cases}$$

- *Step 4: Vehicle Movement.*
  Each vehicle is moved forward according to its new velocity $v_n{=}v_n^{(3)}$, i.e., $x_n \rightarrow x_n + v_n$

Behind each rule, there is a simple interpretation. *Step* 1 expresses the drivers' desire to move as fast as possible, but respecting the speed limit. *Step* 2 guarantees the absence of collisions in the model. *Step* 3 incorporates many effects which play an important role in the dynamics of the model such as random disturbances, road irregularities or drivers' overreactions. This ingredient causes the spontaneous jam formation in this model. The fundamental diagram of the NaSch model consists in an inverted $V$ (Fig. 2.4a) being consistent with the classical view. Nevertheless, it neither reproduces the metastable states with flow nor the synchronized phase. To do so, more sophisticated rules must be implemented.

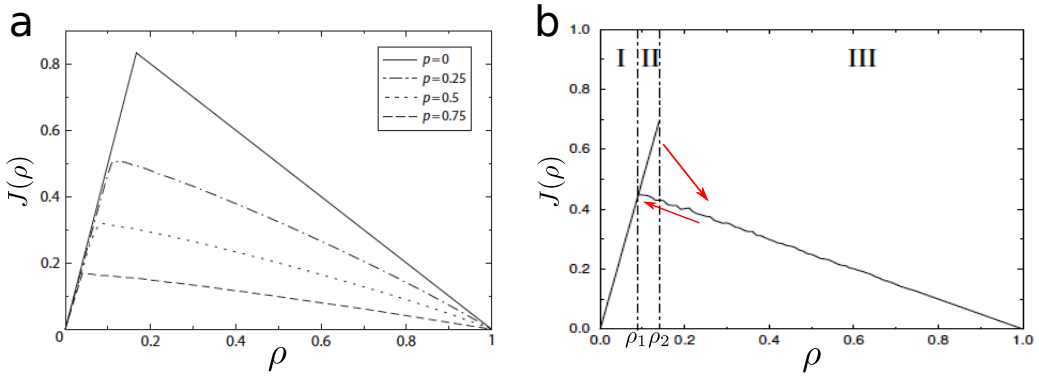


**Figure** 2.4.: **CA fundamental diagrams. (a)** Fundamental diagram of the NaSch model for $v_{max}{=}5$ and different values of $p$. **(b)** Fundamental diagram of the VDR model. The randomization parameter of standing cars is set to $p_0{=}0.5$ and for free flowing vehicles to $p{=}0.01$. The metastable branch in regime II can clearly be identified, red arrows illustrates the hysteresis effect obtained depending on the initial conditions. Here flow is labeled as $J$. Figures are taken from [27]. Copyright (2003) by R. Barlovic.

For instance, the VDR model introduce a velocity-dependent randomization (VDR) parameter $p{=}p(v(t))$, in contrast to the constant randomization in the NaSch model. So, before the acceleration step, the following rule is introduced:

- *Step 0: Determination of the randomization parameter*
  The randomization parameter for the $n^{th}$ car is given by $p{=}p(v_n(t))$.

So that, the randomization parameter used in *Step 3* depends on $v_n(t)$ of the $n^{th}$ car after the previous timestep. Metastable states occur for so-called *slow-to-start* rules where one chooses

$$p(v) = \begin{cases} p_0 & \text{for v=0,} \\ p & \text{for v>0,} \end{cases} \tag{2.6}$$

with $p_0 > p$. Thus, cars which have been standing in the previous timestep have a larger probability $p_0$ of braking in the randomization step than moving cars, explaining the name *slow-to-start* rule. This leads to a reduction of the jam outflow compared to the maximum possible flow, as suggested in the empirical observations. Therefore, the VDR model shows a completely different jam dynamics, i.e., the existence of wide phase separated jams and metastable free-flow states [63–65]. The fundamental diagram of the VDR model is shown in Fig. 2.4b. For densities $\rho_1<\rho<\rho_2$ there are two different states for flow (here labeled as $J(\rho)$) depending on the initial conditions, showing phase separation between jammed and free flowing cars.

While the VDR model shows metastable states and the hysteresis phenomenon, it is no able to reproduce neither the synchronized traffic nor the empirical microscopic structure. Therefore, more realistic aspects as velocity anticipation, retarded acceleration and timely braking must be added to the CA rules. These aspects involve rules with information about the velocity or the velocity difference to the preceding car. Recently, Knospe et al. [66, 67] proposed the brake light model (BL model), which incorporates velocity anticipation through brake lights indicating velocity changes of the preceding car. A smoother acceleration and deceleration are also included by reducing the cell length of 1.5 m instead of 7.5 m (as NaSch model) and, therefore, the vehicles occupy 5 cells. This model is able to reproduce all three phases observed in real traffic and it shows good agreement with empirical single-vehicle data in all phases.

### 2.3.2. A CA Model for Bogotá, Olmos-Muñoz Model

Since the drivers' style is very different from city to city (see Fig. 2.1), a realistic traffic model should keep in mind the particularities of each place. In 2004, Olmos-Muñoz model developed and implemented a CA model for reproducing the behavior of traffic flow in Bogotá [68, 69]. This model keep in mind the particularities of Bogotan drivers, measured directly inside a car running on Bogotá's highways. In this model, each car occupies two cells ($\ell$=2.75 m), and the gaps the driver uses to decide to brake or accelerate are different for each speed ($v_{max}$=7 and $v_{unity}$=10$\frac{km}{h}$). Then, if the headway distance is less or equal to the brake gap,

the car brakes, and if it is greater than the accelerate gap, it accelerates; otherwise, the speed remains constant. The other two elements are delay time on the acceleration $t_{up}$ (the time it takes the car to reach the next discrete speed value) and break lights that force to brake when the car ahead breaks. At time $t$ the $n^{th}$ vehicle is completely defined by: its position $x_n(t)$, its velocity $v_n(t)$ and its brake-light status, $b_n(t)$ (which is $b_n$=1(0) when the driver brakes (or not) at the previous step time $(t-1)$, like [67]). An effective *gap* is defined as $gap(t)$=$\Delta x(t) + \Delta v(t)$, where $\Delta x(t)$=$x_{n+1}(t) - x_n(t) - 1$ is the number of cells empty to the vehicle ahead and $\Delta v(t)$=$v_{n+1}(t) - v_n(t)$ is the speed difference to the car ahead.

The three parameters $gap_{brake}$, $gap_{accel}$ and $t_{up}$, are function of speed and they represent on the whole the drivers' driving. These parameters are summarized in Table 2.1.

**Table** 2.1.: Driving parameters for Bogotá.

*Cars*

| *Speed* | $gap_{brake}$ | $gap_{accel}$ | $t_{up}$ |
|---|---|---|---|
| 0 | 0 | 3 | 1 |
| 1 | 3 | 4 | 1 |
| 2 | 3 | 5 | 1 |
| 3 | 4 | 5 | 1 |
| 4 | 5 | 6 | 2 |
| 5 | 6 | 7 | 2 |
| 6 | 6 | 8 | 2 |
| 7 | 7 | 9 | 2 |
| 8 | 8 | 10 | 3 |
| 9 | 8 | 11 | 3 |
| 10 | 10 | 13 | 3 |

*Buses*

| *Speed* | $gap_{brake}$ | $gap_{accel}$ | $t_{up}$ |
|---|---|---|---|
| 0 | 0 | 4 | 1 |
| 1 | 4 | 6 | 1 |
| 2 | 6 | 7 | 2 |
| 3 | 8 | 9 | 2 |
| 4 | 8 | 10 | 3 |
| 5 | 9 | 12 | 3 |

Every time step, all cars execute in parallel the following set of rules:

1. Compute its $gap(t)$=$\Delta x(t) + \Delta v(t)$.

2. Read its parameters $gap_{accel}$, $gap_{brake}$ and $t_{up}$ from table 2.1.

   - *Normal brake:* If $gap(t) \leq gap_{brake}$, speed down to the maximal speed $v_n(t+1)$ such that $gap'_{brake} \leq gap(t) \leq gap_{accel}$, where $gap'_{brake}$ and $gap'_{accel}$ are the parameters at speed $v_n(t+1)$. In addition, let $delay$=0 and turn on brake lights, $b_n(t+1)$=1.
   - If $gap > gap_{accel}$, then

  - *Instantaneous brake*: If $gap(t) \leq gap_{accel} + 2$ and the brake lights of the car ahead are on ($b_{n+1}(t)$=1), let $v_n(t+1)=v_n(t)-1$ (brake), turn on brake lights ($b_n(t+1)$=1) and let $delay$=0.
  - *Accelerate*: Else, turn off brake lights ($b_n(t+1)$=0) and
    - If $delay == t_{up}$, let $v_n(t+1)=v_n(t)+1$ (accelerate) and let $delay$=0
    - Else, let $delay=delay+1$ and preserve $v_n(t+1)=v(t)$.
- Otherwise, let $delay$=0, turn off brake lights ($b_n(t+1)$=0) and preserve $v_n(t+1) = v_n(t)$.

3. Finally, move $v_n$ cells ahead, $x_n(t+1)=x_n(t)+v_n(t+1)$.

The counter *delay* defines if $t_{up}$ has been completed. The variable $b_{n+1}(t)$ defines the brake light status of the car ahead. The *instantaneous brake* rule represents the braking reaction we have observed when the car ahead also brakes. This reaction is observed for all distances but is just included in the gaps when $gap \leq gap_{accel}$. Thus have included it as an additional rule only it $gap_{accel} \leq gap(t) \leq gap_{accel} + 2$ through a brake light on each car.

As shown in Fig. 2.5, simulations are in very good agreement with the experimental measurements, not just in the shape of the fundamental diagram, but also in the numerical values for both the road capacity and the density of maximal flux. By comparing with other cities, Bogotá seems to have a better behavior not just for the higher value of the maximal flow, but also because it occurs at a higher density. An explanation of these findings is the aggressive driving of the bogotans, i.e., they maintain lower safety distances than in other cities (see Table 2.1).

The model has been improved by including two lanes, dynamic rules for buses (also empirically measured), and then, mixed traffic was studied [70]. With the same CA unities, a bus occupies three cells and its $v_{max}$=5. Table 2.1 (right) show the bus driving parameters. Additionally, a *changing-lane* rule was included just after the step of the gap computation. The inclusion of buses on the highway produces a great effect on the fundamental diagram. Figure 2.5b shows how the critical threshold and the flow capacity are considerably reduced when just the 5 % of vehicles are buses.

More recently, Triana and Muñoz [71] studied the effect of bumps and organized buses stops on the fundamental diagram of two-lane mixed traffic. They showed that the system is very sensitive to both factors explaining, quantitavively, the cost of the disordered and dare-devil style of the bogotans.

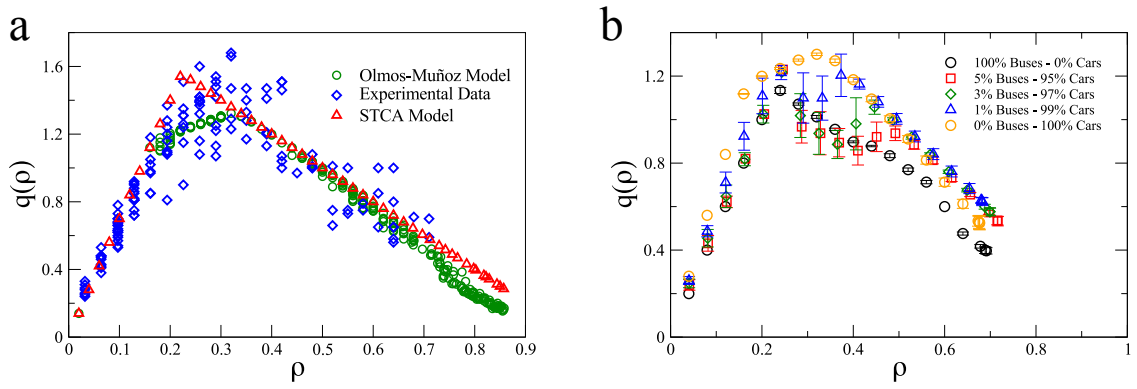


**Figure** 2.5.: **Empirical and simulated fundamental diagrams for Bogotá. (a)** One lane case, obtained empirically (blue diamonds) and with the Olmos-Muñoz model (green circles) with $v_{max}$=7 [68]. For comparison, the fundamental diagram of NaSch with a similar discretization is included (red triangles). **(b)** Fundamental diagram for a two-lane highway with mixed traffic, buses percentages between 5 % and 0 % [70].

## 2.4. CA models for Accidents

Despite accidents are the most frequent reason for the formation of jams in urban traffic, they are usually neglected in modeling approaches. The fact that more than the 90 percent of road accidents are caused by human error, i.e., careless or aggressive drivers' maneuvers, makes the microscopic models more suitable for studying this issue.

Within the framework of CA models, just a few studies have addressed this topic. These approaches focus on modifying the braking rule, such that a fraction of drivers, $q$, do not respect the safety distance in Step 2 on NaSch model, i.e., with probability $p_c$ the velocity after this step for those careless drivers is $v_n^2 = d_n + 1$. This leads to an accident, if the car in front of the careless driver will not move in the same timestep. In other words: An accident occurs with probability $p_c$ if the following three accident criteria are satisfied:

$$(1) : d_n(t) \leq v_{\text{máx}}, \qquad (2) : v_{n+1}(t) > 0, \qquad (3) : v_{n+1}(t+1) = 0. \tag{2.7}$$

It's worth noting that here accidents only occur virtually, i.e., once these criteria are satisfied the accident is counted, but they are replaced by a "safe"dynamics that avoid the accident and any artifact in the simulation. Thus, instead of accidents, it is better to speak about dangerous situations. A critical discussion about this treatment can be found in [59, 72].

This modification on the braking rule was first studied for the deterministic limit of the NaSch model [73]. As one expects, accidents only can occur on the jammed phase of the

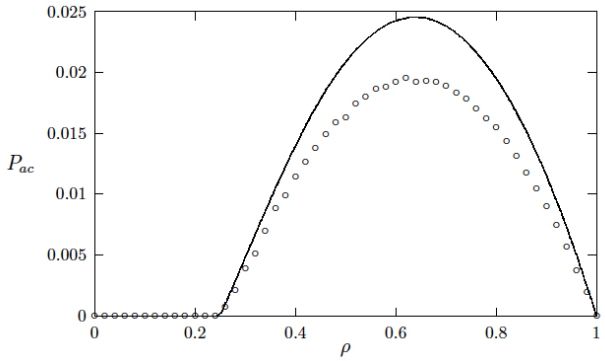


**Figure** 2.6.: **Probability of an accident $P_{ac}$ per car and timestep as a function of the car density.** The accidents are caused by drivers who do not respect the safety distance with a stopped car ahead in deterministic NaSch model with $v_{max}$=3. Figure taken from [73]. Copyright (1997) by IOP Publishing Ltda.

fundamental diagram, as showed in Fig. 2.6. The probability $P_{ac}$ of an accident (per car and timestep) is a parabolic function of the vehicle density and exhibits a maximum at a certain $\rho^* = \rho_c$.

Later studies have generalized this modification to other models, like the probabilistic version of the NaSch model [74–78], the VDR model [79], models of synchronized flow [80], and other situations [81–84]. Nevertheless, in this framework, dangerous situations only occur with stopped cars and thus only at high densities. Contrary, in reality accidents due to careless driving more generally involve vehicles in circumstances like large velocity differences, abrupt velocity changes and small safety gaps. With this in mind, Moussa [85] characterizes a careful driver by lower acceleration capability and a higher value of the deceleration probability $p_1$; these drivers tend to brake more often and accelerate slowly. In addition, aggressive drivers with higher accelerate capability and a lower deceleration value of $p_2$. He found that aggressive driving increases not only the traffic flow but also the number of crashes.

However, these kind of studies have received some criticism, quoting from Schadschneider et al. [59]: *In reality, accidents due to careless driving more generally involve vehicles with large velocity differences. Another source of dangerous situations are abrupt velocity changes and small safety gaps. This poses the question how relevant these investigations are for real traffic accidents. It appears that the probability of dangerous situations is systematically overestimated due to the correlations induced by the fact that accidents are not explicitly modeled. If an accident has occurred it is rather likely that another one, involving the same vehicles, will occur shortly after that because the conditions are usually still fulfilled.*

# 3. Monte Carlo predictions and Accidents

In this chapter we ventured to explore two more ideas about single roads. The first is aimed to inquire how much information can be inferred just from the CA driving rules, without implementing a temporal simulation. Here, we present that a Monte Carlo sampling of all states compatible with the driving rules actually reproduces the measured fundamental diagram, both in mean values and dispersion, when all such states are assumed equally probable. Even more, by using the Wardrop's relation (Eq. 2.5), the same gathered data also approximates the general form of the *time-mean* fundamental diagrams. These results suggest that the assumption of equally probable states plus compatible with the driving rules may be a first model for the statistical description of highways. The results of this were presented in the Conference on Traffic and Granular Flow '13 and were published in the proceedings [1].

The second idea relies on the characterization of a new kind of careless drivers, called hereafter *distracted*, as those who have a braking delay. Everytime rules indicate he must brake, he brakes in the next timestep and, sometimes, causing an accident. Complementing this idea we model accidents more realistically by taking advantage of the technical features of the Olmos-Muñoz CA model. In the original model a car occupies two cells and in it is impossible that two consecutive cars are separated but a single cell. Thus, with the introduction of distracted drivers, an accident occurs when just a single cell separates two cars. Both cars stay at rest for a while, affecting the global state of the system.

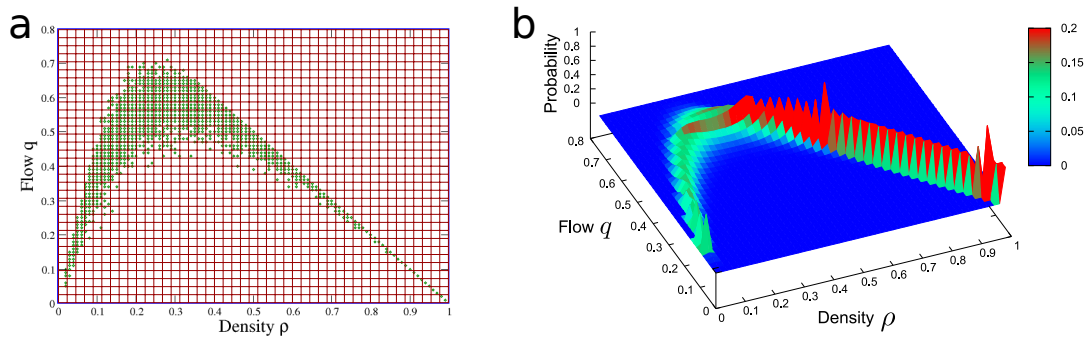


**Figure** 3.1.: **Monte Carlo sampling from the NaSch driving rules to generate at random the traffic states of the road. (a)** Scatter plot of the fundamental diagram and **(b)** density of states obtained from these random configurations.

## 3.1. A Simple Statistical Method for Reproducing the Highway Traffic

Although most cellular automata intend to reproduce the fundamental diagram by measuring mean values at the the limit steady-states from the dynamic simulation, real roads are constantly perturbed by external factors, driving the system to explore a much broader phase space. This arises us the question of which traffic features can be reproduced by a Monte Carlo exploration of the phase space allowed by the driving rules. To solve the question, we implement a Monte Carlo sampling from the driving rules to generate at random all traffic states on the road that, according to the the driving rules, does not change speeds at the next time step. The road is represented by a one-dimensional lattice of $L$ sites with periodic boundaries. Since the empirical data are aggregated for short time periods we must use small road sizes; otherwise, the data dispersion would be reduced. Next, we choose a number of cars $N$ and throw them randomly into the road. Each car computes its distance headway and takes the maximal allowed speed $v_{com}$ (the *comfort speed*) according to the rules of the CA model we are studying. So, we are absorbing both the non-equilibrium characteristic of traffic and the fact that drivers want to move as fast as possible. For each state so generated, we measure the spatial variables $\rho$ and $q$, corresponding to a point in the fundamental diagram. The process is repeated many times for each number of cars $N \leq L$ and the fundamental diagram is obtained by cumulating these samples onto a two-dimensional histogram on the flow-density map (see Fig. 3.1). Our main assumption is that all these randomly generated configurations are equally probable, but not so the macroscopic states of traffic defined by the couple of values $(q, \rho)$. Fig. 3.1(a) shows that for each $\rho$ there is a most likely value of $q$ which just depends on the driving rules. As we will see, the most likely regions can be identified with the realistic states observed in empirical measurements.

**Table** 3.1.: Values of $v_{com}$ for each $gap{=}\Delta x$ in the Olmos-Muñoz model for Bogotá (see first two columns in Table 2.1)

| gap | $v_{com}$ | gap | $v_{com}$ |
|---|---|---|---|
| 0 or 1 | 0 | 6 | 6 |
| 2 | 1 | 7 | 7 |
| 3 | 2 | 8 | 9 |
| 4 | 3 | 9 | 9 |
| 5 | 4 | 10 | 10 |

We studied the driving rules of two CA models. The first one is the deterministic limit of the NaSch model [62] (subsection 2.3.1), where $v_{com}{=}gap$ for $gap \leq v_{max}$ and $v_{\mathrm{com}} = v_{max}$ for $gap{>}v_{max}$. The second one is the Olmos-Muñoz model [68] (subsection 2.3.2) which, as we said before, was developed and implemented for reproducing the behaviour of traffic flow in Bogotá. This second model keeps in mind the particularities of Bogotan drivers, measured directly inside a car running on Bogotá's highways. In this model, each car occupies two cells, and the gaps the driver uses to decide to brake or accelerate are different for each speed. Then, if the headway distance is less or equal to the brake gap, the car brakes, and if it is greater than the accelerate gap, it accelerates; otherwise, the speed remains constant. Here, the comfort speed $v_{\mathrm{com}}$ corresponds to the largest one at which the gap ahead is lower or equal than the accelerate gap. The other two elements are delay time on the acceleration and brake lights that force to brake when the car ahead brakes. Since these last two elements have a dynamical nature, they are not included in our Monte Carlo method. The values of $v_{\mathrm{com}}$ for this second model are summarized in the Table 3.1.

### 3.1.1. Results for the Fundamental Diagram

Fig. 3.2(a) shows the contour plot obtained for the frequency to obtain states with flux $q$ at density $\rho$ for the driving rules of the deterministic NaSch model. This is compared to the steady states of the dynamic simulation of the cellular automata. It is clear that around the value of maximum flow the most probable states do not match with the equilibrium states of the dynamical simulation. This could be expected, since there is not disorder in the deterministic NaSch model and, thus, it describes an unrealistic stationary traffic flow. Nevertheless, by setting a non-zero value for the stochastic parameter, the match can improve. Fig. 3.2(b) shows the comparison between the empirical fundamental diagram measured for Bogotá (builded from *space-mean* measures in [68]) and the result obtained with the Monte

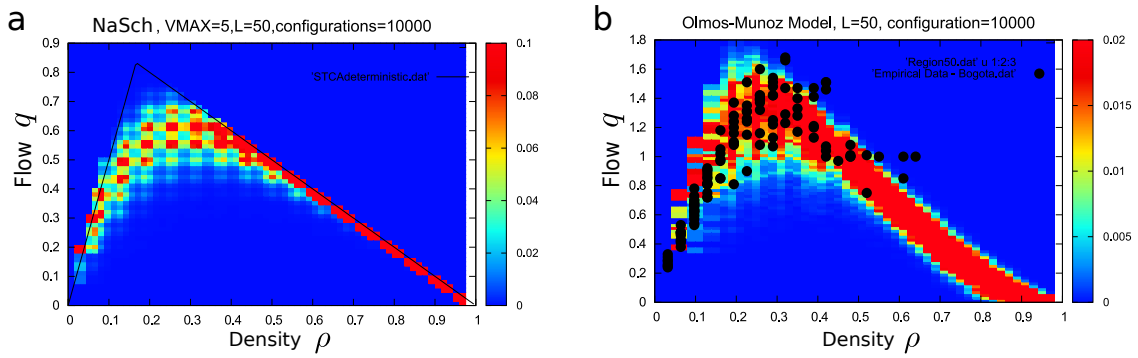


**Figure** 3.2.: **Contour plot of the fundamental diagram obtained from the driving rules of the deterministic NaSch model (a) and of the Olmos-Muñoz model (b) for** $L$=50**.** In **(a)** the right line corresponds to the steady state from a cellular automata simulation. In **(b)** the black dots correspond to the empirical fundamental diagram measured in Bogotá.

Carlo method by using the Olmos-Muñoz driving rules (Table 3.1). This figure shows that the most likely states of the system (red color region) match in a good agreement to the real data measurements of a non-equilibrium system.

As we mentioned above, this method build the fundamental diagrams from *space-mean* variables. This arises the question of how a fundamental diagram is based on *time-mean* quantities. Although our method is not dynamic, we can compute the local quantities by using Eq. 2.5, since $\sigma_s^2$ can be estimated by computing standard deviations on each Monte Carlo configuration. Once $v_t$ is obtained from $v_s$, the flow $q$ remains the same, but the density is recalculated from $\rho = q/v_t$. This step is included in the method before computing the density of the states. Fig. 3.3 shows a striking result: we obtain a fundamental diagram very similar to those measured empirically using temporal averaged variables. Focusing on the most likely states, one can distinguish the free-flow branch with high-flow states and, separated from that, some wide dispersed data appears as the synchronized phase, under the perspective of the three-phases theory [9]. Therefore, the discontinuity appears naturally as a region of unlikely states. Besides that, it appears a region with low flow and a underestimated density, in similarity with real collected data.

### 3.1.2. A Mean Field Approach to the Fundamental Diagram

We are also interested in the features of the microscopic structure that this method can reproduce. Clearly, the *spatial-headway distribution* is the characteristic that we can study directly. Due to the assumption of equally probable microstates, this method neglects the

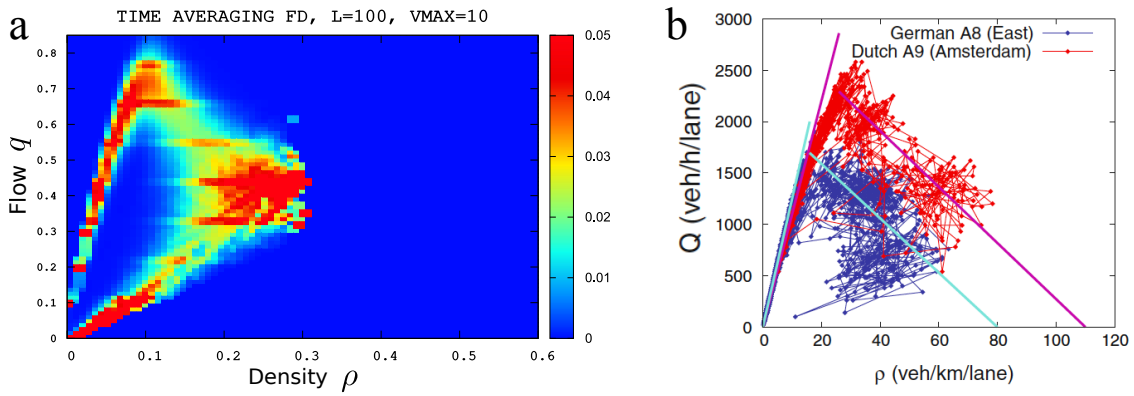


**Figure** 3.3.: **Time-mean fundamental diagrams. (a)** Contour plot of the fundamental diagram (FD) obtained by transforming the *space-mean* variables in *time-mean* by using Eq. 2.5 and the driving rules of the NaSch model. It is clear the similarity to those measured empirically by using temporal averaged variables **(b)** From [13] (copyright (2013) by Springer-Verlag Berlin Heidelberg). It should remark that the discontinuity emerges naturally as a region of unlikely states.

correlation between the gaps in front of successive cars. If we assume further that the length of the road $L \to \infty$, one can analytically derive that the gaps distribute as

$$\wp(gap) = \rho \cdot (1-\rho)^{gap} \text{ and, therefore, } \langle gap \rangle = \sum_{gap=0}^{\infty} gap \cdot \wp(gap) = \frac{1-\rho}{\rho} \quad . \tag{3.1}$$

However, the empirical distribution of distance-headways reveals the inadequacy of this equation. As Fig. 3.5(a) shows, this distribution is surprisingly broad. Even so, it is interesting to see that the right hand side of Eq. 3.1 does predict an average gap decreasing with the inverse density $\frac{1}{\rho}$, as Tilch and Helbing reported [10]. Thus, let us go with the idea more deeply. Since $v_{\text{com}}$ is related with the *gap*, we can study how speed distributes. The distribution of speeds $\wp(v_{com})$ for the deterministic NaSch model, for instance, is the same $\wp(gap)$ for $v_{com} < v_{max}$ and $\wp(v_{\max}) = \sum_{i=v_{\max}}^{\infty} i \cdot \rho \cdot (1-\rho)^i$ for $v_{\max}$. Thus, the average speed can be written as

$$\langle v \rangle = \frac{1-\rho}{\rho} \cdot (1-(1-\rho)^{v_{\max}}) \quad , \tag{3.2}$$

and the flow is immediately obtained as $q{=}\rho \cdot \langle v \rangle$. This mean-field approach match almost perfect for the fundamental diagram of both the NaSch and the Olmos-Muõz models, as shown Fig. 3.4[1]. Note that Eq. 3.2 with $v_{max}{=}1$ reproduces the Greenshields' model [44],

[1]The meanfield approach for the Olmos-Muñoz driving rules (Table 3.1) gives:

$$q = 2\rho[10 - 10\rho - 10\rho(1-\rho) - 9\rho(1-\rho)^2 - 8\rho(1-\rho)^3 - 7\rho(1-\rho)^4 - 6\rho(1-\rho)^5 - 4\rho(1-\rho)^6 - 3\rho(1-\rho)^7 - \rho(1-\rho)^8 - \rho(1-\rho)^9]$$

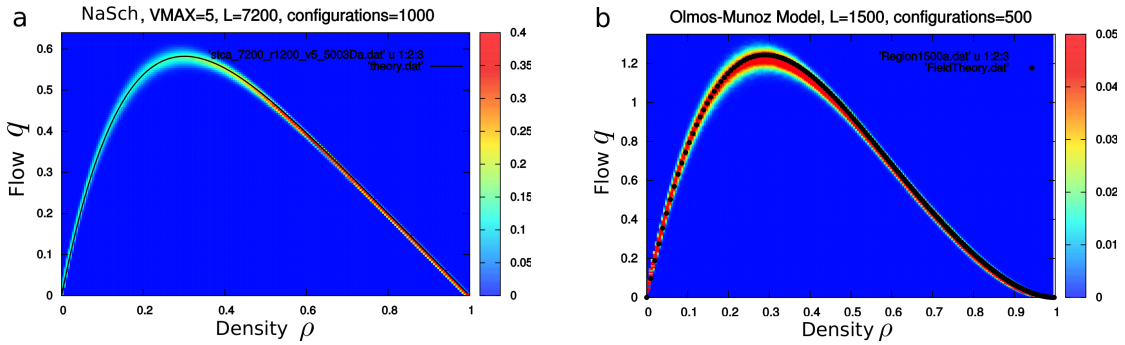


**Figure** 3.4.: Comparison between fundamental diagrams obtained by the Monte Carlo method and the mean-field approach, under the assumption of large road segments for (a) the deterministic NaSch model and (b) the Olmos-Muñoz model.

and even other empirical models can be reproduced with other values of $v_{\max}$ [86]. The kind of analytical calculations resulting in Eq. 3.2 are typical of the naive mean-field theory[2] and its generalizations [41]. These theories were applied with success to the NaSch model at the beginning of the past decade (see [41] and references therein) but, as we already noted in Sec. 2.3, they could not reproduce the distance-headway distribution of the stationary states of the CA model on a large system. Nevertheless, we are not interested in the stationary states of a cellular automaton but in the most likely states one would measure in reality. Therefore, we computed the distance-headway distribution for a finite system just for the most likely states (the red-colored regions in Fig. 3.2(a)). The results, in Fig. 3.5(b), shows the same broad distribution observed in empirical data.

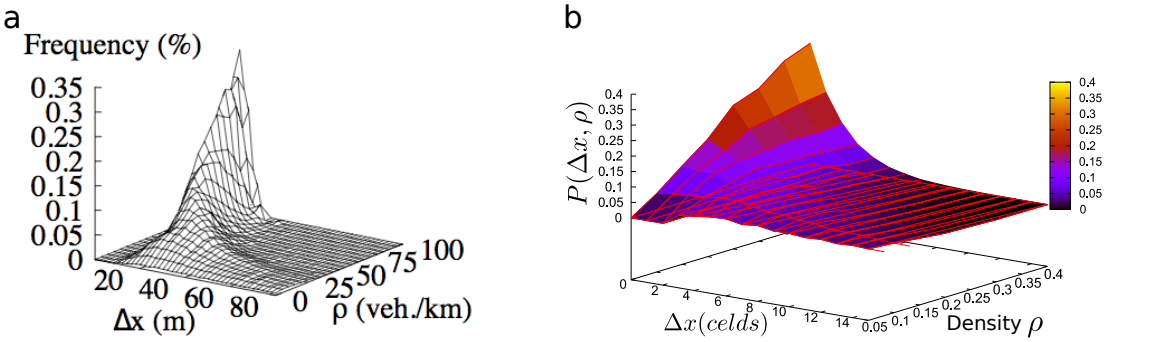


**Figure** 3.5.: **The broad distribution of vehicle distance-headways at all densities $\rho$. (a)** Empirical distribution from Tilch and Helbing [10]. **(b)** Distance-headways distribution for just the most likely states in the Monte Carlo sampling of the NaSch model, showing the same broad distribution observed in the empirical data.

[2] Actually our calculations are more naive than the naive mean-field theory.

## 3.2. Accidents induced by distracted drivers

As we showed above, previous studies have considered dangerous situations instead of accidents, and these situations just involve events with standing cars. But in reality, accidents induced by careless driving generally involve vehicles with large velocity, where the combined effect of an abrupt velocity change and a small safety gap produces the vehicle crash. In addition, a crash usually needs a recovery time to disappear. Here we address a gap in the literature with regard to these two aspects of car accidents.

Let us remark at this point that, in the framework of the Olmos-Muñoz model, the fact that cars occupy two cells becomes an advantage for modeling car accidents. Although in the original model is impossible that two consecutive cars are separated by a single cell, we can relax that rule for distracted drivers, such that two vehicles crash if they are separated by one cell. In that case, because of the model rules, the cars involved will be stayed together for a while.

We characterize a distracted driver as one who delays one time step its braking maneuver if the car ahead is moving. Thus, if the car ahead brakes at time $t$, it is probable that there will be a crash at time $t + 1$. We simulate a single lane periodic road of 2.000 cells (close to 5 km) for a variable percentage of distracted drivers, $f$. Starting from random initial configurations, we let the system to equlibrate during 6.000 timesteps, and just thereafter we turn on the distracted drivers and count the number of accidents that occur in a period of 20.000 timesteps. The influence of the fraction $f$ of distracted drivers on the highway on the number of accidents is shown in figure 3.6. As expected, accidents do not occur for neither free flow ($\rho < 0.3$) nor high congestion conditions ($\rho > 0.8$). The accident zone appears between these limits, and corresponds to the zone of synchronized flow. It seems that the disordered microstructure of this region is the responsible for the crashes, as it increases the dangerous situations [85].

By the way, we realized that these accidents have a tremendous effect on the global state of the system, even for low percentages of distracted drivers. Figure 3.6(b-c) shows space-time diagrams for $f$=0.05 and $f$=0.3 in different stages of the simulation. We can observe how once distracted drivers are turn on, and avalanche of accidents appear in different locations of the road. Each accident produces density waves than can evolve to a long-lasting jams. Thus, the road divides into free-flow and congested sections. At that state, no more accidents appear on the system.

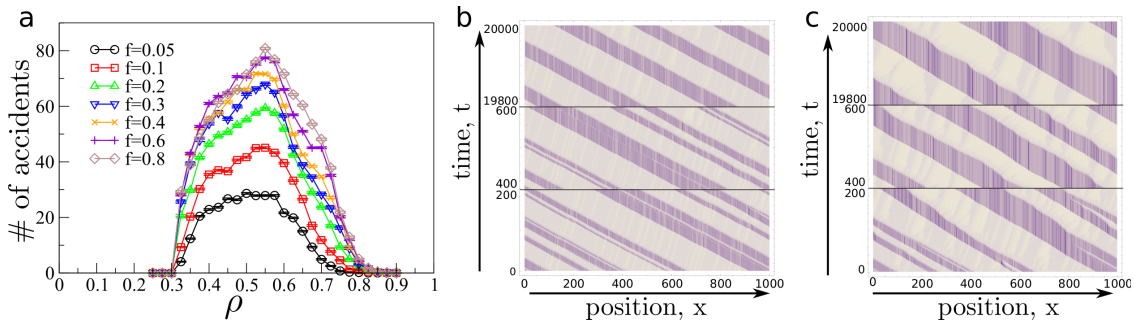


**Figure** 3.6.: **Behavior of the Olmos-Muñoz CA model with accidents. (a)** Average number of accidents (on 100 simulations) as function of car density $\rho$ for several fractions $f$ of distracted. **(b)** and **(c)**, Space-time diagrams at different stages of the simulation for $f$=0.05 and $f$=0.3, respectively. Each horizontal row represents the instantaneous positions of the vehicles moving right, while successive rows represent successive time steps.

## 3.3. Conclusions

We have shown that a Monte Carlo exploration of the driving rules can reproduce the empirical fundamental diagram. By generating states according with the Olmos-Muñoz model, and assuming that all these microstates are equally probable, we have reproduced with good agreement the capacity and the data dispersion of the fundamental diagram measured for Bogotá city. Even more, by using the Wardrop's relation (Eq. 2.5), our data also approximates the general form of the *time-mean* fundamental diagrams, revealing a naturally emergence of both the discontinuity between free-flow and congested phases and the high-flow states in this diagram. In addition, by computing the *distance-headways* distribution according to the driving rules of NaSch model and just for the most likely states of a finite road, we have reproduced the broad distribution observed in reality. All this result suggests that the non-dynamical part of the driving rules can give valuable information about the macroscopic behaviour of the highway traffic flow. They also suggest that the assumption of equal probabilities for all states compatible with the driving rule plus a finite length of road may be a first model for the statistical description of highways. Of course, this hypothesis should be validated on other roads with other automaton rules, and this will be an interest subject of future work.

Regarding accidents, it is worth to mention that our efforts correspond to an incipient stage of our research (early of 2013), when collecting accidents data was unusual and characterizing two totally different driving styles sounded weird. However, the context has changed a lot since then. First, due to the high rates of fatalities on vehicle crashes, very recent initiatives[3]

[3]For instance, see U.S. Department of Transportation - Traffic Fatalities data.

are releasing traffic fatalities data sets (with detailed information about each of these tragic incidents), putting out a call to analyze it. Second, a self-driving cars revolution has started[4], which clearly defines a scenario with two different types of drivers. This can arouse interest again on the modeling of accidents via cellular automata. Our work is, then, a first step on this direction.

[4]Actually, there is already discussion about ethical decisions in their algorithms Why Self-Driving Cars Must Be Programmed to Kill

# 4. Percolation and Phase Transitions

Percolation is one of the simplest mathematical models which exhibits critical phenomena, i.e, phase transitions, scaling laws, fractals and universality. Because of its simplification and abstraction, percolation is especially attractive to describe and understand a wide range of phenomena in disordered systems. Much of what is known about phase transitions in equilibrium systems can be illustrated easily by using isotropic percolation. Although some of those concepts can be extended to its non-equilibrium counterpart, the directed percolation (DP) (an anisotropic case of percolation) is the most important class (model) for describing dynamical phase transitions. In this chapter, we introduce briefly the fundamental concepts in these two percolation versions. We only show the concepts used in our findings that we shall present in the following chapters. For a more comprehensive review of the fundamental concepts in both fields we suggest references [87–91].

## 4.1. Isotropic Percolation

Consider a square lattice composed of $L \times L$ sites, with $L \to \infty$. Each site is occupied at random with probability $p$ independently of all other sites. Two nearest-neighbor sites are called connected if they are both occupied and a group of nearest-neighbouring connected sites is called a *cluster*. For $p$=0 there is no clusters in the lattice, while for $p$=1 the whole system is a cluster. For intermediate values $0<p<1$, at least on average for various realisations, one expects the size of the largest cluster to increase with $p$. We say that the system *percolates* if there is a cluster (called the *percolating cluster*) crossing the entire system from one side to the other. We can see this behaviour in Fig. 4.1, the largest cluster grows as the probability $p$ until a percolating cluster appears for the first time at $p_c \approx 0.59$. Thus, for an infinite network, there is a percolation threshold $p_c$ where a sharp transition in the topological structure of the network takes place, moving from a disconnected structure into a connected one. The obvious variant of this model is to occupy the bonds instead of the lattice sites. Again, above a well-defined value of $p_c$ an infinite cluster of occupied bonds

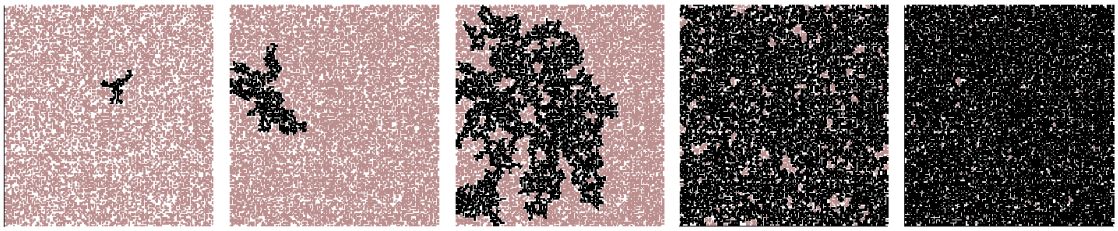


**Figure** 4.1.: **Site percolation in 2D square lattices with system size $L \times L$=150 $\times$ 150 for several occupancy probabilities $p$.** Note that the largest cluster percolates through the lattice from top to bottom when $p$=0.59. Taken from [90]. Copyright (2005) by Imperial College Press.

spans across the network.

At the percolation threshold the system exhibits self-similarity (a fractal structure) and, therefore, is scale free. Thus, many topological properties near the percolation threshold obey power laws. Among the foremost are [87, 88]:

- **Order Parameter, $P_\infty(p)$:** the fraction of occupied sites in the spanning cluster. In the infinite size limit, $P_p \sim |p - p_c|^\beta$ near $p_c$.

- **Correlation Length, $\xi(p)$:** Two occupied sites on the lattice are said to be correlated if they belong to the same cluster. The correlation function $G(r)$, is given by

$$G(r') = \frac{1}{N} \left\langle \sum_{\vec{r}} \sigma(\vec{r}) \cdot \sigma(\vec{r} + \vec{r'}) \right\rangle \ , \tag{4.1}$$

  where $\sigma(\vec{x})$=1(0) if the site at $\vec{x}$ is occupied(empty) and $N$ is the total number of sites. The correlation function usually decays as an exponential, $G(r) \propto \exp(-r/\xi)$, where $\xi$ is known as the correlation length. Near the pecolating threshold, the correlation length diverges as $\xi(p) \sim |p - p_c|^{-\nu}$.

- **Average Cluster Size, $S(p)$:** or mean cluster size in a lattice configuration excluding the percolating cluster. Again in the limit of infinite size, it becomes singular at the percolation threshold, $S(p) \sim |p - p_c|^{-\gamma}$.

The exponents are *universal*, i.e., they only depend on the dimensionality of the system and the coordination number of the lattice. In addition, there are theoretical and experimental indications that the exponents for second-order transitions are not independent but

connected by a *scaling laws*. A scaling law for percolation systems is:

$$2\beta + \gamma = \nu d \ , \tag{4.2}$$

where $d$ is the spatial dimension of the system.

### 4.1.1. Finite-Size Scaling Theory, FSS

The previous discussion is concerned to infinitely large systems, but the practical computations involve finite systems only. To measure those properties in the thermodynamic limit, one can study systems with a wide range of sizes and extrapolate the measurements to the limit of infinite size. That is what address the finite-size scaling theory. The basic concept underlying this theory involves the correlation length of the system. In an infinite system, the correlation length diverges at the critical point, but in a finite one the correlation length is limited by the linear system size $L$, i.e., $\xi<L$. So, for finite sizes near the transition [87,88,90]

$$\xi(p) \sim L \sim |p - p_c(L)|^{-\nu} \ , \tag{4.3}$$

where $p_c(L)$ tends to $p_c$ when $L \to \infty$. Therefore,

$$|p - p_c(L)| \sim L^{-1/\nu} \ , \tag{4.4}$$

which implies

$$P(p) \sim |p - p_c(L)|^{\beta} \sim L^{-\beta/\nu} \ , \tag{4.5}$$

$$S(p) \sim |p - p_c(L)|^{-\gamma} \sim L^{\gamma/\nu} \ . \tag{4.6}$$

Then, the ratios $\beta/\nu$ and $\gamma/\nu$ are estimated from measurements of $P(p_c)$ and $S(p_c)$ as functions of system size $L$. The exponent $\nu$ can be also measured from the wide $\Delta(L)$ of the transition curve $P(p, L)$, since

$$\Delta(p, L) \sim |p - p_c(L)| \ . \tag{4.7}$$

## 4.2. Directed Percolation

Curiously, the vast majority of systems occurring in Nature are not in equilibrium, but open systems that exchange energy, particles and other conserved quantities with external reservoirs. Thus, currents appear through the system, making the time an essential degree of

freedom. The main question focuses on under what conditions a relaxation towards an equilibrium steady-state may occur. Microscopically, this question turns to be if the dynamics satisfies (or not) detailed balance [91]. In the negative case, steady states cannot be equilibrium states, so there is a second-order phase transition from fluctuating (ordered) states into so-called absorbing states (states from which the system cannot leave).

Directed percolation (DP) is the simplest model which displays non-equilibrium transitions to absorbing states. It was introduced in 1957 by Broadbent and Hammersley [92] as a model for water (or a fluid) percolating through a porous medium with a preferred direction (usually defined by a gravitational field). For an illustrative picture, consider a specific case of *directed bond percolation* on a square lattice, where sites represent the pores of the medium, connected by channels (bonds) which are open with probability $p$ and closed otherwise (Fig. 4.2(a)). When a liquid is poured onto the surface, it percolates downwards along the open channels (black and red arrows) and it turns out that there is a well-defined probability $p_c$ for the medium to become macroscopically permeable. DP can be easily conceptualized as a generalization of isotropic percolation.

The dynamic (non-equilibrium) interpretation of DP comes when the preferred direction is naturally associated with a temporal coordinate. Then, one may enumerate horizontal rows by a temporal index $t$ as shown Fig. 4.2(b) and instead of thinking about open channels between sites one can think of sites themselves as active (*wet*) or inactive (*dry*). Knowing the configuration of wet sites at time $t$ we can compute the next configuration at time $t+1$

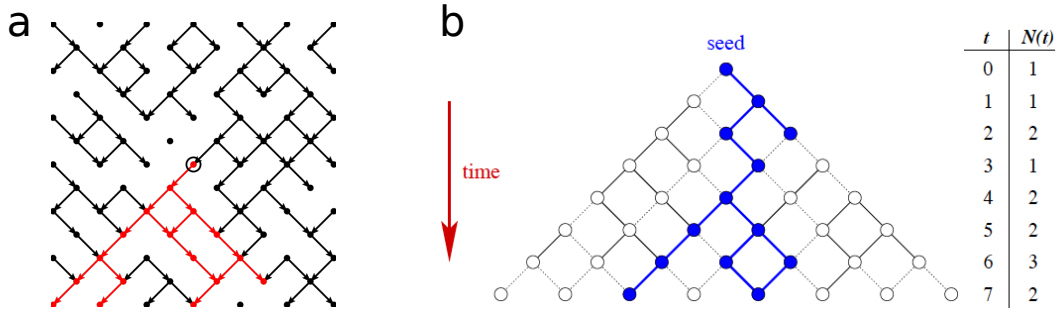


**Figure** 4.2.: **Directed bond percolation. (a)** The figure shows a configuration of open (arrows) and closed (invisible) bonds on a finite square lattice. The arrow at the right shows the preferred direction of percolation. Red arrows correspond to the percolating cluster starting from the site in the middle. Figure taken from Wikipedia- Directed Percolation. **(b)** Dynamic interpretation of bond directed percolation. The process starts with a single active site at the origin. It then evolves through a sequence of configurations along horizontal lines enumerated with $t$. The number $N(t)$ of active sites at each time $t$ is shown in the right table. Figure taken from [91]. Copyright (2008) by Canopus Academic Publishing Limited.

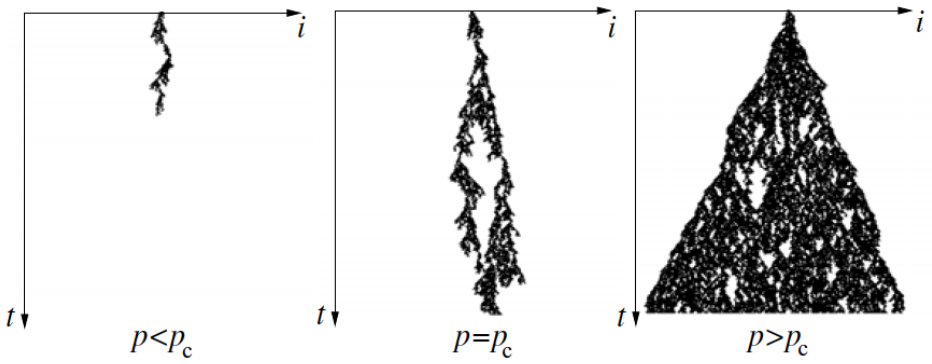


**Figure** 4.3.: **Typical DP clusters grown from a single seed.** Figure taken from [91]. Copyright (2008) by Canopus Academic Publishing Limited.

by means of simple probabilistic rules. For instance, one can implement a cellular automaton in which each active site of the previous configuration activates its nearest neighbors of the actual configuration with probability $p$. Starting from a single seed, figure 4.3 plots the generated clusters for various values of $p$. If $p$ is small, after a while there are no active sites and the thin and finite cluster is generated. If $p$ is sufficiently large, activity may spread over the entire system (percolates) within a cone-like region, generating an infinite cluster of active sites (Fig. 4.3). The transition from one to the other behaviour occurs at $p_c \approx 0.6447$.

The natural quantity to study is the average number of particles $\langle N(t) \rangle$, as shown in Fig. 4.4. Below the critical threshold, $\langle N(t) \rangle$ first increases until it crosses over to an exponential decay. Above the critical point the increase accelerates until becoming linear. At the critical

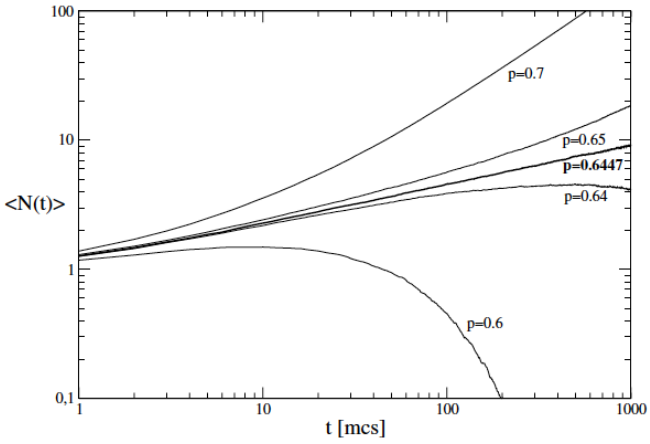


**Figure** 4.4.: **Average number of particles $\langle N(t) \rangle$ as a function of time $t$ for various percolation probabilities p**. Figure taken from [91]. Copyright (2008) by Canopus Academic Publishing Limited.

point, $\langle N(t)\rangle$ increases following a power-law, $\langle N(t)\rangle \sim t^{\theta}$, where the exponent $\theta$ is universal and not depends on the microscopic details of the different DP models but on the initial state. For instance, starting with a fully occupied lattice with $p{=}p_c$, the critical behaviour of $\langle N(t)\rangle$ is totally symmetric to the described above, but $\langle N(t)\rangle \sim t^{-\alpha}$ [91], where again $\alpha$ is universal.

Since there is no symmetry between space and time, the states above $p_c$ can be characterized by a correlation length $\xi_\perp$ and a correlation time $\xi_\parallel$. They both diverge close to the criticality as

$$\xi_\perp \sim (p - p_c)^{-\nu_\perp} \text{ and } \quad \xi_\parallel \sim (p - p_c)^{-\nu_\parallel}, \tag{4.8}$$

where the two exponents $\nu_\perp$ and $\nu_\parallel$ are generally different and the ratio $\nu_\parallel/\nu_\perp$ is the so-called *anisotropic exponent*.

Directed percolation plays an important role in various other models like epidemic spreading [93, 94], roughening transitions [95] and directed lattice animals [96], just for name a few. Nevertheless, except for a recent experiment on turbulent liquid crystals [97], there are no experiments which reliably reproduce the critical behaviour of directed percolation, especially the values for the set of critical exponents[1]. The simplicity of DP lattice models and its robust universality class, makes surprising the rareness of reliable empirical evidence, even more when phenomena like catalytic reactions [91], percolation in porous media [88] or avalanches of flowing granular matter resemble the DP dynamics [99]. Nowadays, it is an open question why experiments of DP are so difficult to perform, and most responses consider that the quenched disorder (microscopic inhomogeneities) is the fundamental factor that destroys the DP critical behaviour.

The single experiment resembling DP [97] consists of a quasi-2D layer of a nematic liquid crystals confined between two glass plates and subject to an external voltage to trigger Carr-Helfrich instability. In this way, one obtains a transition between two different turbulent states, referred to as DSM1 and DSM2, which can be easily detected by a change in the light absorption coefficient. Close to the voltage threshold $V_c$ for the appearance of DSM2, [97] found a regime of spatiotemporal intermittency (appearing as bray spots) where DSM2 plays the role of the active state and DSM1 corresponds to the absorbing state. The spots disappear spontaneously and also induce the creation of new spots nearby, spreading in just the same way as in a 2+1-dimensional contact process, i.e., a particular case of directed percolation.

[1] This is remarked upon by Grassberger in [98]: ... *"there is still no experiment where the critical behavior of DP was seen. This is a very strange situation in view of the vast and successive theoretical efforts made to understand it. Designing and performing such an experiment has thus top priority in my list of open problems."*

By using the density of DSM2 as order parameter, they estimated a non-universal threshold $V_c$ and the critical exponents $\beta$, $\alpha$ and $\nu_\perp$ with values close to the theoretical expectations. Moreover, they also support the directed percolation evidence by a quantitative test of scaling functions (see Fig. 4.5).

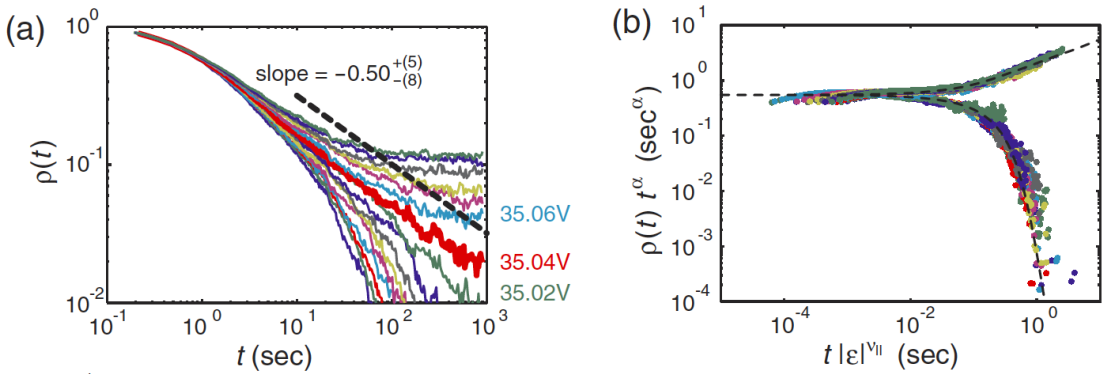


**Figure** 4.5.: **Turbulent liquid crystals. (a)** Empirical data of the temporal behaviour of the density of DMS2, $\rho(t)$, obtained by Takeuchi et al. [97]. **(b)** Data collapse of the experimental data. Both figures taken from [97]. Copyright (2007) by the American Physical Society.

# 5. Uniform Networks

Urban design has a huge impact in transportation. As the travel costs are proportional to the road lengths, the geometry of the urban street networks determines the distribution of vehicular flows which finally leads to congestion [100]. Nowadays, urban street layouts increasingly resemble to a rectangular grid, either as an inheritance of ancient urban planning styles or as product of a densification process related with modern urban concepts. Following this trend, and perhaps because its simplicity, most prominent studies on city traffic adopt square lattices [41, 101, 102]. In this chapter, we first give an overview of the principles supporting city grid planning, while taking the opportunity for reviewing the history of the hexagonal planning, an urbanism design theory very popular by the 1930's that, displaced by the *cul-de-sac* patterns, felt into oblivion. Next, we present two of the most prominent cellular automaton models for city traffic, namely: the Biham Middleton and Levine (BML) model and the Chowdhury-Schadschneider (ChSch) model. Both models are paradigms for reproducing self-organized patterns in traffic flow and jamming transitions.

## 5.1. Urban Planning Designs

### 5.1.1. The Triumph of the City Grid Plan

Despite its widespread association with modern urbanism, grid plan did in fact appeared in ancient times. Many historians contend (with some controversy) that the grid plan was properly invented in about 2154 BCE in the Indus Valley city of Mohenjo-Daro [103]. Remarkably, Mohenjo-Daro had a perfect grid-like street pattern, as precise as Manhattan, with a well organized water supply and plumbing substructure serving about 35,000 inhabitants. Such a city plan was exported to Greece by an anonymous traveler from India, and came into widespread use following the rebuilding of the Greek city of Miletus. Sacked by Persians in 494 BCE and liberated by Athens in 479 BCE, Miletus was rebuilt within a

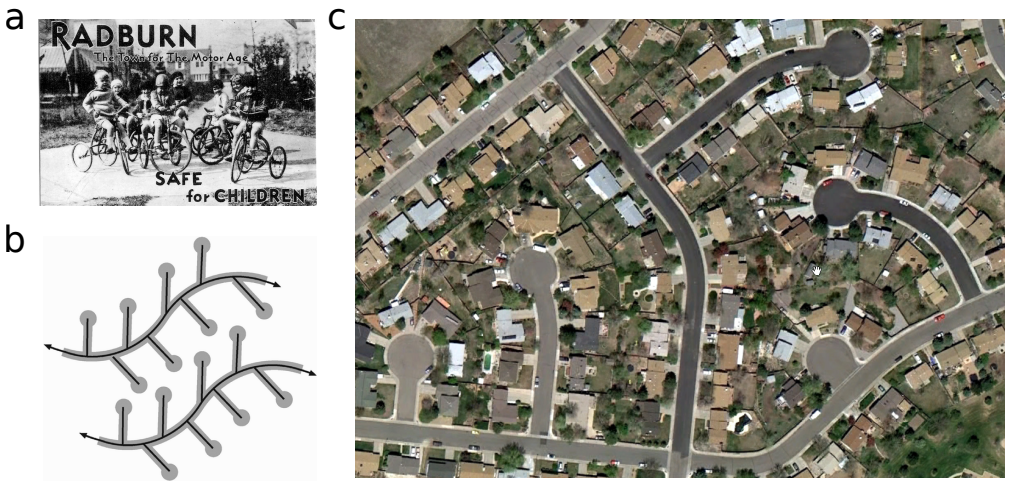


**Figure** 5.1.: **Radburn (*cul-de-sac*) urban design. (a)** Photo of the original Radburn suburb, founded in 1929. **(b)** Cul-de-sac pattern at single road level. **(c)** A typical suburban US neighborhood showing the cul-de-sac pattern. Figures taken from [106, 107].

strictly orthogonal plan. The rest of work was done by the expansion of the Roman Empire. Later, Spanish and Portuguese disseminated this urban planning concept through all Latin America [104].

In the early 20th-century the square grid was the conventional urban pattern design. Nevertheless, the emergence and rapid popularization of the automobile for personal transportation introduced new constraints: noise, excessive pavement and pedestrian safety. These new requirements found response in the Radburn[1] or *cul-de-sac* model, whose geometry adapts to the automobile, excluding traffic at the local street level and permitting good flow at the collector and arterial levels (a street hierarchy). Fig. 5.1 shows the urban street patterns generated for de *cul-de-sac* design. For the perspective of real estate developers, these network patterns were significantly cheaper in infrastructure costs as compared to the square grid plan. Since the 1960's, the *cul-de-sac* has been the dominant road network structure of suburbs in the United States, Canada, and Australia [105].

Nevertheless, in the 1980's, society started to face increasingly traffic congestions and fatal accidents in highways. Thus, new urbanists started to understand about the relative advantages of going back to the old designs, the grid plan. What if such patterns (with streets constantly intersecting with each other) actually force people to drive slower and pay more attention? Lower speed means fewer deadly accidents. More connectivity disperses traffic, increases walkability (less vehicle usage) and, thus, reduces congestion [108]. Moreover, large

[1]The name comes from the pioneering suburb of Radburn, N.J., in 1929

population densities make a more efficient use of services and resource. These principles allowed the final triumph of the grid plan and were the end of the road of the *cul-de-sac*. While there were no conclusive (quantitative) studies supporting those principles, other urban design alternatives fell quickly in the oblivion, e.g., the ideas from the hexagonal planning school.

### 5.1.2. Honeycomb Planning

Honeycomb planning is perhaps the most fascinating part of the story. By 1930, it was a leading theoretical alternative to the rectangular grid for residential subdivisions. Urban designers such as Comey, Charles Lamb, Noulan Cauchon and Barry Parker proposed and demonstrated the economic advantages and efficient land use generated by hexagonal plans. For an unique and charming review of the the various hexagonal planning schemes and their designers see [109].

Interestingly, Cauchon's planning insights are based on scientific approaches. He combined concepts of urban design with his experience as engineer to develop his own theory of honeycomb planning. One of the most visionary Cauchon's insight is related with the accidents on the intersections. He noticed that a three-legs intersection is theoretically superior to a four-legs one, because the 120° angle of the first one improves sight lines, in comparison with the 180° of the second one. Fig. 5.2 shows that the three-legs intersection has only three potential collision points, compared with 16 of a four-legs intersection. Since a pure honeycomb network would only contain three-legs intersections, Cauchon suggested [110, 111] it could be a less complex street network.

Cauchon unveiled his basic honeycomb plan at the 1925 International Town, City and Regional Planning Conference in New York [110, 112, 113]. It included a detailed analysis demonstrating the honeycomb's superiority over the rectangular grid for residential servicing (less roads and more green areas), traffic flow and even public health benefits from better sunlight[2] (see Fig 5.3). Cauchon promoted his theory widely, on a scale comparable with that of Le Corbusier's Ville Contemporaine (1922). Despite the great promotion of his complete plan named *Hexagonopolis* and the strong technical arguments to defend it, not a single hexagon had been built. It was defeated by the powerful *cul-de-sac*. In North America, President Herbert C. Hoover himself discredited hexagonal layouts and adopted the model of *cul-de-sac* as the lineaments of the urban planning in the whole country [114]. Something

[2]Since all rooms in a honeycomb grid pointed due north would receive direct sunlight every day.

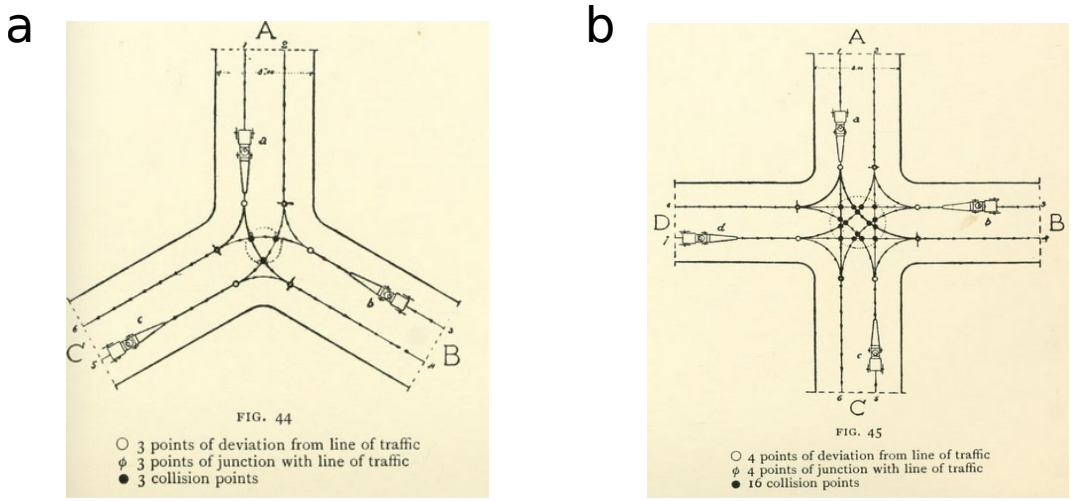


**Figure** 5.2.: **Traffic collision points for intersections types. Comparison between (a) three- and (b) four- legs intersections.** Source I. Triggs, 1909 [111].

similar happened in the rest of the world. More recently, Architect Mazlin Ghazali, from Malasya, has developed a design concept called *tessellation planning*, which in some versions combines hexagons with *cul-de-sac*. The neighbourhood is build by hexagonal blocks with *cul-de-sac* streets inside. The street network connecting the blocks is a honeycomb. This concept has been used to design projects in Kuantan and Singei Petani[3].

Among some frivolous disadvantages exposed against this model were that hexagonal blocks may have looked too unusual. How would be streets named and numbered on a hexagonal plan or how would strangers navigate the streets of Hexagonopolis were some frequent questions. But mathematics gave trivial solutions. Perhaps, people did not like the triangular lots caused by the inside corners of hexagonal blocks. More seriously, urban planners remark that the advantages of hexagonal planning could also be obtained in the *cul-de-sac* and loops scheme, through careful design. Three-way intersections were possible between a *cul-de-sac* and a collector road, while four-way connections between collector and arterial roads could be controlled by traffic signals. A wide angle of view at intersections could be provided by regulations which required larger corner lots with sight triangles. On the cost of infrastructure, the analysts showed (eluding the numbers) that the two options were close, but there is no a conclusive study supported by realistic calculations.

[3]See http://tessellar.blogspot.com.co/

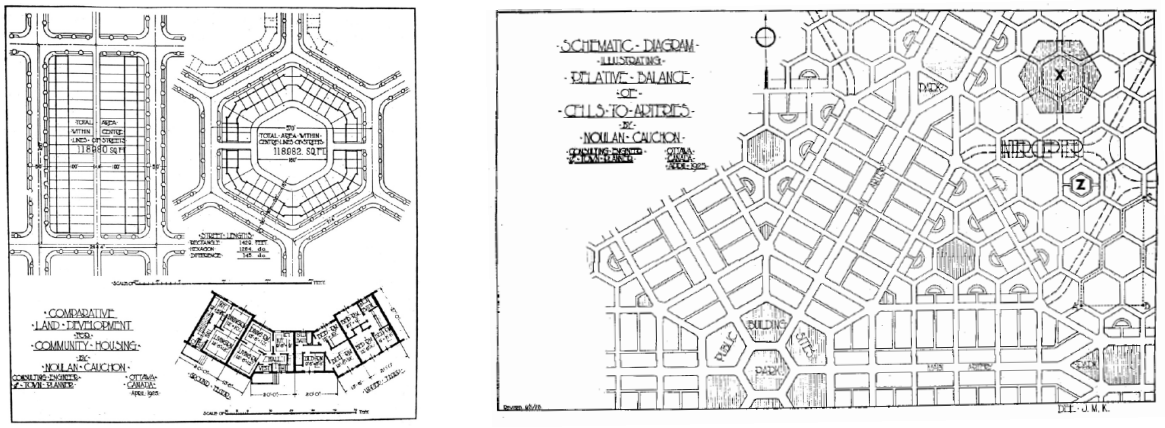


**Figure** 5.3.: **Diagrams of honeycomb designs elaborated by Noulan Cauchon. (left)** Honeycomb block, 1925, with which he demonstrated honeycomb's superiority over the rectangular grid. **(right)** Cauchon promoted his ideas widely, Hexagonopolis (1927), a design which was very popular in to be featured in Canada's largest-circulation magazine. Both diagrams are taken from [109]. Copyright (2000) by Taylor & Francis Ltd.

## 5.2. Modeling the City Traffic with Cellular Automata Models

### 5.2.1. BML traffic model

The Biham-Middleton-Levine (BML) model [16] is, perhaps, the simplest traffic cellular automaton able to exhibit self-organization, pattern formation and phase transitions on a network scale [16–18, 115]. The model considers two types of cars: east-bound (yellow) and north-bound (black), moving on a two-dimensional square lattice with periodic boundary conditions. Each lattice site is in one of three states: empty, occupied by a yellow car, or occupied by a black one. The cars are initially randomly distributed over the lattice sites with spatial density $\rho$ (usually taken to be the same, $\rho/2$, for both north- and eastbound cars). The fully deterministic dynamics is as follows: On even (odd) steps, all eastbound (northbound) cars synchronously attempt to advance one lattice site toward the east (north). If the site eastward (northward) of a car is currently empty, it advances. Otherwise, it remains stationary. The system exhibits, therefore, a preferred north-east direction for the flux. Essentially, this model is the generalization to 2D of the CA 184 rule of Wolfram [116, 117].

For more than a decade, it was believed that at a certain critical car density, $\rho_c$, the system

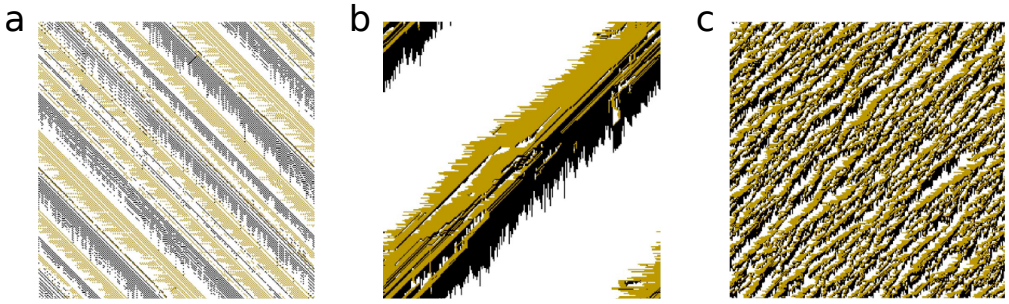


**Figure** 5.4.: **Typical configurations observed for the BML model on an $L \times L$ lattice of size $L$=256.** (a) The free flow state at low density phase. All particles advance during each time, with average speed $v$=1. Ordered stripes of alternating east- and northbound cars appears and their width increases, on average, with density $\rho$. (b) A fully jammed configuration, consisting of one global jam. Note the jam length $\sqrt{2}L$ is larger than the system size. (c) A high density ($\rho \geq 0.50$), random jams configuration. Taken from [19]. Copyright (2005) by The American Physical Society.

exhibits what seems to be a first order phase transition between two phases: a free-flowing phase, where all cars move freely at all time steps (the average velocity of cars $v$=1) and a completely jamming phase, where no car moves at all ($v$=0). In the jammed phase, the vehicles organize into a single jam which becomes more fractal with increasing densities. Then, analyzing the spatial diagonal correlations [115] and the backbones of the clusters structure [17], two jammed phases can be distinguished: the one global jam and the random-jam configurations. Typical configurations of the BML model below and above the transition density are shown in Fig. 5.4. The value of $\rho_c$ decreases with increasing system size, possibly reaching the value $\rho_c$=0 as the system size approaches infinity. Then, it was thought that the BML model would be similar to other well known systems in statistical physics exhibiting phase transitions, e.g., percolation.

Surprisingly, all these conventional beliefs started being reconsidered, since W.K. Yung [21] and R. M. D'Souza [19, 20] realized the existence of intermediate stable phases where free-flowing and jamming phases coexist(see Fig. 5.5). The structure of these states is highly regular, with jams' wavefronts moving through freely flowing traffic in a wide density region, and the value of the average velocity ($0<v<1$) is extremely sensitive to the aspect ratio of the underlying lattice [118]. Thus, instead of a phase transition as a function of car density, the system would exhibit two bifurcation points, limiting a region where intermediate phases would coexist between the two conventional phases above. Even though these states have been described and their asymptotic speeds have been predicted [19,118], the exact locations of the bifurcation points are very difficult to determine and no one knows what truly happens as the system size goes to infinity. Moreover, the origin of the intermediate states remain as a unsolved puzzle.

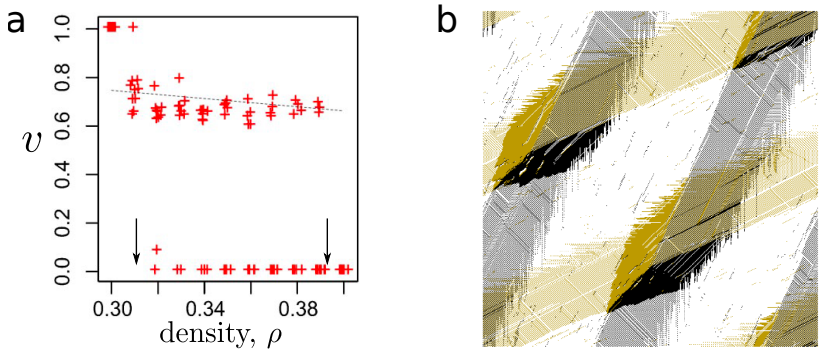


**Figure** 5.5.: **Intermediate stable phases, where jams and freely flowing traffic coexist in the Biham-Middleton-Levine traffic model.** (a) The average velocity for each individual realization $v$ versus the density $\rho$ for a realization. One can observes the well defined intermediate phases. Black arrows mark the bifurcation points. (b) Example of an intermediate state. Note that there are many disordered, random cars in the space between the bands. Figures are taken from [19]. Copyright (2005) by The American Physical Society.

Some extensions of the BML model have been suggested to take into account several realistic features of traffic in cities. Among them are open boundary conditions [119], four-directional traffic [120], jam-avoiding turns [121–123], faulty traffic lights [124], stagnant streets [125] and even 3D implementations [126]. It has also been reported that the intermediate phase disappears when some kind of randomization is introduced [20,127,128], or the traffic periods for the two cars are increased [129]. In contrast, the role played by the network topology has been overlooked and, there are very few studies considering the BML model on different lattices: square lattice generalizations with extra sites in the bonds [130, 131] and triangular lattices where three species of cars are considered [132, 133]. In all cases a more complex behaviour with different jammed phases is observed. A comprehensive overview of these extensions is given by Chowdhury et al. [134].

Although the BML model oversimplifies the city traffic in a way that does not directly resemble an urban network (i.e., with cars at the nodes and not at the links), much extensive research on flux an collective behaviour has been based on it, not just for car traffic (as we show above) but also for pedestrians [135,136] and information packages on the Internet [137]. Currently there are over three-hundred citations in the scientific literature referencing BML and its phase transition.

### 5.2.2. Chowdhury-Schadschneider Model (ChSch)

As the BML neglects completely the vehicle dynamics along road segments, it is not capable to answer questions like how far traffic lights could be optimized or how it is the formation of queues due to that traffic lights. In this context, the Chowdhury-Schadschneider (ChSch) [11] combines the basic ideas from the BML model for city traffic and the Nagel-Schreckenberg (NaSch) model for highway traffic.

The street network is a square lattice with $N$ north-bound and $N$ east-bound streets (see Fig. 5.6). Each link is divided into $D-1$ cells, representing single car-sized cells between each pair of intersections. Moreover, the traffic lights alternate periodically at regular intervals $T > 1$ (instead of every time-step as in the BML) and, also, all of them are synchronized, i.e., they are green for the east-bound vehicles and red for the north-bound vehicles, and conversely. Each vehicle moves forward in accordance with the NaSch rules independently of the traffic light state, even when the distance to the traffic light is smaller than the velocity. In that case, the car will keep on moving for green signals. Otherwise, it has to stop immediately in front of the red signal. In summary, each time step the system state is updated by applying in parallel the following rules on all cars.

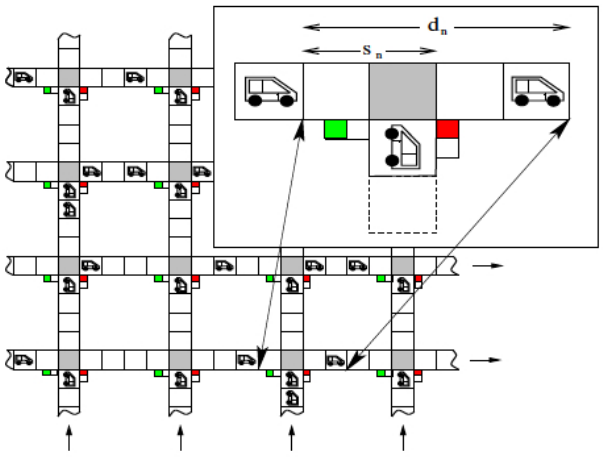


**Figure** 5.6.: **Snapshot of the ChSch model.** The number of intersections in the square network is set to $N \times N$, the distance between neighbohring intersections is $D$ and the length of the streets between them is equal to $D-1$=4. Similarly to the BML model, vehicles can only move from west to east on the horizontal streets or from south to north on the vertical ones. The inset is the zoom in of a horizontal road segment. As the traffic lights are synchronized, vehicles moving from south to north have to wait until all traffic lights switch. Taken from [27]. Copyright (2003) by R. Barlovic.

- Step 1: *Acceleration*:
  $v_n \rightarrow min(v_n + 1, v_{max})$

- Step 2: *Braking due to the other vehicles or red traffic lights:*

  - Case 1: The signal is red in front of the n-th vehicle:
    $v_n \rightarrow min(v_n, d_n - 1, s_n - 1)$

  - Case 2: The signal is green in front of the n-th vehicle:
    If the next two cells directly behind the intersection are occupied
    $v_n \rightarrow min(v_n, d_n - 1, s_n - 1)$
    else
    $v_n \rightarrow min(v_n, d_n - 1)$

- Step 3:*Randomization:*
  With probability p, $v_n \rightarrow max(v_n - 1, 0)$

- Step 4: *Movement.*
  $x_n = x_n + v_n$

Note that *Case 2* of *Step 2* allows a driver to occupy an intersection only if he can leave it again in the next step. This rule avoids the transition into a completely traffic gridlock (as the BML model does), providing a more detailed description of city traffic. Concerning to the jam dynamics, jams may be induced at crossings due to either the red traffic lights or the dynamics itself, as an emergent behaviour. Once they are formed, these jams move through the system according to the model rules and have an immense impact on the overall network flow. Thus, a dynamical phase transition can be observed between free flow and traffic breakdown. Since the signal periods play a relevant role in that transition, most studies based in this model have focused on implementing different traffic light strategies [27], i.e., unsynchronized or a *green wave*, across the whole network, providing insights transferable to realistic scenarios.

## 5.3. Summary and Criticism

The BML model has served as a theoretical underpinning for approaching traffic modelling from physics. Despite the extensive modern studies of traffic flow based on it, a theoretical understanding of the intermediate states is still missing. In the same way, there is a gap in the literature regarding the effect of the topology on the model's behaviour, where a honeycomb lattice seems to be a tantalizing option. Regarding theses issues, we present some results in following two chapters.

The more complete microscopic dynamics used in the ChSch model includes real-time (online) traffic counts, allowing to simulate more realistic scenarios. Due to the interest in traffic management solutions, various software packages based on CA were developed in the early 2000's with the focus on realistic real-time traffic on either highway networks or specific parts of city street networks. Some among them are PAMINA [138], TRANSIMS [139] and BAB-NRW [140]. Nevertheless, if one wants to apply these models to transportation planning, much more than just microsimulations is required. One needs data describing the demand (i.e., reliable origin-destination matrices), a procedure to solve the assignment problem (i.e., how to chose the transportation mode), and also real data for comparison. In addition, one needs to understand how the congestion emerges on a city scale. Fifteen years ago, it was unlikely to study city traffic systematically. A decade later, with the rise of Big Data, we can go back and look at the problem. In the final chapter of this work, we present some own developments on this topic.

# 6. The nature of the intermediate states in the BML traffic model

The Biham-Middleton-Levine (BML) model [16], as described in the previous section, is one of the most fundamental models for the study of traffic congestion in a city network. Nevertheless, some aspects of its behaviour remain unknown. As we mentioned in the previous chapter, W.K. Yung [21] and R. M. D'Souza [19, 20] realized the existence of intermediate stable phases where free-flowing and jamming phases coexist. Thus, instead of a phase transition as a function of car density, the system would exhibit two bifurcation points, limiting a region where intermediate phases would coexist between the two conventional phases above. Even though these states have been described and their asymptotic speeds have been predicted [19,118], the exact locations of the bifurcation points are very difficult to determine, and no one knows what truly happens as the system size goes to infinity. Moreover, the origin of the intermediate states remained, until now, as a unsolved puzzle.

To solve the puzzle, we focus on the clear existence of a preferred direction in the model dynamics. Most previous studies have overlooked this feature, despite - as we will show - - it is the key for unraveling the intriguing intermediate states of the BML model. The presence of anisotropy has been fundamental in the analysis of force networks in granular matter [141, 142] and flocking in collective animal behavior [143], and classical theoretical models with this feature are the next-nearest-neighbor Ising model (ANNNI) [144] and the driven lattice gas model [145]. Such anisotropy should be naturally reflected in the phase transition of BML, making it more akin to the anisotropic equivalent in percolation: directed percolation (DP) [146,147]. By performing a direct anisotropic scaling analysis on the BML model phase transition [148, 149], we will show in this chapter that the jamming process behaves distinctively as two separated phase transitions along different directions, namely, whether the system is longer in the direction of traffic flow (longitudinal system) or in the transversal direction (transversal system). Most results shown here were published in [2].

## 6.1. Studying the anisotropy

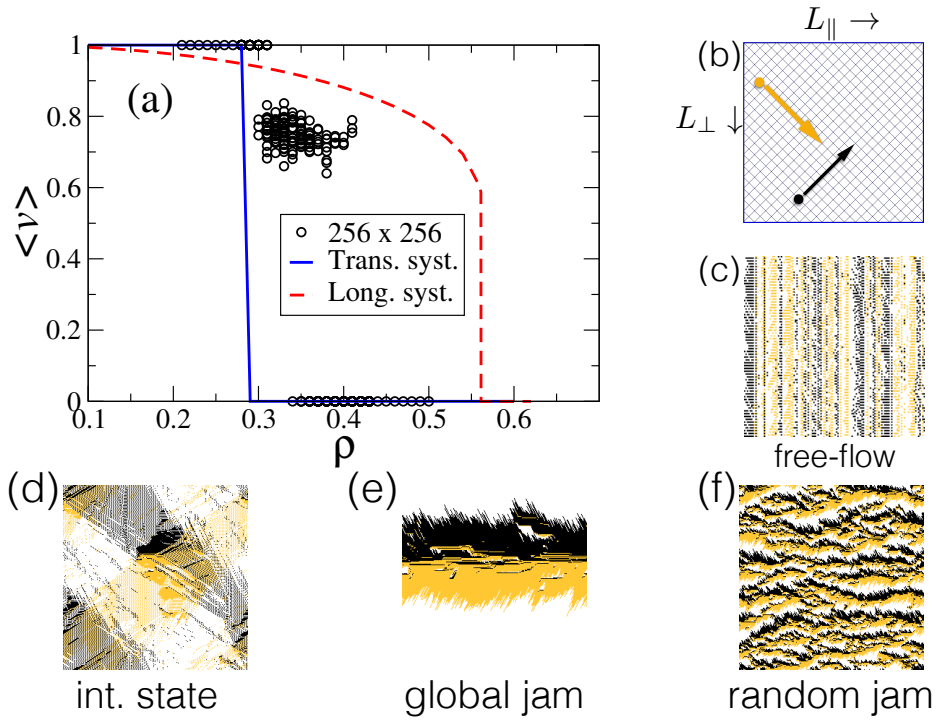


**Figure** 6.1.: **Typical behavior of the Biham-Middleton-Levine model. (a)** Average velocity $\langle v \rangle$ vs density $\rho$ (circles) for a BML model on a 45$^o$-rotated 256 $\times$ 256 lattice (as depicted in **(b)**, with east-bound cars (yellow - light gray) and north-bound cars (black)). The mean-field approach for longitudinal systems (dashed red line) and the numerical prediction for an infinite transverse system (blue solid line) are also included for comparison. Typical configurations for free flow **(c)**, intermediate states **(d)**, one global jam **(e)** and random jams **(f)** are also included.

As a first step, we explicitly rotated 45 degrees the lattice, so we could control the system lengths along the longitudinal ($L_\parallel$) and transversal ($L_\perp$) directions to the car flow. Although this rotation changes the boundary conditions, the system still exhibits the same three phases observed in the original BML model (see Fig.6.1).

In anisotropic systems (Chap. 4), clusters show different correlation lengths along the longitudinal and transversal directions, $\xi_\parallel$ and $\xi_\perp$, respectively, which scale with different exponents as $\xi_\parallel \sim (\rho - \rho_c)^{-\nu_\parallel}$ and $\xi_\perp \sim (\rho - \rho_c)^{-\nu_\perp}$ [146, 148]. An anisotropy exponent, relating the different scaling of the two correlation lengths, is defined as the ratio $\theta = \frac{\nu_\parallel}{\nu_\perp}$. According to [148–150], when the longitudinal and transversal lengths are related by the constraint $L_\perp \sim L_\parallel^{\frac{1}{\theta}}$, the system behaves as it were effectively isotropic, and standard finite-size scaling (FSS) theory applies again for all percolation quantities, just in terms of the length scale $L_\parallel$.

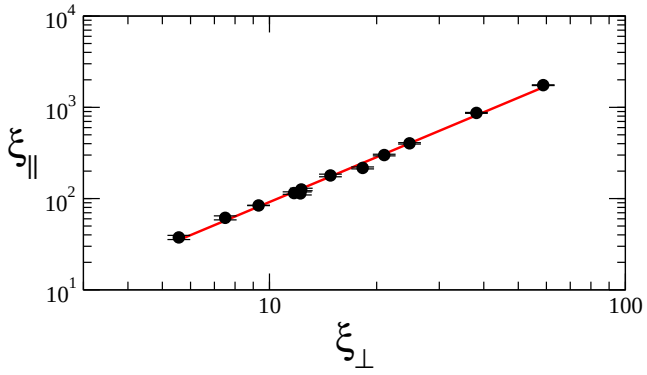


**Figure** 6.2.: **Correlation lenghts.** Longitudinal $\xi_\parallel$ and transversal $\xi_\perp$ correlation lengths from final configurations at densities $\rho$ in the range [0.49-0.54] for square lattices of different sizes. The power-law fit gives $\theta$=1.64(3) for the anisotropy exponent.

Especially the transition width and the percolation threshold, (both obtained by fitting the transition curve with an error function[1]) scale like

$$\Delta(L_\parallel, L_\parallel^{\frac{1}{\theta}}) \sim L_\parallel^{-\frac{1}{\nu_\parallel}} \text{ and } \left|\rho_c - \left\langle \rho_c(L_\parallel, L_\parallel^{\frac{1}{\theta}})\right\rangle\right| \sim L_\parallel^{-\frac{1}{\nu_\parallel}}. \tag{6.1}$$

The symbol $\langle\rangle$ denotes an average over final jammed configurations starting from different random initial conditions. The exponent $\theta$ can be estimated numerically from the fact that, close to the critical point, the two correlations lengths must be related by $\xi_\parallel \sim \xi_\perp^\theta$. With this theory in mind, let us define the parallel (perpendicular) spatial correlation function [115] as

$$G_{\parallel(\perp)}(\vec{r'}) = \frac{1}{N}\left\langle \sum_{\vec{r}} \sigma(\vec{r})\cdot\sigma(\vec{r}+\vec{r'})\right\rangle \ , \tag{6.2}$$

where $\sigma(\vec{x})$=1(0) if the site with position $\vec{x}$ is occupied(empty), $N$ is the total number of cars and $\vec{r'}$ is a vector in the direction $\parallel$ ($\perp$) one want to compute the correlation function along. The correlation functions are fitted with exponentials $G_{\parallel(\perp)} \propto \exp(-r/\xi_{\parallel(\perp)})$ to estimate $\xi_{\parallel(\perp)}$.

Figure 6.2 presents the correlations lengths computed from final configurations of the original BML model for different square lattice sizes at densities close to the threshold transition, averaging over 50 configurations for each point. A linear regression yields an estimate of the anisotropy exponent $\theta$=1.64 $\pm$ 0.03 (here and everywhere in this chapter the error bars are $1\sigma$).

[1]The values of $\rho_c$ and $\Delta(L)$ were determined by fitting the transition curve with a complementary error function $\frac{a}{2}\times \text{erfc}\left[\frac{\rho_c(L)-\rho}{\Delta(L)}\right]$. As the transition on transversal systems occurs between $v$=1 and $v$=0, then $a$=1. For the longitudinal case $a$=0.71, which corresponds to the average speed just before the transition (see Fig. 6.3 (a)).

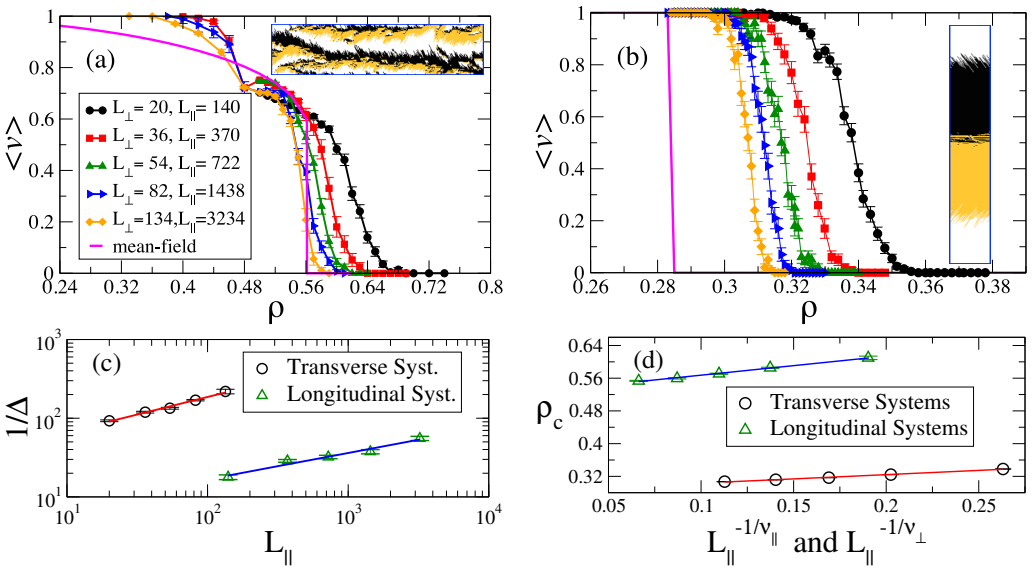


**Figure** 6.3.: **Finite-size scaling analysis for the phase transition of both longitudinal and transversal systems. (a)** Transition curves for several longitudinal systems, including the mean-field prediction (magenta solid line) and a typical configuration for the jammed phase (inset). **(b)** Transition curves for several transversal systems (sizes as in **(a)**, but with $L_\parallel$ and $L_\perp$ interchanged), including the asymptotic limit (magenta solid line) obtained from the FSS analysis. **(c)** Scaling of the transition width $\Delta(L_\parallel)$ for both cases, giving $\nu_\parallel$=3.0(3) and $\nu_\perp$=1.8(2). **(d)** Scaling of the finite critical density gives $\rho_{c_\parallel}$=0.521(2) and $\rho_{c_\perp}$=0.283(2). All systems were simulated for at least $1.5 \times 10^6$ time steps or until convergence ($v$=0 or $v$=1).

## 6.2. Transversal and Longitudinal Phase Transitions

With the exponent $\theta$ in hand, we studied the phase transition for both longitudinal and transversal systems. Longitudinal ones ran on lattices with sizes $L_\parallel^{\frac{1}{\theta}} \times L_\parallel$. Figure 6.3(a) shows that the average velocity begins to decrease smoothly with increasing $\rho$ until the abrupt onset of full jamming ($v$=0) at a certain $\rho_{c_\parallel}$. Right there, an approximately uniform distribution of jams spans through the whole system (Fig. 6.3(a) inset). With Eq.(7.3) in mind, the FSS analysis (Fig. 6.3(c) and (d)) gives $\rho_{c_\parallel}$=0.521(2) and $\nu_\parallel$=3.0(3), which would imply $\nu_\perp$=1.8(2). Quite differently, transversal systems (i.e., lattices with $L_\parallel \times L_\parallel^{\frac{1}{\theta}}$) in the gridlock phase show a single and well localized jam on an empty background (Fig. 6.3(b)). These systems exhibit a sharp phase transition between free-flow and a completely gridlock phase, but at a lower density $\rho_{c_\perp}$. The FSS analysis (also in Fig. 6.3(c) and (d)) gives $\rho_{c_\perp}$=0.283(1) and $\nu_\perp$=2.2(1), in agreement with the previous results. Hence, the intermediate states in square lattices [19] emerge just as a consequence of the combination of these two phase transitions (Fig. 6.3(a) and (b)). At intermediate densities $\rho_{c_\perp} < \rho < \rho_{c_\parallel}$, transversal

jams are already formed, but the system is not narrow enough to completely block the cars; instead, they manage to escape from the jam, only to reach a new one. Fig. 6.3(a) also shows a dip at a density $\rho \simeq 0.48$, below the transition point. An analysis of the time series for the average velocity shows that the system has not stabilized yet, nor for simulations $10\times$ longer, but the point rises monotonically as the simulation time increases. Thus, it can be an effect of an extremely large relaxation time at this density.

## 6.3. Mean-field Treatment

The critical densities for both longitudinal and traverse transitions can be approximated by using a mean-field analysis, inspired by [151]. Consider the mean velocity of yellow cars (by symmetry, the reasoning is also valid for black cars). A yellow car will stop either because it is crossed by a black car or because it queues behind another yellow car. At a random initial configuration, the probability that a car is crossed or queued is $\rho^2$, that is, at the beginning of the simulation the proportion of stopped cars $p_{\rm stop}$ must be equal to $\rho$. Let us define $c_{\rightarrow\uparrow}$ ($c_{\rightarrow\rightarrow}$) as the proportion of stopped cars that are crossed (queued). In previous works [151, 152], it has been assumed that $c_{\rightarrow\uparrow}$=$c_{\rightarrow\rightarrow}$=0.5, but we will see that this is not the case. If $p_{\rm stop} \sim \rho$ for some time steps, the probability a cell to be occupied by a stopped crossed (queued) car will be $c_{\rightarrow\uparrow}\rho^2$($c_{\rightarrow\rightarrow}\rho^2$). Since black cars spend on average a time $1/v$ on a site, they will reduce the speed of yellow cars from unity by $c_{\rightarrow\uparrow}\rho^2/v$. Similarly, the extra amount of time that a yellow car stays on a site will be given by $\frac{1}{v}-1$, reducing the average speed by $c_{\rightarrow\rightarrow}\rho^2(\frac{1}{v}-1)$. Hence, a self-consistency equation for the average speed $v$ will be

$$v = 1 - \frac{c_{\rightarrow\uparrow}\rho^2}{v} - c_{\rightarrow\rightarrow}\rho^2\left(\frac{1}{v}-1\right) \ , \tag{6.3}$$

which gives $\rho_c$ as the critical density at which the equation ceases to give a real solution.

Consider longitudinal systems first, where an uniform distribution of longitudinal jams arise. Before solving Eq.(7.4), let us study the evolution on time of the quantities involved. On one hand, Fig. 6.4(a) shows the time evolution of $p_{\rm stop}$ for different values of the car density in a longitudinal system. At start, $p_{\rm stop}$=$\rho$ for every density, as expected. Later on, $p_{\rm stop}$ declines (grows) for low (high) densities, and this trend changes near the critical density $\rho_c$. Actually, $p_{\rm stop}$ after one time step equals $\rho$ for $\rho \simeq 0.57$ in a large system (Fig. 6.4(b)). On the other hand, $c_{\rightarrow\uparrow}$=$c_{\rightarrow\rightarrow}$=0.5 only at start, but after just one time step they change to $c_{\rightarrow\uparrow}\sim$0.600(5) and $c_{\rightarrow\rightarrow}\sim$0.400(5), remaining there for some time steps (Fig. 6.4(c)). By replacing these two values into Eq.(7.4), the mean-field approach predicts a critical density $\rho_{\parallel}$=0.563(5), in

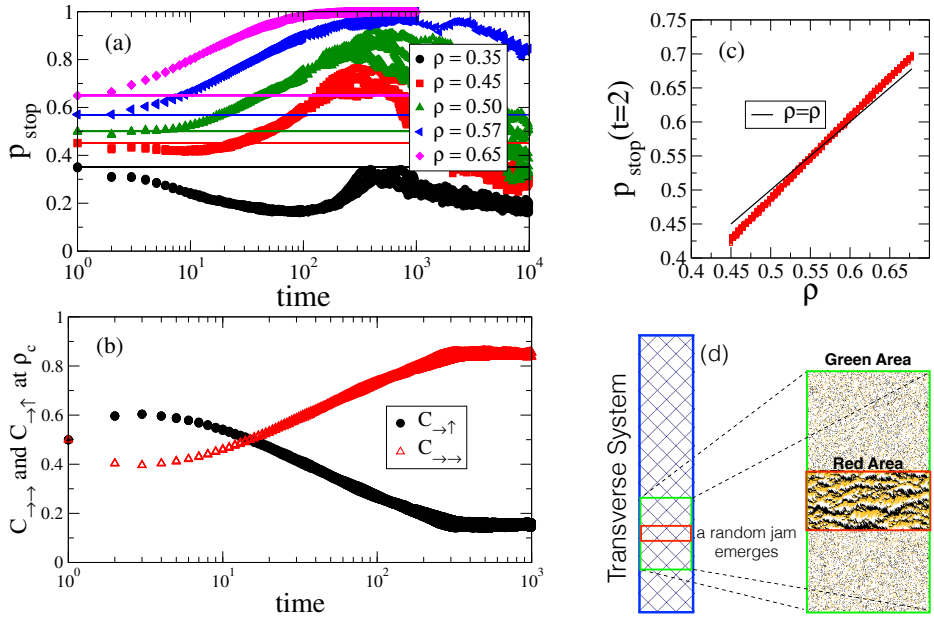


**Figure** 6.4.: **Time evolution of (a) the fraction of stopped cars $p_{\text{stop}}$ and (b) of the fraction of crossed ($c_{\rightarrow\uparrow}$) and queued ($c_{\rightarrow\rightarrow}$) stopped cars in a $1438 \times 82$ longitudinal system.** The value of $p_{\text{stop}}$ after one time step for several densities is shown in **(c)**. **(d)** Schematic representation of the jamming process for transversal systems.

agreement with the value obtained from both finite-size scaling and the change in behaviour of $p_{stop}$ described above.

Transversal systems, in contrast, collapse into a single big jam. Thus, the previous reasoning is impractical here, because the local density becomes inhomogeneous during the collapse: increasing in the vicinity of the growing jam and dropping to zero elsewhere. Let us consider that the density at start is low enough to assume that all cars are moving. At a certain evolution time the cars have condensed into a thinner region (red area in Fig. 6.4(d)) of area $A_{\text{red}}$, where the density has reached the critical value $\rho_{c_{\parallel}}$ for longitudinal systems. All cars in this region come from a larger region of area $A_{\text{green}}$ in the initial configuration (green area in Fig. 6.4(d)). Let us assume that the red area is a fraction of the green one equals to the fraction of cars that have stopped, $A_{\text{red}}/A_{\text{green}}=p_{\text{stop}}$. Because the number of cars does not change, at the critical density

$$\rho_{green} = \rho_{red}\frac{A_{red}}{A_{green}} = \rho_{c_{\parallel}}^2 \quad , \tag{6.4}$$

where we have used the result that $p_{\text{stop}}=\rho$ at the critical density for longitudinal systems. Then, the critical density for transversal systems will be $\rho_{c_{\perp}}=\rho_{c_{\parallel}}^2=0.271(3)$, which approximates quite well the value $\rho_{c_{\perp}}=0.283(2)$ from the simulations (Fig. 7.3(d)).

The values for $c_{\rightarrow\rightarrow}$ and $c_{\rightarrow\uparrow}$ after one time step can also be estimated from the scaling analysis. Consider a typical jam (as the one in Fig. 7.3(a)). It consists of two sets of queues, east-bound (yellow - light gray) and north-bound (black), intersecting along a longitudinal curve. Crossed cars localize on this intersection, and its number is proportional to $L_{\parallel} \propto L_{\perp}^{\theta}$. Queued cars fill the whole jam, and its number is proportional to the jam's area (i.e., to $L_{\parallel} \times L_{\perp}$). Thus, $c_{\rightarrow\uparrow} \propto L_{\perp}^{\theta}$ and $c_{\rightarrow\rightarrow} \propto L_{\perp}^{\theta+1} \propto c_{\rightarrow\uparrow}^{\frac{\theta+1}{\theta}}$. Replacing into $c_{\rightarrow\rightarrow} + c_{\rightarrow\uparrow}=1$, they give $c_{\rightarrow\uparrow}=0.582(1)$ and $c_{\rightarrow\rightarrow}=0.418(1)$, very close to the simulation results. Using these values in the mean-field equation gives $\rho_{\parallel}=0.567(2)$, also close to the simulations.

Taken together, our results suggest that the puzzling intermediate states in the BML model on square lattices are, actually, a consequence of the system's anisotropy, which produces two different phase transitions: one for transverse systems, with $\rho_{c_{\perp}}=0.283(1)$, and another for longitudinal ones, with $\rho_{c_{\perp}}=0.521(1)$. Indeed, the first critical density corresponds with the lower bifurcation point on square lattices, reported at $\rho=0.315$ [19], contradicting the general believe that this would go to zero for infinite systems; similarly, the second critical density perfectly matches with the value of $\rho=0.52$ reported as the transition point between self-organized jams and random jams [17, 115] within the conventional understanding of the original BML model. The asymptotic limit of the curves from simulations on transverse systems (blue solid line in Fig. 6.1(a)) and the mean-field curve for longitudinal systems (Eq. 7.4) and dashed red line in Fig. 6.1(a)) perfectly enclose the zone of intermediate states. In fact, the structure itself of the intermediate states can also be explained if one transition has taken place, but not the other. Fig. 6.1(d) shows how an incipient jam with a similar structure to those of transversal systems (Fig. 7.3(b) inset) begins to form, but it not succeed to block everything, because the system is too width. The cars leaving the jam in both directions create bands of yellow (light gray) and black stripes. These bands will cross to each other to form another incipient global jam and so on, establishing the distinctive periodical structure of such intermediate states.

## 6.4. Discussion

Despite having studied the critical features of the BML phase transitions with the DP formalism, the obtained critical exponents are not compatible with the universality class of the directed percolation. Instead, the critical behaviour here coincides with the reported for the parity-conserving universality class (PC) [146, 147]. The origin of this relationship remains as an open question for future research.

By finding the origin of the intermediate states of the BML model, we have built a very complete description of such a fundamental model for traffic flow, illustrating at the same time the power of the finite-size scaling analysis for anisotropic systems, where the BML model seems to be a paradigmatic example. Because there are very few simple theoretical models exhibiting scaling anisotropy (for instance the next-nearest-neighbor Ising model (ANNNI) [144] and the driven lattice gas model [145]), showing that the BML is one of these systems is a remarkable contribution for the study of anisotropic systems. We look forward to see many future uses of BML as a paradigmatic example of such systems.

Although the BML model oversimplifies the city traffic in a way that does not directly resemble an urban network (i.e., with cars at the nodes and not at the links), the model allow us to show the relevance of the anisotropy on jamming processes. Since the anisotropy is inherent to real traffic demand, e.g., commuting to work on the morning peak hour, our results give some insights into the mechanisms leading congestion. In the same way, the connection between this traffic model and the DP formalism suggests the possibility of studying the urban traffic phenomena from the non-equilibrium statistical physics perspective.

# 7. Honeycomb cities

As cities turn denser, urban networks tend to adopt a squared-lattice shape [153], and many traditional urban planning styles, like the one that spaniards and portuguese disseminated through all Latin America, are grounded on such square patterns [104]. Following this trend, most prominent studies on city traffic adopt square lattices [41, 101, 102]. Despite modern urban planners claim that this design favors connectivity, the question if a square design optimizes traffic flow has not being studied systematically. In contrast, Nature usually opts for other alternatives. Hexagonal structures in two dimensions are present in cellular tissues [154, 155], bee honeycombs [156] and soap bubbles [157, 158]. Such patterns arise by capillary forces that minimizing surface energy on a fixed area [159]. Inspired by Nature, humans have also implemented hexagonal tesselations in a wide range of disciplines, including structured materials [160, 161], wireless networks [162], computer graphics [163]. However, in the realm of the urban design, street patterns based upon hexagonal blocks are just a theoretical alternative which has fallen into oblivion with almost no practical applications (see Section 5.1.2 and refs. therein), but hiding possible unexplored solutions for the overwhelming problem of traffic flow in modern cities.

Regarding the BML model, the role played by the network topology has been overlooked. There are very few studies considering the BML model on different lattices: square lattice generalizations with extra sites in the bonds [130, 131] and triangular lattices where three species of cars are considered [132,133]. In all cases a more complex behaviour with different jammed phases is observed, but the transition has not been characterized. In this chapter, we test the BML traffic model [16] on honeycomb lattices. The intention is to explore if using a different lattice affects the jamming transition and, eventually, when a honeycomb lattice offers a better performance than the square one. The results discussed here will appear in the already submitted paper [3].

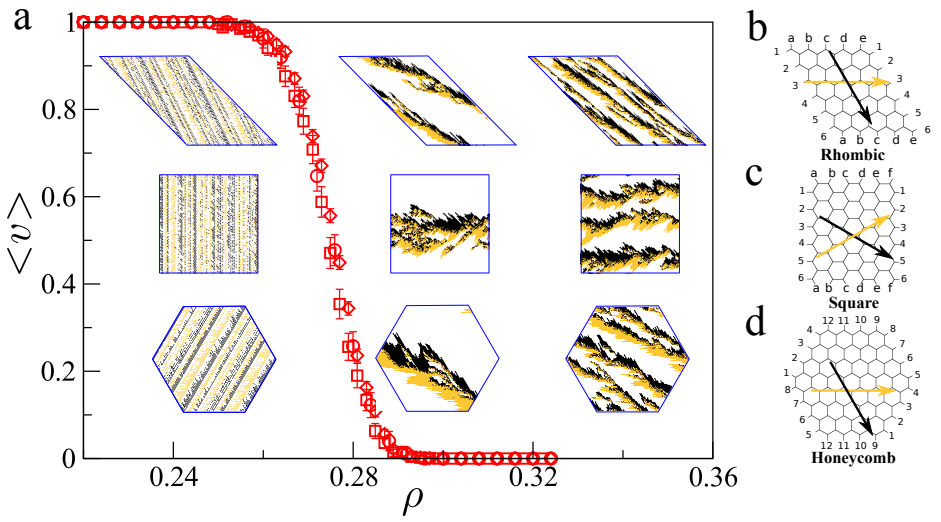


**Figure** 7.1.: **Biham-Middleton-Levine model on a honeycomb lattice. (a)** Average velocity $\langle v \rangle$ vs density $\rho$ (solid red line) for the BML model on $128 \times 128$ honeycomb lattices. Insets show snapshots for free flow (left), one global jam (center) and random jams (right) on lattices with three boundaries: rhombic (diamonds and **(b)**), square (squares and **(c)**) and honeycomb (circles and **(c)**). The flow direction is defined by just two (yellow and black arrows) of the three reflection symmetry axes.

The BML model adapted to honeycomb lattices is as follows: Consider two types of cars moving zig-zag in two different directions, yellow and black, on a honeycomb-like lattice with periodic conditions (Fig. 7.1). Each node is connected with three others and can be in one of three states: empty, occupied by a yellow car, or occupied by a black one. The cars are initially randomly distributed over the lattice sites with spatial density $\rho$. The fully deterministic dynamics is as follows: On even (odd) steps, all yellow (black) cars attempt to advance one lattice site on his zig-zag pattern. If the site ahead of a car (in color direction) is currently empty, it advances; otherwise, it remains stationary. The system is implemented on a torus, i.e., with periodic boundary conditions, as in the original model. Nevertheless, there is no unique way to close an hexagonal lattice on a torus, but three [164]: square, rhombic and honeycomb (Fig 7.1(b-d)). We shall consider all these three tori in the most part of our analysis.

## 7.1. Absence of anisotropy

Starting the simulations from random configurations, the system reaches one of its limiting states after a transient period. If the system size is large enough ($L > 64$), there are only

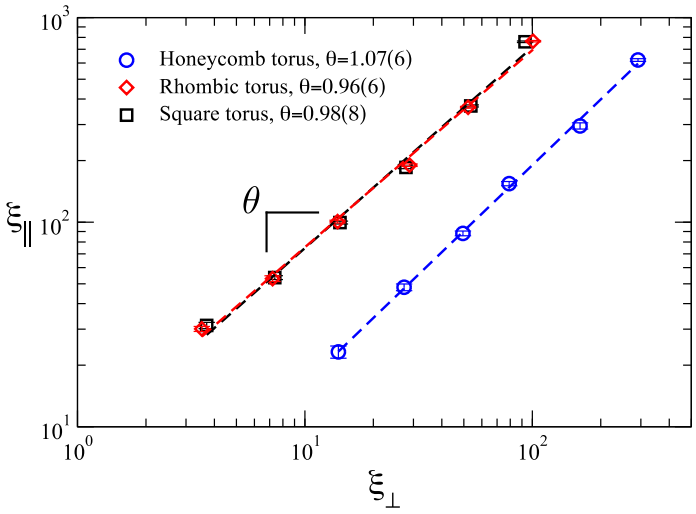


**Figure** 7.2.: **Longitudinal $\xi_{\parallel}$ and transversal $\xi_{\perp}$ correlation lengths from final configurations at densities $\rho$ in the range $[0.265 - 0.310]$ for honeycomb lattices of different sizes with the three boundary conditions.** Each point is an average over 50 configurations. The dashed lines show the power-law fits with anisotropy exponents $\theta \approx 1.0$, i.e. the system behaves isotropic. Here and everywhere in this chapter the error bars are $3\sigma$.

two different limiting states (Fig. 7.1(a)): a free-flow phase, where all cars move freely every time step ($v$=1) and a jammed phase, where no cars move ($v$=0). Contrary to the original model, there are no intermediate states, and the system exhibits a sharp jamming transition between these two phases (Fig 7.1(a)).

As in the original model, there is a preferred flow direction: the one bisecting the two directions for cars and, in consequence, it could be possible to find a similar anisotropy in the correlation length. Let us start by studying the isotropy of the system. If the density is large enough, the system reaches a jamming state after a transient period. Following the methods applied in Chap. 6, we define the parallel (perpendicular) spatial correlation function [115] as

$$G_{\parallel(\perp)}(\vec{r'}) = \frac{1}{N}\left\langle \sum_{\vec{r}} \sigma(\vec{r}) \cdot \sigma(\vec{r}+\vec{r'}) \right\rangle \ , \tag{7.1}$$

where $\sigma(\vec{r})$=1(0) if the site with position $\vec{r}$ is occupied(empty), $N$ is the total number of cars and $\vec{r'}$ is a vector in the direction $\parallel(\perp)$ you want to compute the correlation function along. The symbol $\langle\rangle$ denotes averages over final jammed configurations starting from different random initial conditions at densities slightly above the jamming transition. The correlation functions are fitted with exponentials $G_{\parallel(\perp)} \propto \exp(-r/\xi_{\parallel(\perp)})$ to estimate the correlation lengths $\xi_{\parallel(\perp)}$ in each direction. The anisotropy exponent $\theta$ can be estimated numerically from the fact that, close to the critical point, the two correlations lengths must be related

by $\xi_{\parallel} \sim \xi_{\perp}^{\theta}$ [148, 149].

Figure 7.2 presents the correlation lengths computed from final configurations of the BML model for the three different honeycomb tori with different sizes and at densities close to the threshold transition. A power-law fit gives values for $\theta$ very close to 1, meaning that the system can be considered isotropic, such that the standard finite-size scaling (FSS) theory is suitable for describing the phase transition. Indeed, simulations on systems with different aspect ratios (not shown here) show no difference on the transition. This surprising result is, therefore, not a consequence of the preferred flow direction alone, but also of the grid itself.

## 7.2. The jamming transition

Figure 7.3(a) shows the transition curves for several system's sizes, ranging from $L$=64 to $L$=1024. In the honeycomb-torus case, the size $L$ denotes the torus with the number of nodes closest to $L^2$ [1]. As in many models with phase transitions in statistical physics (e.g., percolation [87]), the value of the critical density $\rho_c$ decreases with system size, reaching a critical value $\rho_c$ as the system size approaches infinity. By fitting the transition curves with a complementary error function

$$\frac{1}{2} \times \mathrm{erfc}\left[\frac{\rho_c(L) - \rho}{\Delta(L)}\right] , \tag{7.2}$$

figures 7.3(b) and (c) show that the transition width and the density threshold scale as [165]

$$\Delta(L) \sim L^{-\frac{1}{\nu}} \text{ and } |\rho_c - \langle \rho_c(L) \rangle| \sim L^{-\frac{1}{\nu}} . \tag{7.3}$$

The values obtained for $\nu$ and $\rho_c(\infty)$ are very similar for the three tori. On average, we obtain $1/\nu$=0.38(3) and $\rho_c(\infty)$=0.244(3).

To investigate the dynamics of the model in the jammed state, let us define $\tau_{1/2}$ [115] as the time when the average speed is one half of the initial speed (Fig. 7.3(d)). This relaxation time follows a lognormal distribution and, therefore, its mean value can be estimated as $\langle \tau_{1/2} \rangle = \exp(\mu + \sigma^2/2)$, with $\mu \simeq \frac{1}{n}\sum_k \ln \tau_{1/2_k}$ and $\sigma^2 \simeq \frac{1}{n}\sum_k (\ln \tau_{1/2_k} - \mu)^2$ . In the jammed phase ($\rho > \rho_c$), Fig. 7.3(e) shows that $\langle \tau_{1/2} \rangle$ is independent of the system size and scales as $\langle \tau_{1/2} \rangle \sim (\rho - \rho_c)^{-\chi}$, with $\chi$=1.55(2). In addition, the values of $\tau_{1/2}$ at the critical density

[1] A honeycomb torus of size $n$ has $6n^2$ nodes and $n$ hexagons between the center and boundary. Thus, a $L^2$ torus actually corresponds to a torus in which $n$ is the closest whole number of $L/\sqrt{6}$

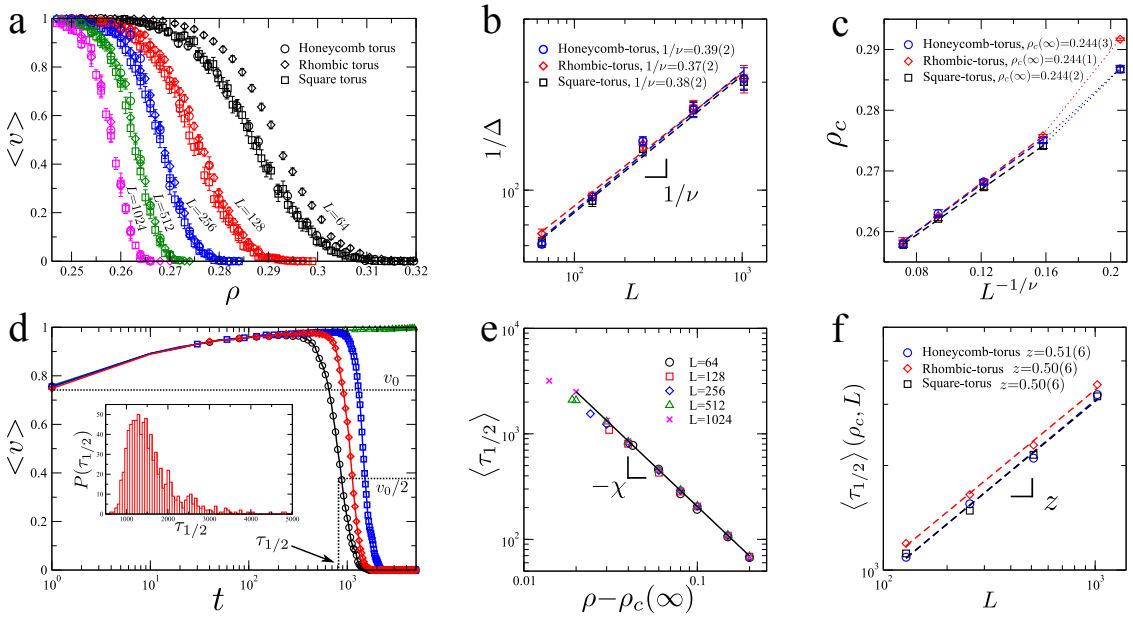


**Figure** 7.3.: **Finite-size scaling analysis for the dynamical phase transition. (a)** Transition curves for the three types of torus (symbols) with five different system sizes (colors), ranging from $L$=64 to $L$=1024. Each point is averaged over 2000 (1000) final configurations for $L\leq$512($L$=1024), obtained after convergence ($v$=0 or $v$=1) or after $2\times10^5$ time steps (whichever comes first). **(b)** Scaling of the transition width $\Delta(L)$. Dashed lines are power-law fits for the three tori, giving $1/\nu$=0.38(3) on average. **(c)** Scaling of the finite critical density. Because of strong finite-size effects, we neglect $L$=64, and obtain $\rho_c(\infty)$=0.244(3) on average. **(d)** Average speed in function of time for five configurations. Dotted lines show the definition of the relaxation time $\tau_{1/2}$. The inset evidences that $\tau_{1/2}$ follows a lognormal distribution. **(e)** Mean relaxation time $\tau_{1/2}$ for densities above $\rho_c(\infty)$ on the honeycomb-torus (results on other tori are quite similar). The slope gives on average a critical exponent $\chi$=1.55(2). **(f)** Scaling of the relaxation time at the critical point $\tau_{1/2}(\rho_c)$. On average, we obtain a dynamical critical exponent $z$=0.50(6). Each point on the last two figures is averaged over 100 configurations.

$\rho_c$ scale with system size as $\langle\tau_{1/2}\rangle(\rho_c, L)\sim L^z$, with $z$=0.50(6) (Fig. 7.3f). The finite size scaling theory suggests that above the transition point $\chi/\nu=z$=0.56(5), in fair agreement with the value above.

## 7.3. A mean-field analysis.

Interestingly, the critical density can be approximated by using a *naive* mean-field analysis, inspired by [151]. Consider the mean velocity of yellow cars (by symmetry, the reasoning

**Table** 7.1.: Critical parameters found from the finite-size scaling and mean-field analysis.

| Exponent/quantity | Value |
|---|---|
| $\rho_c$ | 0.244(3) |
| mean-field $\rho_c$ | 0.250 |
| $1/\nu$ | 0.38(3) |
| $\chi$ | 1.55(2) |
| z | 0.50(6) |
| $\chi/\nu \approx z$ | 0.56(5) |

is also valid for black cars). A yellow car will stop either because it is blocked by a black car or by another yellow car. On honeycomb lattices, there is almost no difference between these two types of interactions. At a random initial configuration, the probability that a car is blocked is $\rho$, that is, at the beginning of the simulation the proportion of stopped cars must be equal to $\rho$. Since black (yellow) cars spend on average a time $1/v$ on a site, they will reduce the speed of yellow cars from unity by $\rho/v$. Hence, a self-consistency equation for the average speed $v$ will be

$$v = 1 - \frac{\rho}{v} \ , \tag{7.4}$$

which gives $\rho_c$ as the critical density at which the equation ceases to give a real solution. That occurs at $\rho_c$=0.25, very close to the value of 0.244(3) obtained from finite size scaling. A summary of all the critical parameters is shown in Table 7.1.

## 7.4. A comparison with the square lattice.

The critical density $\rho_c$=0.244(3) for the BML model on a honeycomb is lower that the value of 0.283(2) for the lowest transition on a square lattice [2]. However, this order is reversed in at least two cases. First, let us remove full synchrony by introducing a random update [128], where a car advances with probability $P$<1 if the target site is empty; a modification that also destroys the intermediate state in of the BML model on square lattices [20, 127, 128]. Figure 7.4(a) compares the critical density of the model as function of $1 - P$ on a rhombic torus with the one on a square lattice. The BML on a square lattice follows a power law behaviour, with $\rho_c \propto (1 - P)^{-0.22(1)}$. Below $P$=0.96, the honeycomb lattice overcomes the square one and behaves better, that is with a higher critical density. Second, we have also studied the effect of increasing the traffic-light periods, that is cars on each direction have the chance to advance in $\tau$ consecutive time steps ($\tau$=1 for the original model). This also

destroys the intermediate states on the original BML model and, furthermore, produces a spatial phase separation with small global speeds at intermediate densities [129]. Again, rhombic tori show higher critical densities than square lattices, even for $\tau$=2 or $\tau$=4 (Figure 7.4b). These results suggest that the model BML on a honeycomb is more resilient against small perturbations than on a square lattice.

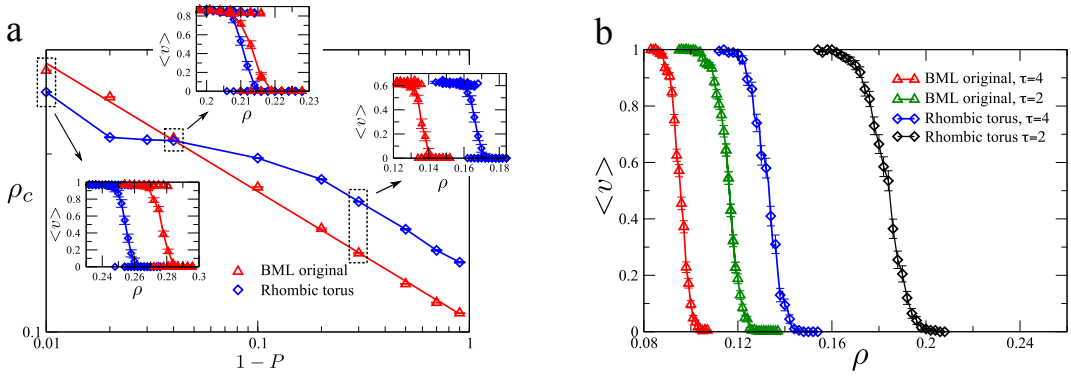


**Figure** 7.4.: **Effects of two modifications of the BML model on both rhombic tori (diamonds) and square lattices (triangles). (a)** Effect of including a random update, where cars move with probability $P$ if the target site is empty. The figure shows the critical density $\rho_c$ as a function of $1-P$ for lattice sizes $L$=128. Insets show the transition curves for three values of $P$. **(b)** Effect of increasing the traffic light period $\tau$. The figure shows transition curves for $\tau$=2 and $\tau$=4 on lattices with size $L$=256. Each point in both figures is averaged on 400 runs. Measurements are obtained after $6 \times 10^5$ time steps or until convergence (whichever comes first).

## 7.5. Conclusion

We have shown that the BML model with two flow directions behaves isotropically on honeycomb networks. There are no intermediate states, and a sharp transition from the moving phase to the jamming phase is observed at a critical vehicle density. Despite the fact that there is a preferred flow direction, the correlation length shows to be isotropic. This surprising result may be a consequence of the symmetries of the honeycomb. Indeed, it has been shown that high-order tensors on a hexagonal lattice (the dual lattice of a honeycomb) are isotropic up to second order in the grid size [166]. If this is the reason for such isotropy or not will be an interesting subject of future research.

By performing a classical scaling analysis, we characterized completely the transition, measuring the critical density and three critical exponents. Although the model shows a lower critical density than on square lattices, this issue is reversed by introducing small and simple perturbations, like increasing the traffic light periods or including a random update with very low probabilities to brake. Street patterns based upon hexagonal blocks were proposed by several planners in the early 20th century [109]. Despite urban designers demonstrated the economic advantages and efficient land use of hexagonal plans, this idea never ceased to be a theoretical alternative to the rectangular grid, barely implemented in urban street patterns. Furthermore, the contemporary movements of New Urbanism claims that square grid layouts increase the connectivity[2], dispersing traffic and reducing driving times, because they are assumed to be mixed-use, walkable, and more pedestrian friendly. However, such assumptions are criticized by practical considerations [109]. Indeed, empirical data about safety [167, 168] suggest that 4-legs intersections, ubiquitous in square grids, increase both the number of crashes and injuries significantly, suggesting to reconsider urban layouts where T-junctions predominates (*cul de sac*, radburn, fused grid). Moreover, city planners use to restrict flow direction emulating T-junctions. Honeycomb grids emerge as an unifying idea. Our results suggest that the BML model on hexagons under perturbations is more robust than on squares. As the perturbations included, i.e., traffic lights and disorder, are crucial in real traffic, this work questions the real role of the square grid-like designs and supports honeycombs as an interesting alternative for urban densification processes.

In general, these results show that topology plays a crucial role on the traffic behavior, to the point that even defines the critical features in the proximity of the collapse. In case of real street networks, geometry not just includes the topology, but also street properties like maximal speed, number of lanes and traffic lights. Therefore, more realistic models are needed to reveal its effect of geometry on urban traffic networks.

[2] see http://www.newurbanism.org/

# 8. A survey of urban traffic gridlock modeling

In contrast to highway traffic, a theoretical framework to describe the urban city traffic is still missing. Congestion at city level is the result of the interplay between the travel distribution of vehicles and physical constraints of the roads, such as: network geometry, road lengths, road capacity and speed limits. This leads to saturation of the most frequently used road segments, spilling over into nearby streets and producing the emergence of large traffic jams. In extreme cases these jams can sometimes collapse the entire system, even lasting for days [5]. The behaviour is so complex, that generally can be only addressed by computer simulations. Nevertheless, the main obstacle in studying traffic congestion has been the lack of data, not just of empirical traffic variables but also of traveling demand for many cities at once. In consequence, most studies on the transition to congestion have been done through simulations with many unrealistic assumptions. This chapter presents an overview of the simulation models for traffic on road networks. The concepts discussed here were the starting point for the ideas we introduce in the next chapter.

## 8.1. Internet inspired models

Most studies about traffic and congestion phenomena on complex networks focus on information systems, especially on the Internet. Thus, several approaches to the urban traffic congestion [22, 23] consist in agent-based models inspired by the traffic dynamics of the Internet [24,25]. In these models, at each timestep, $R$ vehicles/packets (the *inflow*) with random origins and destinations are created and injected into the network. Then, they travel to their destinations, jumping from one node to another following a routing strategy that, in general, involves a nearest neighbor passing of packets. Vehicles are removed from the network once they arrive to their destinations (the *outflow*). An increase of volume demand $R$ in the network beyond a threshold $R_c$ induces a transition to a congested state, where

the number of vehicles in the network $N(t)$ increases steadily in time. The rate of increasing cars per unit time defines the order parameter,

$$\eta(t) = \lim_{t\to\infty} \frac{N(t+\Delta t) - N(t)}{R\Delta t} \ , \tag{8.1}$$

where $\Delta t$ is some certain defined period of time. The aim of this approach consists of identifying the critical value $R_c$ at which vehicles start accumulating in the network and understanding how the various elements of the model (network topology, road capacity or routing strategy [25]) affect the transition to a global congested state (see Fig. 8.1).

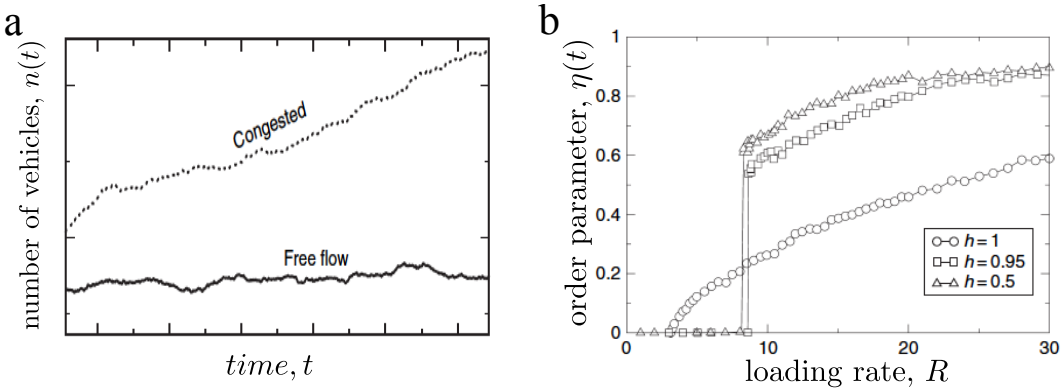


**Figure** 8.1.: **Dynamical traffic transition to congestion on internet-like models. (a)** Evolution in time of the number of vehicles (packets) in the network. If the loading rate, $R$, is not too large (free flow), the number of vehicles on the network fluctuates around a steady-state value. On the contrary, if the arrival of vehicles is not quickly enough, they start accumulating in the network and the load steadily increases with time, defining the jammed phase. Figure taken from [169]), copyright (2008) by the authors A. Barrat, M. Barthelemy and A. Vespignani. **(b)** Jamming transitions for different conditions of the traffic-aware routing strategy proposed in [25]. The case $h$=1 corresponds to the standard shortest path routing with no traffic awareness. Figure taken from [25], copyright (2005) by EDP Sciences.

It seems quite tempting to use internet-like routing strategies in transport networks. However, transport networks present a crucial difference from information systems. Vehicles move along the links (roads) and their interactions favor congestion to spread across the network and eventually affect a large portion of the system. This situation is unlikely on the Internet network, where the congestion locates usually at particular nodes of the system (the hubs). Some recent approaches trying to overcome this obstacle [22, 29] by modeling real road networks considering the detailed vehicular dynamics along the streets. Nevertheless, the use of random origin-destination tables (OD) neglects the inherent spatial heterogeneity in the demand distribution at real cities and defines beforehand a direct relationship between their results and the betweenness centrality of the network. Thus, the connection to the empirical traffic demand is still missing.

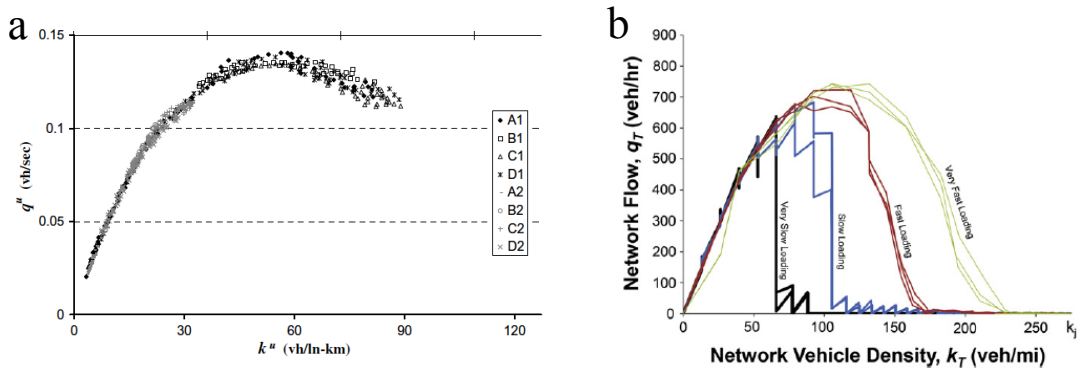


**Figure** 8.2.: **Empirical and simulated network fundamental diagram. (a)** Loop detector data from Yokohama (Japan) suggesting the existence of a network fundamental diagram NFD. The figure shows the average flow $q$ vs. average occupancy $k$ from all detectors in the city across two different days. **(b)** Simulated fundamental diagram for a grid network showing the effect by the demand. Figures taken from [30, 170]. Copyright of both figures by Elsevier Ltd.

## 8.2. Existence of Network Fundamental Diagram (NFD)

Like the fundamental diagram on an individual road segment, several earlier studies suggested that a well-defined relationship between network average flow and average density exists for an urban network [39, 171–175]. However, the evidence for its existence has been given only very recently from empirical data from downtown Yokohama by Daganzo and coworkers [101, 170]. By aggregating the highly scattered plots of flow vs. density from individual loop detectors, they found a well-defined Network Fundamental Diagram (NFD) between space-mean flow and density (see Fig. 8.2). They also showed evidences that the NFD is a property inherent to the network infrastructure and control, and not to the demand. Indeed, space-mean flow reaches a maximum for the same value of critical vehicle density, independently of time-dependent origin-destination tables. Based on these findings and the assumption that traffic distributes homogeneously in space, Daganzo & Geroliminis [176] and Helbing [177] have derived analytical theories for the urban fundamental diagram, using either a density-based or a use-based approach, respectively. NFDs derived from these theories fit well the data obtained from the Yokohama experiment. As a result, many simulation-based studies rely on the existence and observability of the network fundamental diagram. In these approaches, the traffic dynamics is modeled via dynamic traffic assignment [26], as well as macroscopic calculations based on car-following [30, 178] or cellular automata models [28–31]. So, variations in flow and density can be measured at the road segment level. Considering the network density as the control parameter (similarly to the single road case), a congested state at the network level is defined as a drop in the cars outflow when the density exceeds certain threshold value.

Nevertheless, this well-defined NFDs seems not to be universal. For instance, Buisson & Ladier [179] showed with real data from Toulouse that heterogeneity has a strong impact on the shape of the NFD and, in some cases it is not even similar with wide scatter for high densities. Even worse, it is well known that traffic conditions may significantly vary for similar travel activities and traffic volumes; that is, different congestion levels can take place in different week days with similar origin-destination tables. Therefore, the description of city traffic in terms of a fundamental diagram with aggregated data appears to be incomplete and, thus, other general descriptions must be formulated.

## 8.3. Relevance of the outflow and the recovery time

In [26], Mahmassani et al. claim that real networks are more richer than a fundamental diagram, because urban traffic dynamics includes features such as outflow, inherent spatial heterogeneity of origins and destinations, cycles of loading and unloading with hysteresis effects (empirically observed in [175, 180–183]) and adaptive driver behaviors. Thus, the major limitation of the existing simulation-based studies (like the mentioned above) is the lack of exit flows and recovery periods. As vehicle density is the control parameter in those approaches, every time a vehicle arrives to the destination is reinserted into the network (with other random OD), and the system never recovers. If a network keeps loading indefinitely, it will eventually reach a state of gridlock and empirical phenomena like hysteresis loops are unlikely to observe. Therefore, those kind of simulations are missing important elements for the understanding of the urban traffic dynamics.

With this in mind, Mahmassani et al. [26] proposed a model to reproduce hysteresis and gridlock when homogeneity and steady-state conditions do not hold. They calibrated and tested the model for the Chicago road network. The input is the 5 hours morning peak origin-destination demand estimated from real observations (detectors) of individual link flows. Once you have the ODs, the traffic dynamics is modeled with dynamic traffic assignment (DTA) [184, 185]. The aim of this method is to assign routes based on the maximization of some criterion, e.g., the system optimum or user equilibrium. So, the method reroutes until the solution converges with the chosen criterion.

Figure 8.3(a) shows the simulated loading profile, which consists of the 5 hours morning peak period plus 9 hours recovery time with no loading. Such a long recovery time allows to observe the dynamics of the long-lasting gridlocks in the network.

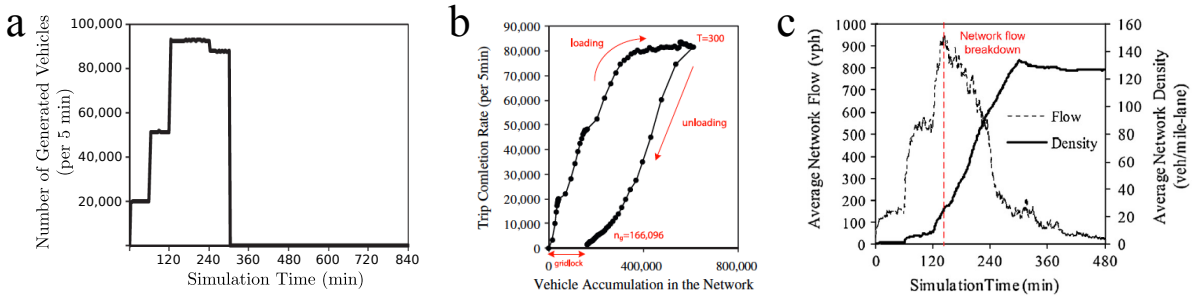


**Figure** 8.3.: **Realistic simulation of Chicago traffic dynamics (a)** Simulation loading profile. **(b)** Network-wide relationship between vehicle accumulation in the network and trip completion rate. **(c)** Network fundamental digaram of Chicago Central Business District sub-network. Figure taken from [26]. Copyright (2013) by Elsevier Ltd.

A remarkable result is that they could observe the hysteresis phenomenon. Figure 8.3(b) shows the relationship between vehicle accumulation and trip completion rate (outflow). The large hysteresis formed is the result of the exit flow and the recovery period, and it is amplified by the abrupt stop of the loading and the formation of gridlocks. When loading sharply stops, a large portion of the network (mostly in the outer regions) quickly becomes empty, while the central part of the network remains congested with some vehicles still moving toward their destinations or trapped in the gridlock. More interestingly, when they focus on the Chicago Central Business District sub-network, a flow breakdown can be observed long before the loading stops. Following that breakdown, the average network density constantly increases up to the end of the loading process, and remains thereafter almost invariant until the end of the simulation, as seen in Fig. 8.3(c). This suggest the emergence of a gridlock. This work could characterize urban gridlock using descriptive measurements from simulations of the Chicago road network, although its connection with other global characteristics of urban travel remained missing.

## 8.4. Traffic Percolation

The first attempt to theoretically understand the problem of the dynamical organization of traffic in road networks was provided very recently by D. Li et al. [32]. In that work, the authors propose a quantitative framework based on percolation theory, where the number of road links below a certain speed threshold form a giant component in the network. Based on taxi data, they collected the average velocities of the roads in the central area of Beijing. As the data contain the velocities along the day for every road $e_i$, one can define for each road a ratio $r_i$ between its current velocity and its maximal velocity measured during the

day. Then, for a given threshold $q$, the road $e_i$ can be classified into two states: functional (1) when $r_i \geq q$ and disfunctional (0), otherwise. In this way, a traffic dynamical network can be constructed for a given $q$ value, which allows to observe how global traffic is dynamically composed of clusters of connected roads with high velocity.

Figures 8.4(a)-(c) shows the dynamics during a typical noon period. For $q$=0.69, only small clusters emerge. As the value of $q$ decreases to 0.19, these small clusters merge together to form a giant cluster, where the functional network covers almost the entire road network. For the intermediate value $q$=0.38, the size of the second-largest cluster becomes maximal, which identifies a critical threshold $q_c$ separating the fragmented phase from the connected phase of the traffic network, as seen in Fig. 8.4(d). This percolation-like process evolves during the day. Figure 8.4(e) shows the temporal evolution of $q_c$, and one can see a dramatical decrease close around the rush hours. The authors argue that the percolation threshold $q_c$ can be an estimator for traffic efficiency that reveals the interaction between roads, network structure and flow. Nevertheless, the relation between traffic parameters (volume and routing choice) and the system percolation properties has not been studied systematically.

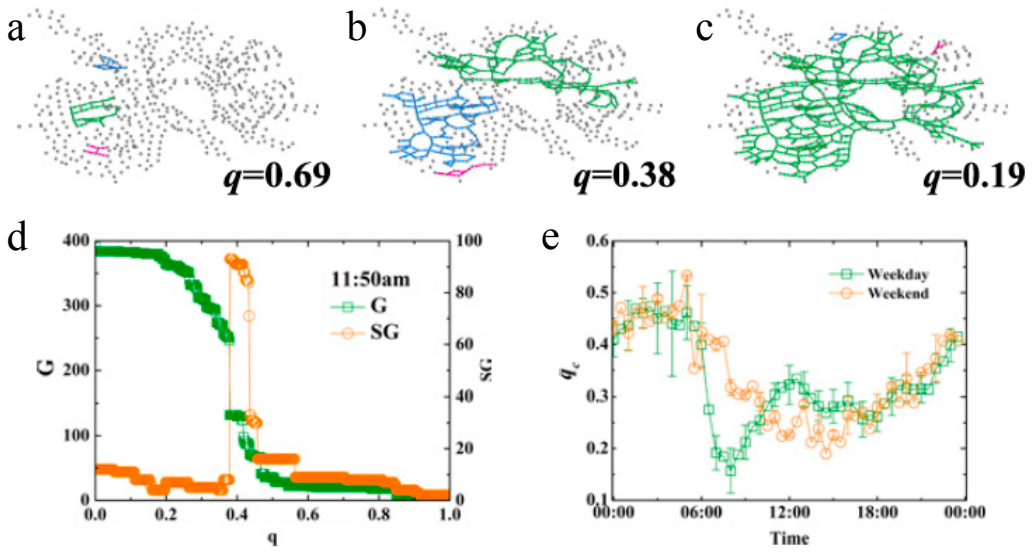


**Figure** 8.4.: **Percolation of traffic networks during the noon period. (a)-(c)** show the traffic networks under different $q$ values representing states of high ($q$=0.69), medium ($q$=0.38), and low ($q$=0.19) velocity thresholds. Only the largest three clusters are plotted, which are marked in green (largest), blue (second-largest), and magenta (third-largest). **(d)** Size of the largest cluster (G) and the second-largest cluster (SG) of traffic networks as a function of $q$. The critical value, $q_c$ is determined where SG becomes maximal. **(e)** $q_c$ as a function of time, averaged separately over weekdays and weekends. Figures taken from [32]. Copyright (2015) by the authors D. Li et al.

## 8.5. Discussion

Until now, the lack of data for travel demand has prevented large-scale comparative studies of the relation between the empirical urban congestion and global traffic parameters such as car volume, road network supply and travel times. Namely, there are two limitations in the simulation-based studies. One is the use of random origin-destination tables (OD), which neglects the inherent spatial heterogeneity in the demand distribution. The other is the interpretation of transition to congestion as a loading process, where the order parameter is defined by the amount of accumulated vehicles. These limitations generate two main consequences. First, the transition to congestion occurs at unrealistic high car densities. Second, random ODs have no relation to the empirical travel demand, which creates gridlocks in most used streets. Mahmassani et al. [26] characterized urban gridlock by using descriptive measurements from simulations of the Chicago road network. This work pioneered the concept of the recovery time as an important metric to diagnose urban congested states. Yet its connection with other global characteristics of urban travel remained missing.

However, the recent availability of data on personal tracking devices allows us to overcome these limitations. Travel information for entire cities, i.e., origin-destination tables (ODs), can be extracted from the analysis of call detailed records (CDRs) from mobile phones [33–36]. Using these data as the input of a cellular automaton simulation, we propose in the next chapter a novel framework to characterize the transition to congestion at a city network level.

# 9. Non-equilibrium dynamics in urban traffic networks

As we said in the previous chapter, there are mainly two obstacles in studying traffic in a network scale. The first obstacle is the lack of data for city travel demand which forces to use random origin-destination tables (OD), and thus, neglects the inherent spatial heterogeneity in the demand distribution. The second is the the lack of valid methods to characterize the emergence of congestion in the road network. Most previous approaches interpret the transition to congestion as a purely loading process, being quite far from reality.

To overcome the first obstacle, the recent availability of data on personal tracking devices could be helpful. Some recent studies have been able to extract the travel information from the analysis of call detailed records (CDRs) [33–36] from mobile phones. Particularly, Çolak et al. [37], from the HuMNet Lab - MIT, have estimated the origin-destination tables (ODs) during the morning peak hour for five major cities around the world: Boston, San Francisco Bay, Rio de Janeiro, Lisbon and Porto. Using these travel information, along with a cellular automata microsimulation of the five subject cities, here we propose a novel framework to characterize the transition to congestion in the same cities. This is a first step to overcome the second obstacle.

## 9.1. Travel Demand Information

As we said above, Çolak et al. [37], have estimated the origin-destination tables (ODs) during the morning peak hour for Boston, San Francisco Bay, Rio de Janeiro, Lisbon and Porto. Using these ODs, along with road networks publicly available on OpenStreetMaps and a dynamic traffic assignment method (DTA) [184, 185], the authors estimated the congested travel time ($t_{ue}$) for each road and at network scale. So, the information we had access

consisted in:

- **City road networks:** In the OpenStreetMap (OSM) data, nodes represent corners (intersections) and links represent road segments. Roads contain attributes such as length, speed limit (thus free travel time), number of lanes and its classification varying between motorway, trunk, primary, secondary, tertiary, residential and trunk roads. For their purpose, Çolak et al. [37] filtered out roads with irrelevant categories (deleting the last two classes) and simplified the network by collapsing roads with only one incoming and one outgoing road, if they were in the same road classification.

- **Congested travel time:** After running the dynamic traffic assignment method, roads also have the congested travel time $t_{ue}$, this is the travel time under traffic conditions, using the user equilibrium criterion (drivers choose the shortest travel time).

- **Origin-destination tables (ODs):** These tables correspond to the total disaggregated trips during the morning peak hour (from 7:00 to 8:00) for each city (see Table 9.1).

With this information, we implemented a cellular automata model for the whole network. For simplicity we assume that each link only has one lane. Therefore, every road segment is discretized in cells of equal length. The trips routes in the road networks are pre-calculated with the congested traveled time $t_{ue}$ as weights. Thus, we assign initial routes to each vehicle by means of shortest time path.

## 9.2. Traffic Dynamics

Vehicles are created at origin nodes (intersections) and then, we try to insert them in the network (roads) right away according to the initial routing strategy. In case of high insertion rates, queues of *new* vehicles can be formed at origin nodes. Vehicle dynamics along road segments is modeled with the deterministic NaSch model [62] (see also subsection 2.3.1). When a car is traveling in free flow and approaches an intersection it decreases its speed to $v_{uts}$. In the implementation presented here our unit time step (uts) is $\Delta t = 1.2375[s]$ and the cell sizes are $l$=5.5$[m]$. This defines the minimum distance per unit time step that vehicles can travel in the absence of congestion, which corresponds to $v_{uts}$=16$[km/h]$ or $1cell/\Delta t$ in the simulation. Each vehicle keeps a gap distance which creates congestion when cars accumulate in the streets taking speeds in the range $[0, v_{max}]$, $v_{max}$ is taken from the speed

limit of the road network data (see Fig. 9.1). At each time step, all vehicles update in parallel their velocities and move according to the rule $v_{t+1}{=}min(v_t + 1, gap, v_{max})$ where $gap$ is the distance from the car ahead or to next intersection.

The dynamic at the intersections has three steps. First, the first *new* vehicle in the queue is chosen to pass. Secondly, incoming streets are checked in a random sequence asking for the destination of the first vehicle in the street. If the intersection is just the destination

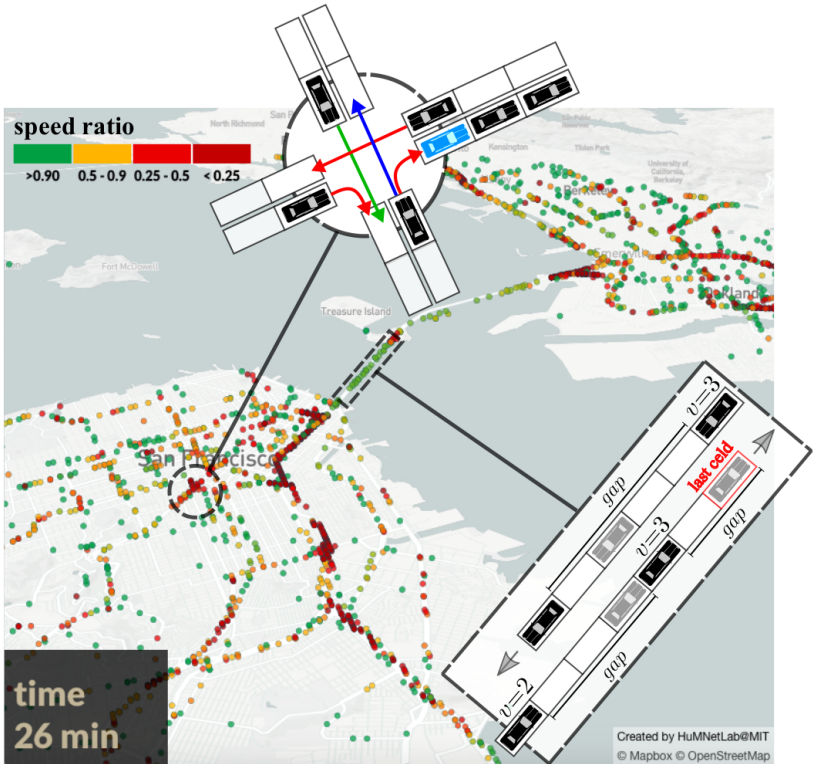


**Figure** 9.1.: **Model dynamics.** Once vehicles are inserted in the network, the trip toward their destinations are determined by two process: the dynamics along the streets and the routing at the intersections. (**Right**) Vehicle dynamics along road segments is modeled with the deterministic Nagel-Schreckenberg CA model [62]. The snapshot illustrates some cases of the dynamics, black vehicles correspond to the configuration at time $t$ and grey ones correspond to the position at $t{+}1$ after the velocity updating. (**Top**) Each timestep in a random sequence, the intersections transmit the first vehicles of the in-going streets. The vehicles can be routed (1) if the first cell in the desired outgoing street is empty and (2) if the road capacity of the ingoing street allows it. In the last case, the vehicle is delivered with a probability $p$ proportional to the road capacity of the incoming street, $C_e$. In case of long waiting times, vehicles re-route. In the snapshot colored arrows illustrate several possibilities of crossing: green (successful), red (not successful) and blue (a new route chosen). Light-blue vehicle means that the cell is occupied by a vehicle that has crossed before or by one that just entered the network.

node, then the vehicle is removed from the network. Otherwise, if the first cell of the desired outgoing street is free, the vehicle is delivered with a probability $p$ proportional to the empirical flow capacity of the incoming street, $C_e$. Consequently, here is where the bottlenecks begin, due to capacity limitations and spill back effects. Finally, in case of long waiting times, we introduce a basic dynamic routing strategy: A vehicle that has been stopped at an intersection during more than $t_{wait}$=96 time steps (approx. 2 minutes), it can decide to reroute to a less congested outgoing street and recomputes its route. Under low traffic conditions, this strategy softens the artifacts that can be generated by short-length cycles, e.g., roundabouts intersections, where the turning maneuvers can create unsolvable gridlocks. In high traffic cases, the possibility of re-routing helps to solve gridlocks, and to reach a recovery period for congestion.

Rush hours can be described as a loading and unloading process. Thus, to model the morning peak hours, we load the road network during one hour; i.e., every $\Delta t$, the network is loaded with $R$ random trips chosen from the ODs. After that, we stop the loading and let the system recover within a time window of 9 hours. We select a sufficiently long time of observation that allows us later to observe the dynamics of long-lasting traffic jams.

## 9.3. Current Traffic Conditions

First, we focus on understanding the system behavior under actual traffic conditions. Due to the one-lane representation, the total volume demand ($V$) is re-scaled by the ratio between the space demands in simulated and real networks, i.e.,

$$V_s = \frac{\sum\limits_{e \in E} x_e \cdot \ell_e}{\sum\limits_{e \in E} x_e \cdot \ell_e \cdot n_e} \cdot V, \tag{9.1}$$

where $x_e$, $\ell_e$ and $n_e$ are the vehicle flow, length (in km) and number of lanes of a road segment $e$. Despite the differences in road infrastructure, there are slight differences between these ratios for the considered cities, as seen in Table 1. This is just further evidence of how traffic streams are concentrated on a few arterial roads only. Next, we distribute the re-scaled volume demand ($V_s$) in the one hour loading, such that $R_s = \frac{V_s}{1h} \cdot \Delta t$ random chosen trips are inserted each time step $\Delta t$.

Figure 9.2(a) shows the schematic representation of the percentage of vehicles in the network, $n(t) = \frac{N(t)}{V_s}$. We can see that the network responds differently to loading and unloading, sho-

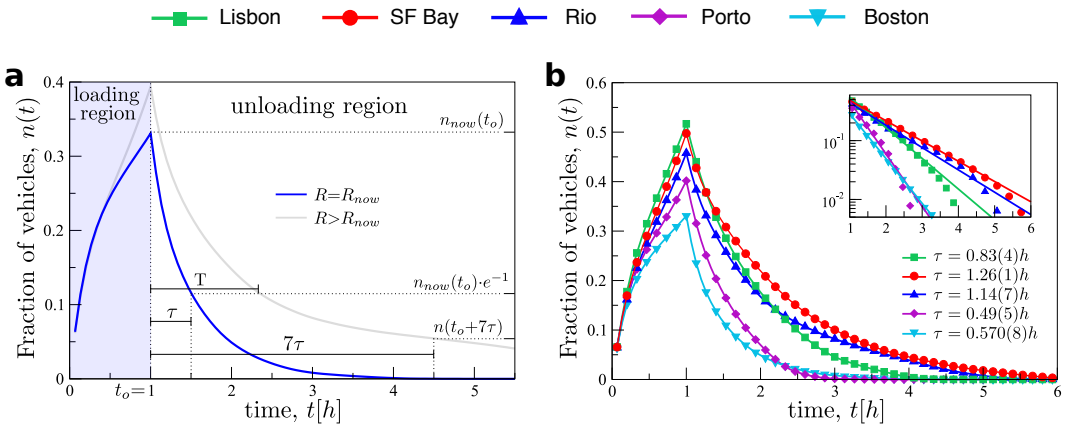


**Figure** 9.2.: **Comparison of congestion levels for the five considered cities.** (**a**) Scheme of the fraction of vehicles in the network, $n(t){=}\frac{N(t)}{N_{total}}$, for simulations of the morning peak hours. (**b**) During the $1st$ hour every city is loaded homogenously with a rescaled loading rate $R{=}R_s$ (see Table 9.1). Inset shows the log-lin plot of the recovery period with the unloading time $\tau$ of the fitted exponential function depicted in the legend. Every curve here is an average over 20 realizations.

**Table** 9.1.: A comparison of the general properties of the subject cities.

| | City | | | | |
|---|---|---|---|---|---|
| | Boston | Porto | Lisbon | Rio | SF Bay |
| roads (th. miles) | 12 | 3 | 7 | 6 | 30 |
| all trips (mil.) | 0.916 | 0.171 | 0.324 | 0.432 | 1.015 |
| $V_s/V$ | 0.417 | 0.403 | 0.414 | 0.439 | 0.391 |
| $R_{now}[veh/\Delta t]$ | 131 | 24 | 48 | 64 | 134 |

wing hysteresis effects, as other studies have also uncovered [26, 180, 182, 183]. Interestingly, for all five cities the recovery period follows an exponential decay,

$$n(t)_{t\geq 1h} = n(1h)e^{-\frac{t-1h}{\tau}}, \tag{9.2}$$

with the unloading time $\tau$ ranging from 0.49 to 1.26 hours (see inset Fig. 9.2(a)). This behavior implies a proportionality between the outflow rate and the number of vehicles in the network,

$$\frac{dN(t)}{dt} = -\tau \cdot N(t), \tag{9.3}$$

which in fact is confirmed by simulations (see Fig. 9.3).

We are interested in understanding what characterizes this exponential recovery. Therefore, we begin by analyzing the travel demand. Similar to [37], commuting trip distances, $d$, can

be approximated by a log-normal distribution (see Fig. 9.4(a)) ,

$$P(d;\mu,\sigma) = \frac{1}{\sqrt{2\pi}\sigma d_b} e^{-(\ln(d)-\mu)^2/2\sigma^2} \ , \tag{9.4}$$

with medians ranging from 10 to 16 km ($\mu$=2.31 − 2.77) and the s.d. ranging from 2.13 to 2.91 km ($\sigma$=0.76 − 1.07).

After the 1*st* hour there are some vehicles that have not reached their destination. The

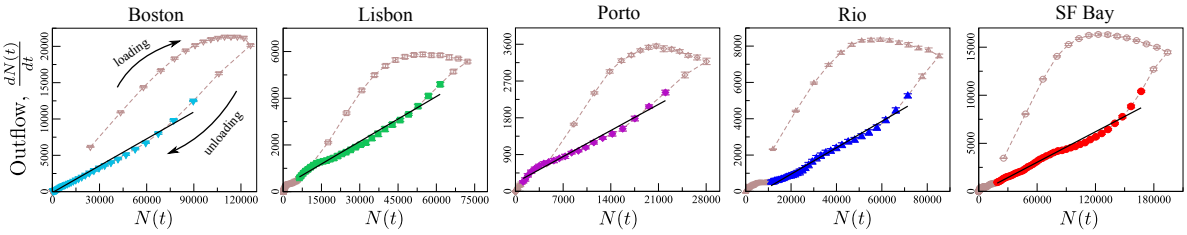


**Figure** 9.3.: **Relationship between network outflow rate $\frac{dN(t)}{dt}$ and the number of vehicles in the network $N(t)$ for the five cities.** Shortly after finishing the loading, all cities exhibit a linear relationship. More precisely, starting from the $t$=1:08$h$, color symbols represent 3$h$ within the recovery period. The hysteresis effect is also observed.

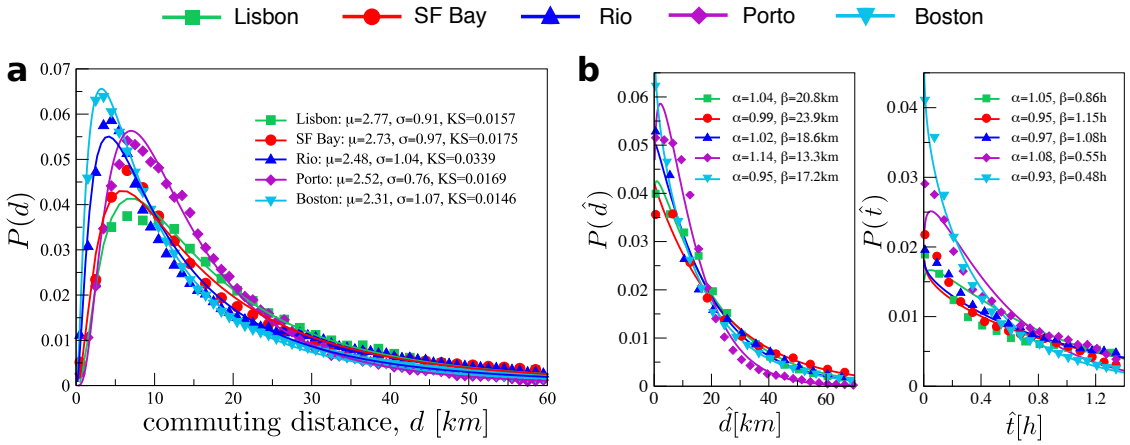


**Figure** 9.4.: **Comparison of the travel demand properties of the subject cities under free-flow and congested conditions.** (**a**) Distribution of commuting distance, d[km], in the morning peak. All curves are fitted to a lognormal distribution. The distribution parameters and the Kolmogorov-Smirnov test are depicted in the legend. (**b**) After the loading hour, the remaining distance $\hat{d}$ and the remaining travel time $\hat{t}$ for the cars in the network can be fitted by a Weibull distribution with parameters shown in the legends (see also Table 9.2). This explains the exponential behavior in (**b**). Every curve here is an average over 20 realizations.

remaining distance $\hat{d}$ of these vehicles follows a Weibull distribution (Fig. 9.4(b) left),

$$P(\hat{d};\alpha,\beta) = \frac{\alpha}{\beta}\left(\frac{\hat{d}}{\beta}\right)^{\alpha-1} e^{-(\hat{d}/\beta)^{\alpha}} \ . \tag{9.5}$$

In a non-collapsed state, the remaining travel times, $\hat{t}$, follow the same distribution, as shown in Fig. 9.4(b) right. Thus, in the recovery period, the number of vehicles as a function of time, $t_r$=$t-1$, can be estimated as

$$N(t_r) = N(1h)\cdot\left(1-\int_0^{t_r} P(\hat{t};\alpha,\beta)\ d\hat{t}\right) = N(1h)\cdot e^{-(t_r/\beta)^{\alpha}} \ . \tag{9.6}$$

As $\alpha$ takes values very close to 1.0 (see legends in Fig. 9.4(b) right) and the $\beta$ values are similar to the $\tau$ of each city, this explains the exponential recovery time.

The network response to the traffic demand can be measured by how long it takes to the network to be unloaded. We argue that $\tau$ quantifies the congestion level of the road network. With this in mind, we now focus on how the travel demand and network features explain congestion levels. To that end, we measure two parameters for each city. The first is the demand-to-supply ratio defined as [37]

$$\Gamma = \frac{\sum_{e\in E}\ell_e x_e}{\sum_{x_e>0, e\in E}\ell_e C_e} \quad , \tag{9.7}$$

which is a dimensionless metric that captures the spatial distribution of the loading on the available road infrastructure of the city. The second, is the median of the free flow travel time $t_{ff}$, defined as the travel time at the speed limit over all the trips in the rush hour, if they occurred without congestion. This provides a time dimension and captures a feature of the travel demand related to the form of the city and the distribution of residential places respect to the required destinations. The values of both parameters are shown in Table 9.2. Remarkably, there is a clear linear relation between $\tau$ and the product $\Gamma\times t_{ff}$ (see Fig. 9.5(a)) such that the congestion level of each city can be defined only by these two observable parameters that synthesize travel demand, road infrastructure and road usage. We also compare our parameter $\tau$ with the empirically measured TomTom Traffic Index (reported in 2016)[1] as shown in Fig. 9.5(b). The outlier appearance of the Bay Area data is a consequence of the fact that TomTom considers San Francisco and San Jose independently, as $\tau$ depends on the trip distances (included in $t_{ff}$), the trips between these two regions (almost the 30 %) increase the value of $\tau$.

[1]The leading GPS company TomTom reports every year the data for more than 200 cities around the World `https://www.tomtom.com/en_gb/trafficindex/`

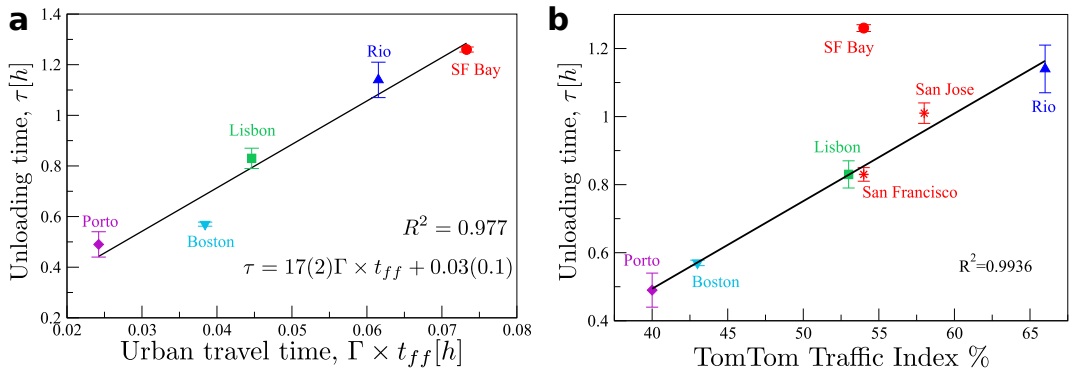


**Figure** 9.5.: **Comparison of congestion levels for the five considered cities. (a)** Linear relation between $\tau$ and the product of the demand to supply ratio with the free travel time of the median travel distance, $\Gamma \times t_{ff}$, for the five subject cities, error bars show the s.d. **(b)** Strikingly, we also found a linear relationship between $\tau$ and the TomTom Traffic Index reported in 2016.

**Table** 9.2.: Comparison of the travel demand properties of the subject cities under free-flow and congested conditions.

| | City | | | | |
|---|---|---|---|---|---|
| | Boston | Porto | Lisbon | Rio | SF Bay |
| Demand-to-supply, $\Gamma$ | 0.129 | 0.101 | 0.121 | 0.180 | 0.213 |
| Mean commuting dist. $d[km]$ | 10.07 | 12.45 | 15.99 | 11.98 | 15.33 |
| s.d. commuting dist. $[km]$ | 2.91 | 2.13 | 2.48 | 2.82 | 2.64 |
| Mean free-travel-time, $t_{ff}[h]$ | 0.184 | 0.188 | 0.267 | 0.218 | 0.234 |
| Mean remaining dist. $\hat{d}[km]$ | 17.69 | 12.69 | 20.47 | 18.44 | 24.00 |
| Mean remaining travel time, $\hat{t}[h]$ | 0.496 | 0.534 | 0.843 | 1.094 | 1.177 |

## 9.4. Phase Transition to Urban Gridlock

Although the considered cities already face a high traffic demand, the studied exponential decay indicates a rapid recovery without the occurrence of long-lasting traffic jams, because the minority of the available streets are in congested state. In this section, we study controlled increments of the cars volume, while maintaining the same spatial distribution of ODs.

Figure 9.6(a) shows the recovery period for all five cities under different loading rates. As $R$ increases, the initially exponential unloading becomes a power law decay beyond a critical value $R_c$. For $R > R_c$, the unloading follows a slower recovery until an inflection point

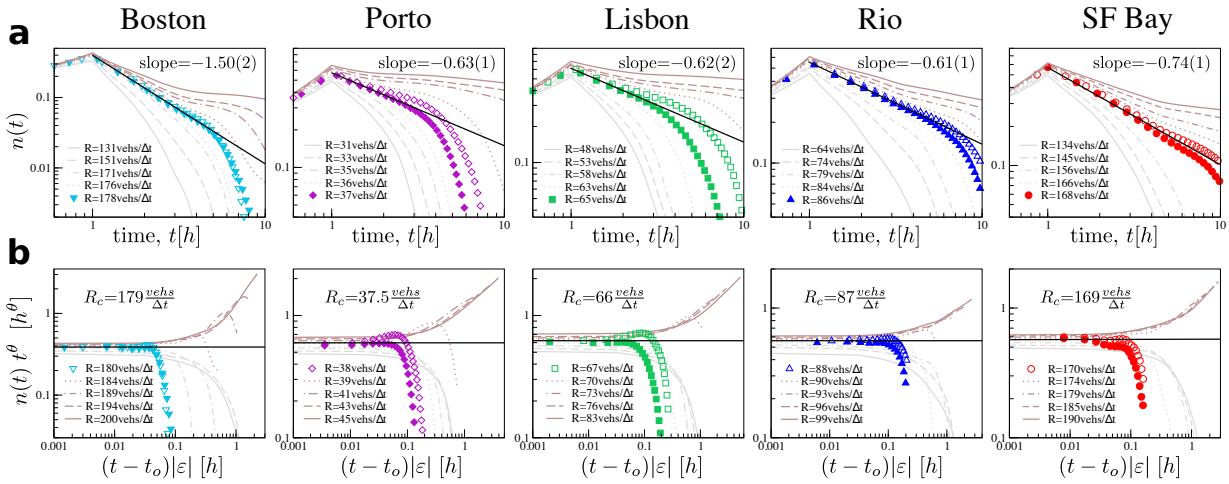


**Figure** 9.6.: **Critical behavior of the fraction of vehicles in the network** $n(t)$. To study the transition to urban gridlocks, we systematically increase the car demand per time step on each city. (**a**) Time series of $n(t)$ after the loading, for several loading rates. Critical condition is indicated by the solid black lines where the $n(t)$, the order parameter, follows a power law $t^{-\theta}$. The non-universal values of the critical exponent $\theta$ are shown for each city. The critical loading rate $R_c$ is estimated as the average loading rate of the two colored curves. (**b**) Scaling plot of data in (**a**), where $\varepsilon = \frac{|R_c^2 - R^2|}{R_c^2}$ is the deviation from criticality. Above the critical point $R > R_c$, the system falls into a gridlock state, from which the system can escape only after several hours. This behavior is typical in non-equilibrium phase transitions (see Fig. 4.5).

appears, where the outflow rate decreases to very low levels and remains so, for a considerable time. Eventually, due to the rerouting possibilities, the system returns to its normal unloading (not shown here). By defining the percentage of vehicles in the network $n(t)$ as the order parameter, the above description resembles the critical behavior of the models in the directed percolation (DP) universality class, with the difference that our system does not have absorbing state due to the rerouting rules. From the slopes of the algebraic regimes for the two R values (curves marked with symbols) closest to the transition threshold, we estimate the critical loading rate $R_c$, and the critical exponent $\theta$. Furthermore, by following the scaling approach in the DP framework [89, 98, 146], the curves collapse when $n(t) \cdot t^{\theta}$ is plotted as a function of $(t-1)\varepsilon$, where $\varepsilon = \frac{|R^2 - R_c^2|}{R_c^2}$ is the deviation from criticality (see Fig. 9.6(b)). Even though $\theta$ is different for each city, indicating non-universality, this behavior evidences that the onset of the traffic gridlock has a non-equilibrium phase transition nature [89, 98, 146].

We further study the transition using the loading rate as control parameter. We define the remaining percentage of vehicles in the network at long times $n(t >> 1 + \tau)$ as an order parameter. We arbitrarily test here $t = 1h + 7\tau$. Note this is a factor of the current recovery

time ($\tau$), allowing us to compare cities and the magnitude of traffic collapse of respect to the current state. In this case, in Fig. 9.7(a) we show $n(1h + 7\tau)$ as a function of $\frac{R}{R_c}$ for all cities. As depicted, with increasing $\frac{R}{R_c}$, $n(1h + 7\tau)$ increases continuously at the vicinity of $\frac{R}{R_c}$=1.0. For this transition of second-order, the variation of $n(t_o + 7\tau)$ follows a power law, $n(t_o + 7\tau) \sim \varepsilon^{\beta}$ shown in the inset of Fig. 9.7(a).

Let us define a second order parameter, associated with the temporal dynamic. First, the value of $n(\tau)$ is identified for the empirical loading rate $R_{now}$ in cities today (see Fig 9.2(a)). We then measure the recovery time T, defined as how long it takes to reach the current value of $n(\tau)$ when the vehicle rate increases. In order to compare the response of various cities, we define $\left(\frac{\mathrm{T}}{\tau}\right)^{\theta}$ as the temporal order parameter. As expected, Fig. 9.7(b) shows how this quantity diverges at the vicinity of $\frac{R}{R_c}$=1.0.

Figure 9.8 depicts the temporal evolution of the five city road networks for $R{>}R_c$. Let us focus on Boston, after the $1st$ hour, the system reaches a high occupancy with some traffic jams formed around low-capacity configurations as roundabouts and intersections of two-way streets. Then, during a slow and short recovery period, vehicles with reasonably congested routes can reach their destinations. However, most of the vehicles remain stuck in large traffic jams that become long-lasting gridlocks. Finally, only when these gridlocks are resolved, the system return to its normal unloading. In analogy to the DP framework, the emergence of long-lasting gridlocks play the role of the absorbing states with the difference that they can be solved due to the re-routing behavior.

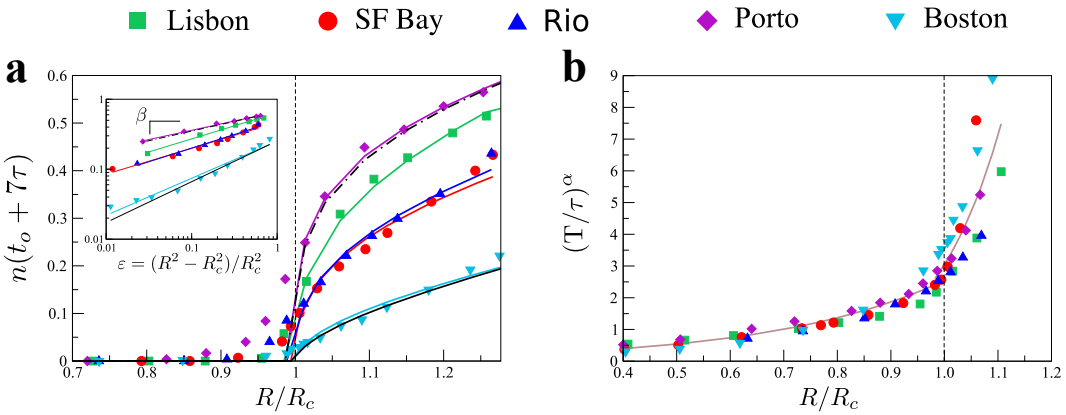


**Figure** 9.7.: **Phase transition in terms of the control parameter** $R/R_c$. (**a**) Fraction of vehicles at $t$=$1h + 7\tau$ vs $R/R_c$ is plotted for the five cities. Inset: same data in logarithmic scales, the solid lines show $\varepsilon^{\beta}$. (**b**) Recovery time T diverges at the critical point. A data collapse can be obtained by plotting the quantity $(\mathrm{T}/\tau)^{\theta}$.

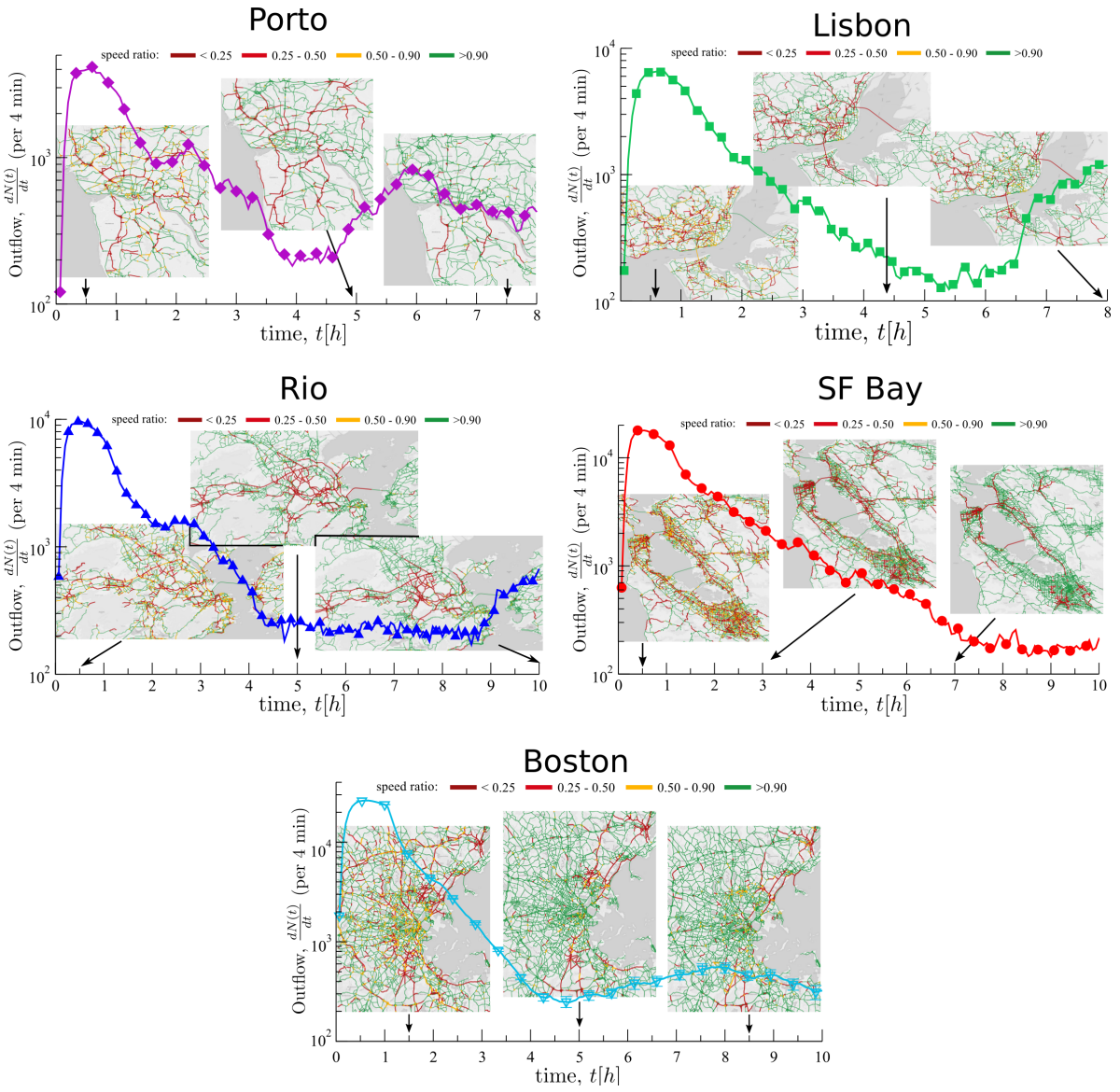


**Figure** 9.8.: **Snapshots of the city networks at three different times of its evolution using $R>R_c$.** We consider the normalized velocity on every link, that is, the current speed (with 4-minutes resolution) divided by its limited maximal velocity. Thus, the road segments are classified into three categories according to the speed ratio: below 0.5 (red), between 0.4-0.9 (yellow) and above 0.9 (green). Let us focus in the Boston case. Observing the clusters of each color, one can realize that at $t$=1$h$, giant traffic jams have already been formed. At $t$=1$h + \tau$, most vehicles are trapped in the gridlock. Finally at $t$=1$h + 7\tau$, the long-lasting traffic jams are still being resolved.

## 9.5. Discussion

We have studied the transition to congestion in urban road networks informed by empirical travel demand and road capacity. For the first time, this transition is defined in terms of an unloading time or recovery period ($\tau$) that has analogies with a non-equilibrium phase transition, resembling directed percolation. We focus on analyzing the urban traffic congestion as a loading and unloading process. From realistic simulations of the morning peak hours, we show that the congestion level of the five subject cities can be described by two observable quantities, car demand to road supply ratio ($\Gamma$) and the median of the free travel time distribution ($t_{ff}$). Our results offer quantitative insights of the interplay in urban traffic dynamics between the available capacity of road infrastructure and the travel demand defined by both the distances traveled and the number of cars. In addition, we study the emergence of congestion increasing the number of cars, keeping the trip distributions and street capacities unchanged. In this case, our findings strongly support the notion that the transitions to urban traffic gridlock resemble the DP universality class, and can be approached with the framework of non-equilibrium phase transitions. Future challenges include unveiling nature of the critical behavior and quantifying the clustering dynamic of the congested roads. We have uncovered a novel relevance on the dynamics of the recovery period and related it to measurable urban quantities based on actual travel demand. This work suggests a change of paradigm in the study of traffic congestion, in the sense that the unloading process can give us more insights about the interplay between topology and travel demand.

# 10. Conclusions

In addition to the economic and environmental impacts, traffic congestion itself represents a contradiction in human life, as the motor vehicle - a symbol of freedom and autonomy - now is a source of stress and unhappiness [6]. This perception was one of the underlying motivation for undertaking this research. Throughout this thesis, we try to convey the idea that the concepts of statistical physics allow us to better understanding the emergence of traffic congestion. We have covered three levels of complexity, ranging from traffic jams on a single road to the urban traffic gridlock on real cities, including the jamming processes in simple models on lattice grids. Curiously, in all three levels the traffic dynamics was based on cellular automata models. In the following, we summarize the main findings for each part of this thesis.

**Part I: The Street**

At the highway level the problem is focused on the macroscopic properties of vehicular traffic produced by microscopic evolution rules, which can be addressed by the dynamic behaviour of simple cellular automata (CA). But, what part of these features is determined by the driving rules alone? In Chapter 3, we proposed a Monte Carlo method that, without any dynamical simulation, can reproduce some of those crucial features in a highway traffic dynamics. By generating states according with CA rules and assuming all micro-states as equally probable we have reproduced with good agreement the fundamental diagram for both the NaSch and the Olmos-Muñoz models. The procedure also reproduces the data dispersion observed in empirical diagrams. Even better, in the case of the Olmos-Muñoz model this method reproduce the empirical fundamental diagram measured for Bogota city. Moreover, by using the Wardrop's relation (Eq. 2.5) it was possible to generate a *time-mean* fundamental diagram that exhibits not just the *discontinuous* phase separation between free-flow and synchronized phases but also the high-flow states. Additionally, by computing the *distance-headways* distribution according to the driving rules of NaSch model, and just for the most likely states of a finite road, we obtained the broad distribution observed in reality.

What these evidences suggest is that most part of the macroscopic behaviour of highway traffic flows is a consequence of the non-dynamical part of the driving rules, confirming the decisive role played by the local driving style. Since we just assumed equally probable equilibrium states, our findings become a novel statistical approach to describing the flow on a single road. Of course, these results should be validated on other roads with other automaton rules, and this will be an interest subject of future work. These results were presented in the Traffic and Granular Flow 2013 conference in Aachen (Germany) and published in the proceedings of the event [1].

Regarding accidents, in Chapter 1 we showed how previous studies have considered dangerous situations instead of real crashes where the involved cars remain stationary for a while. In reality, accidents induced by careless driving generally involve vehicles with large velocities, because the combined effect of an abrupt velocity change and a small safety gap produces the vehicle crash. In addition, a crash usually needs a recovery time to disappear. Considering these two aspects of car accidents, the Olmos-Muñoz CA model allows a deeper study, as follows. We characterized a distracted driver as one who delays one time step its braking maneuver if the car ahead is moving. Thus, if the car ahead brakes at time $t$, it is probable that there will be a crash at time $t + 1$. Because in the original model a car occupies two cells, this is also the minimal distance between two consecutive cars. So an accident occurs when only a single cell separates two cars. Because of the driving rules themselves, both cars stay at rest for a while, generating a local perturbation on the event place. In fact, we realized the tremendous effect that these accidents have on the global state of the system, even for low percentages of distracted drivers. Once distracted drivers appear, an avalanche of accidents occurs in different locations of the road, the generated density waves evolve to a long-lasting jams and, thereafter, the road is divided into free-flow and congested sections. This strong effects made pause our efforts and rethink the scope of this idea, with the hope that with the recent availability of data this idea can be resumed in the future.

**Part II: The Grid**

In this part, concerning traffic model on regular grids (like in many neighbourhoods), we have focused on the Biham-Middleton and Levine model (BML), which over the last two decades has become a theoretical underpinning for the study of jamming phenomena and congestion patterns on vehicular traffic research. Originally defined on square lattices, the model exhibits three phases; the typical free flow and jammed phases plus an intermediate phase where jams and freely traffic coexist. The origin of the latter phase remained as a mystery during almost a decade time, and only few efforts were disposed to investigate the

effect of other grids on the model's behaviour. We addressed both issues by studying the BML on square and honeycomb-like lattices.

**Square lattices (Chapter 6):** We found the origin of the intermediate phase and solved most of the open questions on the BML model by studying it as an anisotropic system with a preferred (north-east) direction, an aspect that has shown to be fundamental for the analysis of many systems in granular matter and animal collective behaviour, but overlooked in most previous studies on BML. By performing an anisotropic scaling analysis on the BML model phase transition, inspired on the directed percolation formalism (DP), we arrived to the interesting result that the jamming process behaves distinctively as two separated phase transitions along different directions, namely, whether the system is longer in the direction of traffic flow (longitudinal system) or in the transversal direction (transversal system). The critical densities for these transitions enclose the density interval of intermediate states and can be approximated by mean-field analysis, all derived from the anisotropic exponent relating the longitudinal and transversal correlation lengths. Therefore, we show that the intriguing intermediate states in the original model are just a superposition of these two different behaviours of the phase transition, solving, by the way, most mysteries behind the BML model. Moreover, establishing the BML as a paradigmatic model with scaling anisotropy, adds a new instance to the scare list of such anisotropic models like the Anisotropic Nearest-Neighbor Ising model (ANNI) and the Driven Lattice-Gas Model. These results were published in PRE Rapid Communications [2].

**Honeycomb lattices (Chapter 7):** We presented a comprehensive analysis of the BML model, also with two car directions, but on a hypothetical city with a perfect honeycomb street network. In contrast with the same model on a square lattice, there is no intermediate phase, but a sharp phase transition between free and totally congested flow. Surprisingly, despite the fact that the system still has a preferred flow direction, there is no anisotropy in the correlation length. This fact could be a consequence of the symmetries of the honeycomb network, already reported in other contexts [160, 166]. If this is the reason for such isotropy or not will be an interesting subject of future research. A manuscript with these results was submitted to PRE [3].

With an isotropic behaviour, the system can be studied with the tools of classical finite-size scaling. So, we characterized completely the transition, measuring the critical density (lower than the square case) and three critical exponents. What is more interesting is that the BML model on honeycomb lattices shows to be more resilient against perturbations than the original model on a square lattice. Although the critical density is lower for the honeycomb than for the square, this order reverses when we introduce small and simple

perturbations, like increasing the traffic light periods or including a random update with very low probabilities to brake. Since such perturbations are ubiquitous in real traffic, these results question the actual role of the square grid-like urban designs and supports honeycombs as a more efficient alternative for traffic; suggesting, by the way, a change of paradigm in urban design concepts. Thinking on practical applications, its worth nothing that what makes a street network a honeycomb is not the hexagons, but the network connections, with three streets at each intersection; therefore, a brick-like structure is also a honeycomb, but easier to implement. Indeed, a normal square network can be transformed into a brick like structure by changing some streets to pedestrian zones. Since this result is in a sense controversial, it had a remarkable impact in the media, as shown in Appendix D.

Taken together, our findings point out the relevance of anisotropy, either in the flow dynamics or inherent to the network. As we demonstrated, the topology plays so a crucial role on the traffic behaviour than even determines the critical features in the proximity of the collapse. In case of real street networks, topology not just includes the geometry, but also street capacity properties like maximal speed, number of lanes and traffic lights. The work presented here was the starting point for our attempts in Part III to tackle the congestion at city scale.

**Part III: The City**

As a complex phenomenon, urban traffic has emergent patterns that we can observe and quantify in the streets. Non-equilibrium relations between the flow of cars and their spatial density have successfully informed traffic models over the years. However, at urban scale, characterizing the transition that gives rise to the appearance and growth of congestion bottlenecks remains an elusive task. The connection between streets topology and the spatial dynamics of the population is still a missing component to comprehensively describe the emergence of urban congestion.

To investigate such connection, we ran cellular automata simulations at the car level on the road network of five cities: Rio, Lisbon, Porto, S. Francisco Bay and Boston, with origin-destiny matrices obtained by [37] from empirical mobile phones data. The model implements the NaSch model on each link, and intersections are solved by assigning turns on a simple and heuristic way. The simulation reproduces qualitatively the congestions reported by Google Maps for those cities. Next, the model was employed to simulate the recovering period after a 1h charge at rush hours, a recovering period that exhibits an exponential decay of characteristic time $\tau$ in the numbers of cars in the network. We found that such a characteristic time depends on two quantities that can be measured in cities. The first one is the

distribution of free flow travel times ($t_{ff}$) given by trip distances, and the second is the road usage ($\Gamma$), given by the total vehicle demand divided by the road supply. Since changing either of these two quantities to improve $\tau$, this finding would directly inform interventions to improve congestion in any city. Our results offer quantitative insights of the interplay in urban traffic dynamics between the available capacity of road infrastructure and the travel demand defined by both the number of cars and the traveled distances. Our findings point out to that the recovery process can give more insights about congestion than even the loading process. Thus, this work suggests a change of paradigm in the study of traffic congestion.

In addition, by increasing the volume of cars in the network and keeping the road capacity and the empirical spatial dynamics from origins to destinations unchanged, we identified a distinctive phase transition to a collapsed state. The temporal dynamics of the system could be described in terms of an unloading time or recovery period, in analogy with a non-equilibrium phase transition and resembling directed percolation. Finally, we characterized the transition to congestion by measuring two critical exponents that demonstrate the non-equilibrium nature of the urban traffic gridlock phenomenon. Future challenges include unveiling the nature of the critical behaviour and quantifying the clustering dynamic of the congested roads.

The next question that arises is: what are the next steps? Several answers come naturally. At network level, a first goal is to extend the network analysis to different times of the day, intending to reproduce how the macroscopic traffic behaviour evolves dynamically during the day [32]. The model itself can also be improved by implementing the real number of lanes and traffic lights in order to verify that our findings remain qualitatively the same. But even more interesting is to quantify, still within the non-equilibrium phase transitions context, the spreading dynamics of the traffic jams. Complementing this ideas, the understanding of human behaviour in choosing routes is a topic we need to go deeper. Although we have assigned route with the shortest time path routing algorithm, very recent works using GPS data [186, 187] have given evidence that this is not the case. Once this was well understood, one can start studying strategies for congestion mitigation which opens up a wide range of possibilities. Among them, I have particular interest in re-routing strategies and in the evaluation of scenarios where road segments are added (or removed) to the network.

At the road level, a first goal consists on comparing different strategies to simulate accidents with the real data that has is only recently at disposal [188]. But even more interesting is to explore the effect of such car accidents on the global behaviour of real city street networks, testing different strategies to mitigate the effects. Also, making the link between Part II and

III of this work, it would be intriguing to investigate what the performance would be of a real city with a square street network (like Manhattan) if it is turned to a honeycomb-like street structure, but keeping the same travel demand. Such a work would give valuable insights in the discussion of different urban planning strategies for neighbourhood and cities.

This work has explored traffic problems at three levels: road (street), grid (neighbourhoods) and network (cities) by using cellular automata models plus analysis tools of statistical mechanics. So, it combines the power of a computational description at the level of each car with a solid theoretical framework, allowing to derive more reliable conclusions. This combined strategy looks as a promising path to address the modeling of such a complex system as the vehicular traffic flow in large cities, an issue that plays a relevant role in the quality and productivity of everyday's life for more than one half of the world population.

# A. Appendix A: A Simple Statistical Method for Reproducing the Highway Traffic

# A Simple Statistical Method for Reproducing the Highway Traffic

**Luis Eduardo Olmos and José Daniel Muñoz**

**Abstract** Some of the most important questions concerning the traffic flow theory are focused on the correct functional form of the empirical flow-density fundamental diagram. Although most cellular automata intend to reproduce this diagram by measuring the limit steady-states from the dynamic simulation, real roads are constantly perturbed by external factors, driving the system to explore a much broader phase space. Hereby, we show that a Monte Carlo sampling of all states compatible with a driving rule (previously derived for Bogota) actually reproduces the measured fundamental diagram, both in mean values and dispersion, when all such states are assumed equally probable. Even more, by using the Wardrop's relation, the same gathered data also approximates the general form of the *time-mean* fundamental diagrams. These results suggest that driving rules are much richer in information than usually expected and, that the assumption of equally probable states plus a finite length of road may be a first model for the statistical description of highways.

## 1 Introduction

Since the beginnings the investigation in traffic flow is mainly focused on the functional relationships between the flow $q$, the space-mean speed $v_s$ and the density of vehicles on a road $\rho$ and even Greenshields [1] found a linear relationship between speed and density. The first fundamental diagrams were found just by fitting a relation $q(\rho) = \rho \cdot v(\rho)$ of the empirical data, where $v(\rho)$ is again the fitted empirical velocity-density relationship. However, this is much more complex than just a well-defined function. It is discontinuous and, for high densities, the data are widely scattered, which is usually interpreted as an effect of fluctuations or of an instability in vehicle dynamics. This property shows that rather than the fundamental diagram, the microscopic structure is the key for the understanding of the traffic flow characteristics. That is why microscopic models have been more successful over other models. Among those, cellular automata models (CA) have been some of the most fruitful, as they have reproduced the more complex properties of the

L.E. Olmos (✉) • J.D. Muñoz
Universidad Nacional de Colombia, Av. Carrera 30 # 45 Bogotá, Colombia
e-mail: leolmoss@unal.edu.co; jdmunozc@unal.edu.co



M. Chraibi et al. (eds.), *Traffic and Granular Flow '13*,
DOI 10.1007/978-3-319-10629-8_46

traffic flow. The success of these models is due to its simplicity and flexibility in the introduction of individual driving features, which are ultimately the responsible for the complex behaviour. Nevertheless, the traffic flow is a open system that, in general, is continuously perturbed at random by real factors (like pedestrians, or road imperfections) which make the system walks about several states. This arises the question of which traffic features can be reproduced by a Monte Carlo exploration of the phase space allowed by the driving rules.

## 2 Data Collection

Most empirical data are collected by stationary inductive loops at many highway locations. The loop detects a vehicle, it records the time of passing and it can also calculated the vehicle speed $v_i$. Quantities as $q$ and $v$ can be derived and presented in aggregated values for a time period, for instance, 1 or 5 min. The flow $q$ is given by the number of cars $N(\Delta t)$ passing the detector per time interval $\Delta t$, i.e. $q = \frac{N(\Delta t)}{\Delta t}$. The time-mean speed, $v_t$, is obtained as the arithmetic average $v_t = \frac{1}{N}\sum_{i=1}^{N} v_i$. However, the determination of density is rather problematic. The difficulty arises from the fact the density is derived from the hydrodynamic relation $\rho = \frac{q}{v}$ and, when $v_t$ is used, standing or slow cars are not detected, so then density is underestimated. By assuming stationary conditions, some authors avoid this difficulty by computing the space-mean speed as the harmonic mean of the time measurements [2, 4, 6, 10]:

$$v_s = \frac{1}{\frac{1}{N}\sum_{i=1}^{N}\frac{1}{v_i}} \quad . \tag{1}$$

The harmonic mean value corrects the detection of slow cars, but it does not allow to account for standing cars. Even so, this relation is the mostly used in the empirical data analysis. On respect to the differences between these two speed averages Wardrop [11] found that under homogeneous and stationary conditions:

$$v_t = \frac{\sigma_s^2}{v_s} + v_s \quad , \tag{2}$$

where $\sigma_s^2$ is the variance of space mean speed. Equation 2 is not useful if one has just local measurements (real case). This difficulty makes the single-vehicle data more interesting over aggregated data for the study of traffic flow. In other words, the histograms of quantities such as the time interval between consecutive cars (*temporal-headway*) or the spatial distance between them, *distance-headway* or *gap*, contains much more valuable information that simple relationships among average values [2, 6].

## 3 Methods

Let us implement a simple Monte Carlo sampling from the driving rules to generate at random the traffic states on the road in such a way that the states so obtained fulfill the driving rules. With this aim, the road is represented by a one-dimensional lattice of $L$ sites with periodic boundaries. Since the empirical data are aggregated for short time periods we must use small road sizes, otherwise, the data dispersion would be reduced. Then, we choose a number of cars $N$ and throw them randomly into the road. After that, each car computes its distance headway and takes the maximal allowed velocity $v_{com}$ (comfort velocity) according to the rules of the CA model we are studying. So, we are absorbing both the non-equilibrium characteristic of traffic and the fact that drivers want to move as fast as possible. For each state so generated, it measured the spatial variables $\rho$ and $q$ which corresponds to a point in the fundamental diagram. The process is repeated many times for each number of cars $N \leq L$ and the fundamental diagram was obtained by cumulating these samples onto a two-dimensional histogram on the flow-density map (see Fig. 1). The main assumption of this work is that all randomly generated configurations, understood as the disposition of the cars on the road, are equally probable. But it is not the same for the macroscopic states of the traffic defined by the value of $q$, $v$ and $\rho$. Figure 1 right shows that for a value of $\rho$ there is a value of $q$ more probable which just depends on the driving rules. We identify the most likely regions as the realistic states observed in empirical measurements.

We studied the driving rules of two CA models. The first one is the deterministic case of the well known NaSch model [5] where $v_{com} = gap$ for $gap \leq v_{max}$ and $v_{com} = v_{max}$ for $gap > v_{max}$. The second one is the Olmos-Muñoz model [7, 8] which was developed and implemented by the authors for reproducing the behavior of traffic flow in Bogota. This model keep in mind the particularities of Bogotan drivers, measured directly inside a car running on Bogota's highways. In this model, each car occupies two cells, and the gaps the driver uses to decide to brake or

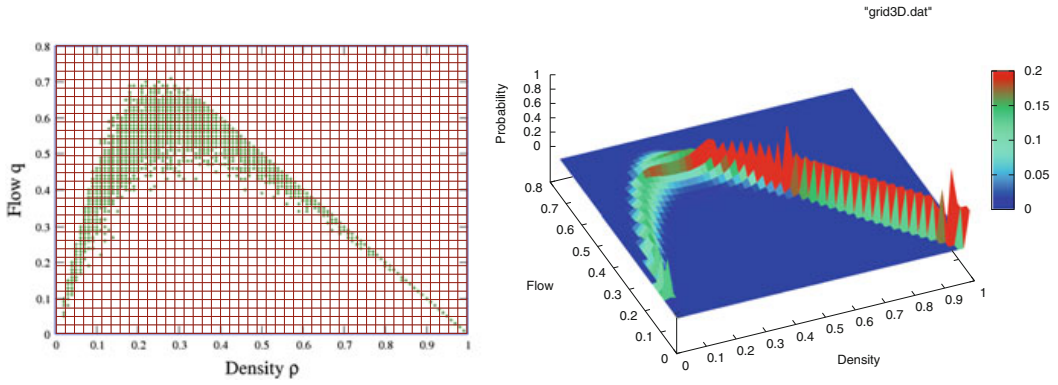


**Fig. 1** Monte Carlo sampling from driving rules to generate at random the traffic states of the road. Scatter plot of the fundamental diagram (*left*) and density of states (*right*) obtained from the highway traffic states of these random configurations

**Table 1** Values of $v_{com}$ for each *gap* in the Olmos Muñoz model

| Gap | $v_{com}$ | Gap | $v_{com}$ |
|---|---|---|---|
| 0 or 1 | 0 | 6 | 6 |
| 2 | 1 | 7 | 7 |
| 3 | 2 | 8 | 9 |
| 4 | 3 | 9 | 9 |
| 5 | 4 | 10 | 10 |

accelerate are different for each speed. Then, if the headway distance is less or equal to the brake gap, the car brakes, and if it is greater than the accelerate gap, it accelerates; otherwise, the speed remains constant. Here, the comfort speed $v_{com}$ corresponds to the largest one at which the gap ahead is lower or equal than the accelerate gap. The other two elements are delay time on the acceleration ( the time it takes the car to reach the next discrete speed value) and break lights that force to brake when the car ahead breaks. Since these last two elements have a dynamical nature, they cannot be included in our method. This model is not as simple as the NaSch model but the value of $v_{com}$ is summarized in the Table 1.

## 4 Results for the Fundamental Diagram

Figure 2 up shows the contour graph obtained for the frequency to obtain states with flux $q$ at density $\rho$ for the driving rules of the deterministic NaSch model. This is compared to the steady states of the dynamic simulation of the cellular automata. It is clear that around the value of maximum flow the most probable states do not match with the equilibrium states of the dynamical simulation. This could be expected, since there is not disorder in the deterministic NaSch model and, thus, it describes an unrealistic traffic flow. Nevertheless, by setting a non-zero value for the stochastic parameter, the match can improve. Figure 2 down shows the comparison between the empirical fundamental diagram measured for Bogota (built from *space-mean* measures in [7]) and the result obtained with the Monte Carlo method by using the Olmos-Muñoz driving rules (Table 1). This figure shows that the most likely states of the system (red color region) match in a good agreement to the real data measurements of a non-equilibrium system.

As we mentioned above, this method build the fundamental diagrams from *space-mean* variables. This arises the question of how a fundamental diagram is based on *time-mean* quantities. Although our method is not dynamic, we can compute the local quantities by using the Eq. 2, since $\sigma_s^2$ can be estimated from the histogram by computing standard deviations on horizontal sections of the diagram. So then, $v_t$ can be obtained from $v_s$, the flow $q$ remains the same but the density is recalculated from $\rho = \frac{q}{v_t}$. This step is included in the method before computing the density of the states. Figure 3 shows the surprising result. We obtain a fundamental diagram very similar to those measured empirically using temporal

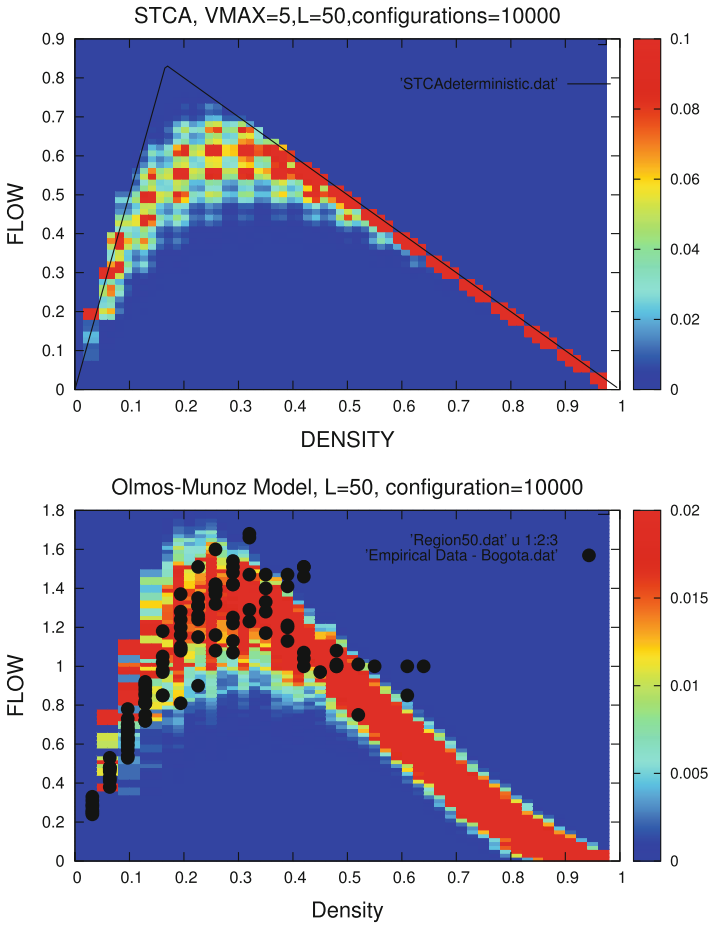


**Fig. 2** Contour graph of the fundamental diagram obtained from the driving rules of the deterministic NaSch model (*top*) and of the Olmos-Muñoz model (*down*) for $L = 50$. *Top*: the right line corresponds to the steady state from a cellular automata simulation. *Down*: the *black dots* correspond to the empirical fundamental diagram measured in Bogota

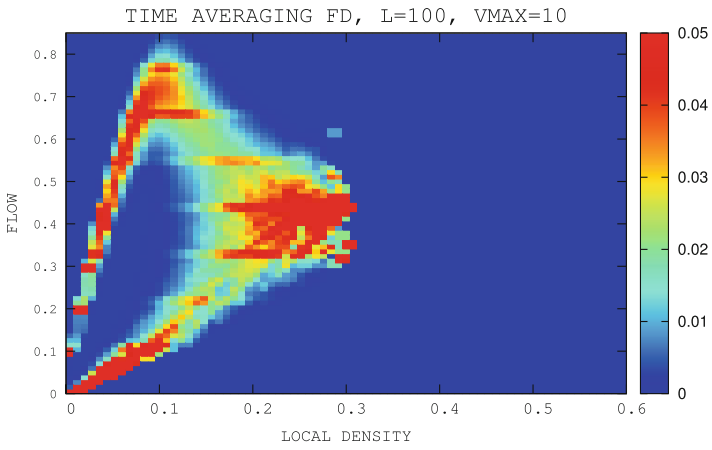


**Fig. 3** Contour plot of the fundamental diagram obtained by transforming the *space-mean* variables in *time-mean* by using the Eq. 2 and the driving rules of the NaSch model. It is clear the similarity to those measured empirically using temporal averaged variables. It should remark that the discontinuity emerges naturally as a region of unlikely states

averaged variables. Focusing on the most likely states, one can distinguish the free-flow branch with high-flow states, and separated from this, a wide dispersed data appears as the synchronized phase under the perspective of the three-phases theory [3]. Therefore, the discontinuity appears naturally as a region of unlikely states. Besides that, it appears a region with low flow and a underestimated density, in similarity with the real collected data.

## 5 Analytical Approach and Distribution of Spatial Headways

We are also interested in the features of the microscopic structure that this method can reproduce. Clearly, the *spatial-headway distribution* is the characteristic that we can study directly. Due to the assumption of equally probable microstates, this method neglects the correlation between the gaps in front of successive cars. If we assume further that the length of the road $L \to \infty$, one can analytically derive that the gaps distribute as

$$\wp(gap) = \rho \cdot (1-\rho)^{gap} \text{ and, therefore, } \langle gap \rangle = \sum_{gap=0}^{\infty} gap \cdot \wp(gap) = \frac{1-\rho}{\rho} \tag{3}$$

However, the empirical distribution of distance-headways reveals the inadequacy of this equation. As Fig. 4 left shows, this distribution is surprisingly broad. Even so, it is interesting to see that the right hand of the Eq. 3 predicts an average gap decreasing with the inverse density $\frac{1}{\rho}$, as Tilch and Helbing reported [10]. Thus, let us go more deeply with the idea. Since the $v_{com}$ is related with the *gap*, we can study the distribution of speeds. The distribution of speeds $\wp(v_{com})$ for the deterministic NaSch model, for instance, is the same $\wp(gap)$ for $v_{com} < v_{max}$ and $\wp(v_{max}) = \sum_{i=v_{max}}^{\infty} i \cdot \rho \cdot (1-\rho)^i$ for $v_{max}$. Then, the average speed can be written as

$$\langle v \rangle = \frac{1-\rho}{\rho} \cdot (1-(1-\rho)^{v_{max}}) \quad , \tag{4}$$

and one can obtain the flow immediately as $q = \rho \cdot \langle v \rangle$. Note that Eq. 4 with $v_{max} = 1$ reproduces Greenshield's model, and even other empirical models can be reproduced with other values of $v_{max}$. The kind of analytical calculations resulting in Eq. 4 are typical of the naive mean-field theory[1] and its generalizations [9]. These

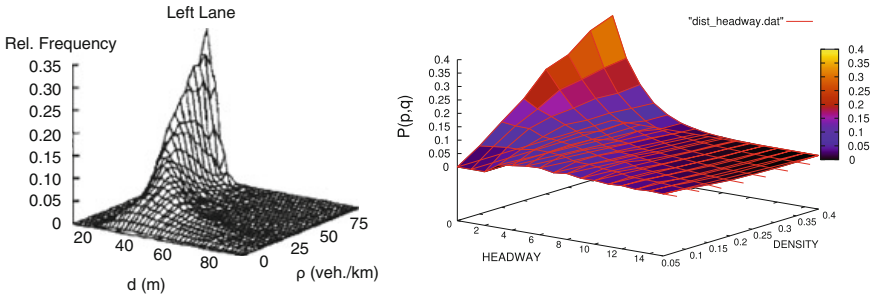


**Fig. 4** The broad distribution of vehicle distance-headways at all densities $\rho$. *Left*: Empirical distribution from Tilch and Helbing [10]. *Right*: Distance-headways distribution just for most likely states in the Monte Carlo sampling of the NaSch model. Figure shows the same broad distribution observed in empirical data

[1] Actually our calculations are more naive than the naive mean-field theory.

theories were applied with success to the NaSch model at the beginning of the past decade but, as we already noted, they could not reproduce the distance-headway distribution of the stationary states of the CA model on a large system. Nevertheless, we are not interested in the stationary states of a cellular automaton but in the most likely states one would measure in reality. Therefore, we computed the distance-headway distribution for a finite system just for most likely states (the red color regions in Fig. 2 up). The results, in Fig. 4 right, shows the same broad distribution observed in empirical data.

**Conclusions**

Hereby, we have showed that a Monte Carlo exploration of the driving rules can reproduce the empirical fundamental diagram. Indeed, by generating states according with the Olmos-Muñoz model, and assuming that all these microstates are equally probable, we have reproduced with good agreement the capacity and the data dispersion of the fundamental diagram measured for Bogota city. Even more, by using the Wardrop's relation (Eq. 2), our data also approximates the general form of the *time-mean* fundamental diagrams, revealing a naturally emergence of both the discontinuity between free-flow and congested phases, and the high-flow states in this diagram as a consequence of such relation. In addition, by computing the *distance-headways* distribution according to the driving rules of NaSch model and just for the most likely states of a finite road, we have reproduced the broad distribution observed in reality. All this result suggests that the non-dynamical driving rules are more than a simulation mechanism; they can give valuable information about the macroscopic behaviour of the highway traffic flow. In addition, they also suggest that the assumption of equal probabilities for all states compatible with the driving rule plus a finite length of road may be a first model for the statistical description of highways. Of course, this hypothesis should be validated on other roads with other automaton rules, and this will be an interest subject of future work.

## References

1. B.D. Greenshields, A study of traffic capacity, in *Highway Research Board Proceedings*, vol. 14, (Washington DC, 1935), p. 448
2. D. Helbing, Traffic and related self-drive many-particle systems. Rev. Mod. Phys. **73**, 1067–1141 (2001)
3. B. Kerner, *The Physics of Traffic: Empirical Freeway Pattern Features, Engineering Applications and Theory*. Understanding Complex Systems (Springer, 2004)
4. V. Knoop, S.P. Hoogendoorn, H. van Zuylen, Empirical differences between time mean speed and space mean speed, in *Traffic and Granular Flow'07 Proceedings* (Springer, Orsay, France, 2008), pp. 351–356

5. K. Nagel, M. Schrekenberg, A cellular automaton model for freeway traffic. J. Phys. I Fr. **2**, 2221–2229 (1992)
6. L. Neubert, L. Santen, A. Schadschneider, M. Schreckenberg, Single-vehicle data of highway traffic: a statistical analysis. Phys. Rev. E **60**, 6480 (1999)
7. L.E. Olmos, J.D. Muñoz, Traffic flow in Bogotá, in *Traffic and Granular Flow'05 Proceedings* (Springer, Berlin, Germany, 2006), p. 403
8. L.E. Olmos, J.D. Muñoz, A cellular automaton model for the traffic flow in Bogotá. Int. J. Mod. Phys. C **15**, 1397 (2004)
9. A. Schadschneider, Traffic flow: a statistical physics point of view. Physica A **313**, 153–187 (2002)
10. B. Tilch, D. Helbing, Evaluation of single vehicle data in dependence of the vehicle-type, lane, and site, in *Traffic and Granular Flow'99* (Springer, Berlin, Stuttgart, Germany, 2000), p. 333
11. J.G. Wardrop, Some theoretical aspects of road traffic research, in *Proceedings of the Institution of Civil Engineers*, vol. 1 of 2, (London, Great Britain, 1952)

# B. Appendix B: Unraveling the puzzling intermediate states in the Biham-Middleton-Levine traffic model

PHYSICAL REVIEW E **91**, 050801(R) (2015)

# Unraveling the puzzling intermediate states in the Biham-Middleton-Levine traffic model

L. E. Olmos* and J. D. Muñoz†

*Simulation of Physical Systems Group, CeiBA-Complejidad, Physics Department, National University of Colombia, Bogotá, Colombia*

(Received 16 February 2015; published 18 May 2015)

The Biham-Middleton-Levine (BML) traffic model, a cellular automaton with eastbound and northbound cars moving by turns on a square lattice, has been an underpinning model in the study of collective behavior by cars, pedestrians, and even internet packages. Contrary to initial beliefs that the model exhibits a sharp phase transition from freely flowing to fully jammed, it has been reported that it shows intermediate stable phases, where jams and freely flowing traffic coexist, but there is no clear understanding of their origin. Here, we analyze the model as an anisotropic system with a preferred fluid direction (northeast) and find that it exhibits two differentiated phase transitions: the system is either longer in the flow direction (longitudinal) or perpendicular to it (transversal). The critical densities where these transitions occur enclose the density interval of intermediate states and can be approximated by mean-field analysis, all derived from the anisotropic exponent relating the longitudinal and transversal correlation lengths. Thus, we arrive at the interesting result that the puzzling intermediate states in the original model are just a superposition of these two different behaviors of the phase transition, solving by the way most mysteries behind the BML model, which turns out to be a paradigmatic example of such anisotropic critical systems.

DOI: 10.1103/PhysRevE.91.050801 PACS number(s): 89.40.Bb, 05.20.Dd, 05.65.+b, 87.10.Hk

In the recent urbanization era, society faces an inevitable increase of traffic congestion, turning its attention to urban road networks. Nowadays, it is widely assumed that a proper understanding of the mechanisms leading jamming processes is indispensable for improving the efficiency of transportation systems. The Biham-Middleton-Levine (BML) model [1] is, perhaps, the simplest traffic cellular automaton able to exhibit self-organization, pattern formation, and phase transitions [1–4]. Although the BML model oversimplifies the city traffic in a way that does not directly resemble an urban network (i.e., with cars at the nodes and not at the links), much extensive research on flux and collective behavior has been based on it, not just for car traffic (see [5,6] and references in [7,8]) but also for pedestrian traffic [9,10] and information packages on the Internet [11]. For more than a decade, it has been believed that at a certain critical car density $\rho_c$, the system exhibits what seems to be a first order phase transition between two phases: a free-flowing phase, where all cars move freely at all time steps (the average velocity of cars $v = 1$), and a completely jamming phase, where no car moves at all ($v = 0$). The value of $\rho_c$ decreases with increasing system size, possibly reaching the value $\rho_c = 0$ as the system size approaches infinity. Then, it was thought that the BML model would be similar to other well-known systems in statistical physics exhibiting phase transitions, e.g., percolation. However, all these conventional beliefs started to be reconsidered since Yung [12] and D'Souza [13,14] realized the existence of intermediate stable phases where free-flowing and jamming phases coexist (see Fig. 1). The structure of these states is highly regular, with jams' wave fronts moving through freely flowing traffic in a wide density region, and the value of the average velocity ($0 < v < 1$) is extremely sensitive to the aspect ratio of the underlying lattice [15]. Thus, instead of a phase transition as a function of car density, the system would exhibit two bifurcation points, limiting a region where intermediate phases would coexist between the two conventional phases above. Even though these states have been described and their asymptotic speeds have been predicted [13,15], the exact locations of the bifurcation points are very difficult to determine, and no one knows what truly happens as the system size goes to infinity. Moreover, the origin of the intermediate states remain an unsolved puzzle.

In this Rapid Communication we focus on the clear existence of a preferred direction in the model dynamics. Most previous studies have overlooked this feature, even though, as we will show, it is the key for unraveling the puzzling intermediate states of the BML model. The presence of anisotropy has been fundamental in the analysis of force networks in granular matter [16,17] and flocking in collective animal behavior [18]. Classical theoretical models with this feature are the next-nearest-neighbor Ising model (ANNNI) [19] and the driven lattice gas model [20]. The anisotropy should be naturally reflected in the phase transition of BML, making it, in principle, more akin to the anisotropic equivalent in percolation: directed percolation (DP) [21,22]. By performing an anisotropic scaling analysis on the BML model phase transition [23,24], we found that the jamming process behaves distinctively as two separated phase transitions along different directions; namely, the system is longer either in the direction of traffic flow (longitudinal system) or in the transversal direction (transversal system). Our main result is that the puzzling intermediate states in the BML model on square lattices emerge just as a superposition of these two different transitions, solving, by the way, most mysteries behind the BML model.

*Model.* The original BML model considers two types of cars: eastbound (yellow) and northbound (black), moving on a two-dimensional square lattice with periodic boundary conditions. Each lattice site is in one of three states: empty, occupied by a yellow car, or occupied by a black one. The cars are initially randomly distributed over the lattice sites with spatial density $\rho$ (usually taken to be the same, $\rho/2$, for both

*leolmoss@unal.edu.co
†jdmunozc@unal.edu.co

 

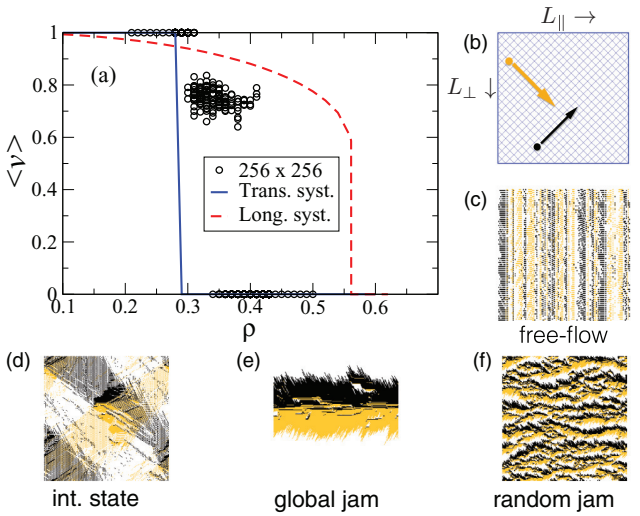


FIG. 1. (Color online) (a) Average velocity $\langle v \rangle$ vs density $\rho$ (circles) for a BML model on a 45°-rotated $256 \times 256$ lattice [as depicted in (b), with eastbound cars in yellow (light gray) and northbound cars in black]. The mean-field approach for longitudinal systems (dashed red line) and the numerical prediction for an infinite transverse system (blue solid line) are also included for comparison. Typical configurations for (c) free flow, (d) intermediate states, (e) one global jam, and (f) random jams are also included.

north- and eastbound cars). The fully deterministic dynamics is as follows: On even (odd) steps, all eastbound (northbound) cars synchronously attempt to advance one lattice site toward the east (north). If the site eastward (northward) of a car is currently empty, it advances. Otherwise, it remains stationary. The system exhibits, therefore, a preferred northeast direction for the flux.

To study the system as an anisotropic one, we explicitly rotated the lattice 45°, so we could control the system lengths along the longitudinal ($L_\parallel$) and transversal ($L_\perp$) directions to the car flow. Although this rotation changes the boundary conditions, the system still exhibits the same three phases observed in the original BML model (see Fig. 1). In anisotropic systems, clusters show different correlation lengths along the longitudinal and transversal directions, $\xi_\parallel$ and $\xi_\perp$, respectively, which scale with different exponents as $\xi_\parallel \sim (\rho - \rho_c)^{-\frac{1}{\nu_\parallel}}$ and $\xi_\perp \sim (\rho - \rho_c)^{-\frac{1}{\nu_\perp}}$ [21,23]. An anisotropy exponent, relating the different scalings of the two correlation lengths, is defined as the ratio $\theta = \frac{\nu_\parallel}{\nu_\perp}$. According to [23–25], when the longitudinal and transversal lengths are related by the constraint $L_\perp \sim L_\parallel^{\frac{1}{\theta}}$, the system behaves as it were effectively isotropic, and standard finite-size scaling (FSS) theory applies again for all percolation quantities, just in terms of the length scale $L_\parallel$. Especially, the transition width and the percolation threshold (both obtained by fitting the transition curve with an error function [26]) scale as

$$\Delta\left(L_\parallel, L_\parallel^{\frac{1}{\theta}}\right) \sim L_\parallel^{-\frac{1}{\nu_\parallel}}, \left|\rho_c - \left\langle \rho_c\left(L_\parallel, L_\parallel^{\frac{1}{\theta}}\right)\right\rangle\right| \sim L_\parallel^{-\frac{1}{\nu_\parallel}}. \quad (1)$$

The exponent $\theta$ can be estimated numerically from the fact that, close to the critical point, the two correlations lengths must be related by $\xi_\parallel \sim \xi_\perp^\theta$. The symbol $\langle \cdot \rangle$ denotes averages over final

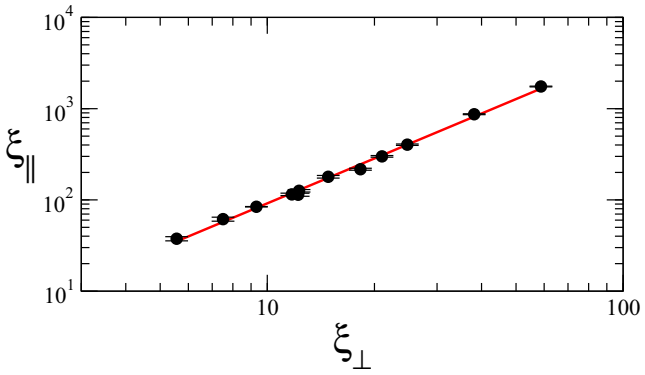


FIG. 2. (Color online) Longitudinal $\xi_\parallel$ and transversal $\xi_\perp$ correlation lengths from final configurations at densities $\rho$ in the range [0.49–0.54] for square lattices of different sizes. The power-law fit gives $\theta = 1.64(3)$ for the anisotropy exponent.

jammed configurations starting from different random initial conditions. With this theory in mind, let us define the parallel (perpendicular) spatial correlation function [2] as

$$G_{\parallel(\perp)}(\vec{r}') = \frac{1}{N}\left\langle \sum_{\vec{r}} \sigma(\vec{r}) \cdot \sigma(\vec{r} + \vec{r}') \right\rangle, \quad (2)$$

where $\sigma(\vec{x}) = 1$ (0) if the site with position $\vec{x}$ is occupied (empty), $N$ is the total number of cars, and $\vec{r}'$ is a vector in the direction $\parallel$ ($\perp$) you want to compute the correlation function along. The correlation functions are fitted with exponentials $G_{\parallel(\perp)} \propto \exp(-r/\xi_{\parallel(\perp)})$ to estimate $\xi_{\parallel(\perp)}$.

Figure 2 presents the correlations lengths computed from final configurations of the original BML model for different square lattice sizes at densities close to the threshold transition, averaging over 50 configurations for each point. A linear regression yields an estimate of the anisotropy exponent $\theta = 1.64 \pm 0.03$ (Here and everywhere the error bars are $1\sigma$). With the exponent $\theta$ in hand, we studied the phase transition for both longitudinal and transversal systems. Longitudinal ones ran on lattices with sizes $L_\parallel^{\frac{1}{\theta}} \times L_\parallel$.

Figure 3(a) shows that velocity begins to decrease smoothly with increasing $\rho$ until the abrupt onset of full jamming ($v = 0$) at a certain $\rho_{c_\parallel}$. Right there, an approximately uniform distribution of jams spans the whole system [Fig. 3(a), inset]. With Eq. (1) in mind, the FSS analysis [Figs. 3(c) and 3(d)] gives $\rho_{c_\parallel} = 0.521(2)$ and $\nu_\parallel = 3.0(3)$, which would imply $\nu_\perp = 1.8(2)$. Quite differently, transversal systems (i.e., lattices with $L_\parallel \times L_\parallel^{\frac{1}{\theta}}$) in the gridlock phase show a single and well-localized jam on an empty background [Fig. 3(b)]. These systems exhibit a sharp phase transition between free-flow and completely gridlock phases, but at a lower density $\rho_{c_\perp}$. The FSS analysis [also in Figs. 3(c) and 3(d)] gives $\rho_{c_\perp} = 0.283(1)$ and $\nu_\perp = 2.2(1)$, in agreement with the previous result. Hence, the intermediate states in square lattices [13] emerge as a consequence of the combination of these two phase transitions [Figs. 3(a) and 3(b)]. Figure 3(a) also shows a dip at a density $\rho \simeq 0.48$, below the transition point. An analysis of the time series for the average velocity shows that the system has not stabilized yet and does not stabilize for simulations 10 times longer, but the point rises monotonically as the simulation

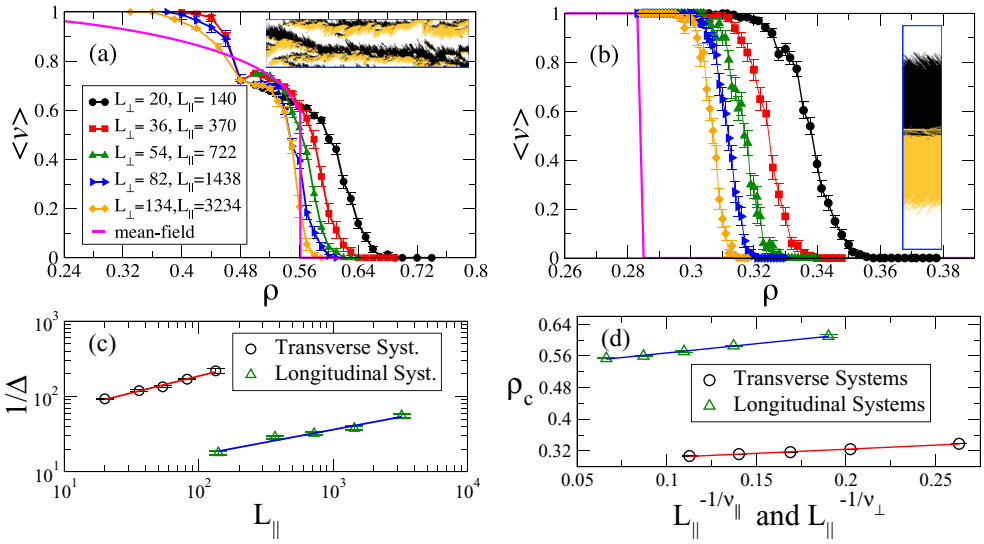


FIG. 3. (Color online) Finite-size scaling analysis for the phase transition of both longitudinal and transversal systems. (a) Transition curves for several longitudinal systems, including the mean-field prediction (magenta solid line) and a typical configuration for the jammed phase (inset). (b) Transition curves for several transversal systems [sizes as in (a), but with $L_\parallel$ and $L_\perp$ interchanged], including the asymptotic limit (magenta solid line) obtained from the FSS analysis. (c) Scaling of the transition width $\Delta(L_\parallel)$ for both cases, giving $\nu_\parallel = 3.0(3)$ and $\nu_\perp = 1.8(2)$. (d) Scaling of the finite critical density gives $\rho_{c_\parallel} = 0.521(2)$ and $\rho_{c_\perp} = 0.283(2)$. All systems were simulated for at least $1.5 \times 10^6$ time steps or until convergence ($v = 0$ or $v = 1$).

time increases. Thus, it could be an effect of an extremely large relaxation time at this density.

The critical densities for both longitudinal and traverse transitions can be approximated by using a mean-field analysis, inspired by [27]. Consider the mean velocity of yellow cars (by symmetry, the reasoning is also valid for black cars). A yellow car will stop either because it is crossed by a black car or because it queues behind another yellow car. At a random initial configuration, the probability that a car is crossed or queued is $\rho^2$; that is, at the beginning of the simulation the proportion of stopped cars $p_{\text{stop}}$ must be equal to $\rho$. Let us define $c_{\rightarrow\uparrow}$ ($c_{\rightarrow\rightarrow}$) as the proportion of stopped cars that are crossed (queued). In previous works [27,28], it has been assumed that $c_{\rightarrow\uparrow} = c_{\rightarrow\rightarrow} = 0.5$, but we will see that this is not the case. If $p_{\text{stop}} \sim \rho$ for some time steps, the probability of a cell being occupied by a stopped crossed (queued) car will be $c_{\rightarrow\uparrow}\rho^2$ ($c_{\rightarrow\rightarrow}\rho^2$). Since black cars spend, on average, a time $1/v$ at a site, they will reduce the speed of yellow cars from unity by $c_{\rightarrow\uparrow}\rho^2/v$. Similarly, the extra amount of time that a yellow car stays at a site will be given by $\frac{1}{v} - 1$, reducing the average speed by $c_{\rightarrow\rightarrow}\rho^2(\frac{1}{v} - 1)$. Hence, a self-consistency equation for the average speed $v$ will be

$$v = 1 - \frac{c_{\rightarrow\uparrow}\rho^2}{v} - c_{\rightarrow\rightarrow}\rho^2\left(\frac{1}{v} - 1\right), \qquad (3)$$

which gives $\rho_c$ as the critical density at which the equation ceases to give a real solution.

Consider longitudinal systems first, where a uniform distribution of longitudinal jams arises. Before solving Eq. (3), let us study the evolution over time of the quantities involved. On the one hand, Fig. 4(a) shows the time evolution of $p_{\text{stop}}$ for different values of the car density for a longitudinal system. At the start, $p_{\text{stop}} = \rho$ for every density, as expected. Later on, $p_{\text{stop}}$ declines (grows) for low (high) densities, and this trend changes near the critical density $\rho_c$. Actually, $p_{\text{stop}}$ after one time step equals $\rho$ for $\rho \simeq 0.57$ in a large system [Fig. 4(b)]. On the other hand, $c_{\rightarrow\uparrow} = c_{\rightarrow\rightarrow} = 0.5$ only at the start, but after just one time step they change to $c_{\rightarrow\uparrow} \sim 0.600(5)$ and $c_{\rightarrow\rightarrow} \sim 0.400(5)$, remaining at those values for some time steps [Fig. 4(c)]. By replacing these two values into Eq. (3), the mean-field approach predicts a critical density $\rho_\parallel = 0.563(5)$, in agreement with the value obtained from both finite-size scaling and the behavior change of $p_{\text{stop}}$ described above.

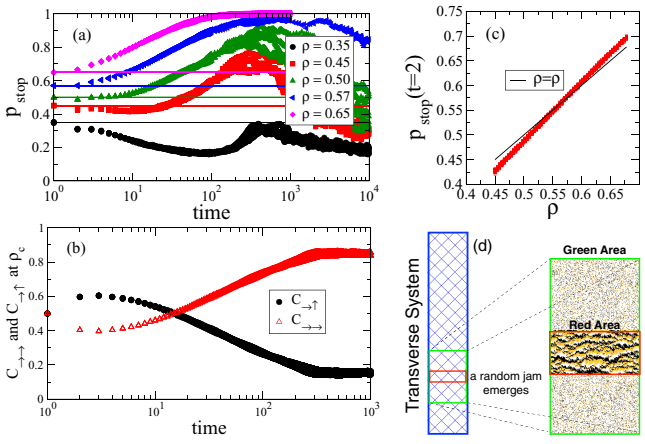


FIG. 4. (Color online) Time evolution of (a) the fraction of stopped cars $p_{\text{stop}}$ and (b) of the fraction of crossed ($c_{\rightarrow\uparrow}$) and queued ($c_{\rightarrow\rightarrow}$) stopped cars in a $1438 \times 82$ longitudinal system. (c) The value of $p_{\text{stop}}$ after one time step for several densities is also shown. (d) Schematic representation of the jamming process for transversal systems.

Transversal systems, in contrast, collapse into a single big jam. Thus, the previous reasoning is impractical here because the local density becomes inhomogeneous during the collapse: increasing in the vicinity of the growing jam and dropping to zero elsewhere. Let us consider that the density at the start is low enough to assume that all cars are moving. At a certain evolution time the cars have condensed into a thinner region [red area in Fig. 4(d)] of area $A_{\text{red}}$, where the density has reached the critical value $\rho_{c_\parallel}$ for longitudinal systems. All cars in this region come from a larger region of area $A_{\text{green}}$ in the initial configuration [green area in Fig. 4(d)]. Let us assume that the red area is a fraction of the green one equal to the fraction of cars that have stopped, $A_{\text{red}}/A_{\text{green}} = p_{\text{stop}}$. Because the number of cars does not change, at the critical density

$$\rho_{\text{green}} = \rho_{\text{red}} \frac{A_{\text{red}}}{A_{\text{green}}} = \rho_{c_\parallel}^2, \tag{4}$$

where we have used the result that $p_{\text{stop}} = \rho$ at the critical density for longitudinal systems. Then, the critical density for transversal systems will be $\rho_{c_\perp} = \rho_{c_\parallel}^2 = 0.271(3)$, which approximates quite well the value $\rho_{c_\perp} = 0.283(2)$ from the simulations [Fig. 3(d)].

The values for $c_{\rightarrow\rightarrow}$ and $c_{\rightarrow\uparrow}$ at $t = 1$ can also be estimated from a mean-field analysis. Let us assume the car distribution is still uniform after one timestep. Remember that the fraction of cars that stop at $\rho = \rho_c$ is $p_{\text{stop}} = \rho$ [Fig. 3(c)]. The number of crossed cars at $t = 1$ will be the contribution of three factors: the cars that were moving at $t = 0$ but stopped and are now crossed $(c_{\rightarrow\uparrow}^{(t=1)}(1-\rho))$ , the crossed cars at $t = 0$ that remain crossed $(c_{\rightarrow\uparrow}^{(t=0)}\rho$, because the site ahead of the crossed couple is occupied) and the queued cars that turned into crossed ones $(c_{\rightarrow\rightarrow}^{(t=0)}\frac{\rho}{2}(1-\rho)$, which takes place if the site ahead of the queued couple is empty and a car moving in the other direction points to the header of the couple). Thus, we have $c_{\rightarrow\uparrow}^{(t=1)} = c_{\rightarrow\uparrow}^{(t=1)}(1-\rho) + c_{\rightarrow\uparrow}^{(t=0)}\rho + c_{\rightarrow\rightarrow}^{(t=0)}\frac{\rho}{2}(1-\rho)$. As $c_{\rightarrow\uparrow}^{(t=0)} = c_{\rightarrow\uparrow}^{(t=0)} = 0.5$ and $\rho = \rho_c$, then, $c_{\rightarrow\uparrow}^{(t=1)} \approx \frac{3-\rho_c}{4} \approx 0.61$ and $c_{\rightarrow\rightarrow}^{(t=1)} \approx 0.39$, very close to the simulation results. Using these values in the Eq. (3), gives $\rho_\parallel = 0.562(2)$, also close to the simulations.

Taken together, our results suggest that the puzzling intermediate states in the BML model on square lattices are, actually, a consequence of the system's anisotropy, which produces two different phase transitions: one for transverse systems, with $\rho_{c_\perp} = 0.283(1)$, and another for longitudinal ones, with $\rho_{c_\perp} = 0.521(1)$. Indeed, the first critical density corresponds to the lower bifurcation point on square lattices, reported at $\rho = 0.315$ [13], contradicting the general belief that this would go to zero for infinite systems; similarly, the second critical density perfectly matches the value of $\rho = 0.52$ reported as the transition point between self-organized jams and random jams [2,4] within the conventional understanding of the original BML model. The asymptotic limit of the curves from simulations on transverse systems [blue solid line in Fig. 1(a)] and the mean-field curve for longitudinal systems [Eq. (3) and dashed red line in Fig. 1(a)] perfectly enclose the zone of intermediate states. In fact, the structure of the intermediate states can also be explained if one transition has taken place but not the other. Figure 1(d) shows how an incipient jam with a structure similar to those of transversal systems [Fig. 3(b), inset] begins to form, but it not succeed in blocking everything because the system is too wide. The cars leaving the jam in both directions create bands of yellow (light gray) and black stripes. These bands will cross each other to form another incipient global jam and so on, establishing the distinctive periodic structure of such intermediate states.

Despite having studied the critical features of the BML phase transitions with the DP formalism, the obtained critical exponents are not compatible with the universality class of the directed percolation. Instead, the critical behavior here coincides with that reported for the parity-conserving universality class [21,22]. The origin of this relationship remains an open question for future research.

By finding the origin of the intermediate states of the BML model, we have built a very complete description of such a fundamental model for traffic flow, illustrating at the same time the power of the finite-size scaling analysis for anisotropic systems, where the BML model seems to be a paradigmatic example. We look forward to seeing many more results of this enlightening analysis technique in the future.

## ACKNOWLEDGMENTS

We thank the Complex Systems Research Center CeiBA-Complejidad and the National University of Colombia for financial support.

[1] O. Biham, A. A. Middleton, and D. Levine, Phys. Rev. A **46**, R6124 (1992).
[2] S. I. Tadaki and M. Kikuchi, Phys. Rev. E **50**, 4564 (1994).
[3] J. Torok and J. Kertész, Phys. A (Amsterdam, Neth.) **231**, 515 (1996).
[4] H. S. Gupta and R. Ramaswamy, J. Phys. A **29**, 022812 (1996).
[5] J.-R. Xie, R. Jiang, Z.-J. Ding, Q.-L. Li, and B.-H. Wang, Phys. Rev. E **87**, 022812 (2013).
[6] Y. Sun and I. Timofeyev, Phys. Rev. E **89**, 052810 (2014).
[7] T. Nagatani, Rep. Prog. Phys. **65**, 1331 (2002).
[8] D. Chowdhury, L. Santen, and A. Schadschneider, Phys. Rep. **329**, 199 (2000).
[9] H. Yue, H. Hao, X. Chen, and C. Shao, Phys. A (Amsterdam, Neth.) **384**, 567 (2007).
[10] J. Cividini, H. J. Hilhorst, and C. Alpert-Rolland, J. Phys. A **46**, 345002 (2013).
[11] T. Ohira and R. Sawatari, Phys. Rev. E **58**, 193 (1998).
[12] W. K. Yung, Master's thesis, University of Hong Kong, 1998.
[13] R. M. D'Souza, Phys. Rev. E **71**, 066112 (2005).
[14] R. M. D'Souza, Complexity **12**, L547 (2006).
[15] N. J. Linesch and R. M. D'Souza, Phys. A (Amsterdam, Neth.) **387**, 6170 (2008).
[16] S. Ostojic, T. J. H. Vlugt, and B. Nienhuis, Phys. Rev. E **75**, 030301(R) (2007).

[17] D. Bi, J. Zhang, B. Chakrabortty, and R. P. Behinger, Nature (London) **480**, 355 (2011).
[18] T. Vicsek and A. Zafeiris, Phys. Rep. **517**, 71 (2012).
[19] M. Pleimling and M. Henkel, Phys. Rev. Lett. **87**, 125702 (2001).
[20] B. Schmittmann and R. P. Zia, *Statistical Mechanics of Driven Diffusive System*, Phase Transitions and Critical Phenomena, Vol. 17 (Academic, London, 1995).
[21] H. Hinrichsen, Adv. Phys. **49**, 815 (2001).
[22] M. Henkel, H. Hinrichsen, and S. Lubeck, *Non-Equilibrium Phase Transitions*, Theoretical and Mathematical Physics, Vol. 14 (Springer, Berlin, 2008).
[23] K. Binder and J.-S. Wang, J. Stat. Phys. **55**, 87 (1989).
[24] S. Redner and P. R. Mueller, Phys. Rev. B **26**, 5293 (1982).
[25] J. K. Williams and N. D. Mackenzie, J. Phys. A **17**, 3343 (1984).
[26] The values of $\rho_c$ and $\Delta(L)$ were determined by fitting the transition curve with a complimentary error function $\frac{a}{2}\mathrm{erfc}[\frac{\rho_c(L)-\rho}{\Delta(L)}]$. As the transition on transversal systems occurs between $v=1$ and $v=0$, then $a=1$. For the longitudinal case $a=0.71$, which corresponds to the average speed just before the transition [see Fig. 3(a)].
[27] B. H. Wang, Y. F. Woo, and P. M. Hui, J. Phys. A **29**, L21 (1996).
[28] T. Nagatani, J. Phys. Soc. Jpn. **62**, 2656 (1993).

# C. Appendix C: Traffic gridlock on a honeycomb city.

# Traffic gridlock on a honeycomb city

L. E. Olmos* and J. D. Muñoz†
*Simulation of Physical Systems Group, Physics Department, National University of Colombia, Bogotá, Colombia*
(Received 20 October 2016; published 31 March 2017)

Inspired by an old and almost in oblivion urban plan, we report the behavior of the Biham-Middleton-Levine (BML) model—a paradigm for studying phase transitions of traffic flow—on a hypothetical city with a perfect honeycomb street network. In contrast with the original BML model on a square lattice, the same model on a honeycomb does not show any anisotropy or intermediate states, but a single continuous phase transition between free and totally congested flow, a transition that can be completely characterized by the tools of classical percolation. Although the transition occurs at a lower density than for the conventional BML, simple modifications, like randomly stopping the cars with a very small probability or increasing the traffic light periods, drives the model to perform better on honeycomb lattices. As traffic lights and disordered perturbations are inherent in real traffic, these results question the actual role of the square gridlike designs and suggest the honeycomb topology as an interesting alternative for urban planning in real cities.

DOI: 10.1103/PhysRevE.95.032320

As cities turn denser, urban networks tend to adopt a squared-lattice shape [1], and many traditional urban planning styles, like the one Spaniards and Portugueses disseminated through all Latin America, are grounded on such square patterns [2]. Following this trend, most prominent studies on city traffic adopt square lattices [3–5]. Despite modern urban planners' claim that this design favors connectivity, the question of whether a square design optimizes traffic flow has not being studied systematically. In contrast, Nature usually opts for other alternatives. Hexagonal structures in two dimensions are present in cellular tissues [6,7], bee honeycombs [8], and soap bubbles [9,10]. Such patterns arise by minimizing surface energy on a fixed area [11]. Inspired by Nature, humans have also implemented hexagonal tesselations in a wide range of disciplines, including structured materials [12,13], wireless networks [14], computer graphics [15], etc. However, in the realm of the urban design, street patterns based upon hexagonal lock are just a theoretical alternative which has fallen into oblivion with almost no practical applications (see [16] and references therein), but hiding possible unexplored solutions for the overwhelming problem of traffic flow in modern cities.

The BML model is the simplest traffic cellular automaton able to exhibit self-organization, pattern formation, and phase transitions [17–20]. The original model describes two species of cars (east-running and north-running cars) moving by turns on a two-dimensional square lattice with periodic boundary conditions. Thus, the dynamics considers the city as a closed system with a constant number of cars and, does not allow cars to change direction. Despite these oversimplifications, the model allows us to focus on the nature of the phase transition between free and congested flow, and much extensive research has been based on it [3,21–23]. Driven by car density, the control parameter, the system falls into three different phases according to its asymptotic velocity $v$: free flow (all vehicles move $v = 1$), jammed phase (all vehicles are stuck $v = 0$), and intermediate states where jams and free flow coexist on a wide density range ($0 < v < 1$) [24–26]. A recent study has shown that such intermediate states are a consequence of the anisotropy inherent to the model [27], which produces two different phase transitions: one if the system is longer in the flow direction (longitudinal) and the other if the system is longer in the perpendicular one (transversal). It has also been reported that this intermediate phase disappears when some kind of randomization is introduced [25,28,29], or the traffic periods for the two cars are increased [30]. Some other extensions include free boundary conditions [31], four directions for the cars [32], or three-dimensional (3D) implementations [33]. In contrast, the role played by the network topology has been overlooked and, there are very few studies considering the Biham- Middleton-Levine (BML) model on different lattices: square lattice generalizations with extra sites in the bonds [34,35] and triangular lattices where three species of cars are considered [36,37]. In all cases a more complex behavior with different jammed phases is observed.

The main goal of this work is to test the BML traffic model [17] on honeycomb lattices. The intention is to explore how the topology (i.e., the node degree) affects the jamming transition and, eventually, when a honeycomb lattice offers a better performance than the square one. As in the original model, we will implement two car species moving by turns on a lattice with periodic boundary conditions, which can be closed on a torus in three different ways. Surprisingly, all systems show a single well-defined phase transition, although there is still a preferred flux direction and, moreover, there are cases where the BML performs better on honeycomb lattices than on square ones. So, this work questions the assumption that square grids are always optimal and suggests honeycombs as interesting alternatives for urban designers.

*Model.* Consider two types of cars moving zigzag in two different directions, yellow and black, on a honeycomblike lattice with periodic conditions (Fig. 1). Each node is connected with three others and can be in one of three states: empty, occupied by a yellow car, or occupied by a black one. The cars are initially randomly distributed over the lattice sites with spatial density $\rho$. The fully deterministic dynamics is as follows: On even (odd) steps, all yellow (black) cars attempt to advance one lattice site on their zigzag pattern. If the site ahead

*leolmoss@unal.edu.co
†jdmunozc@unal.edu.co

 

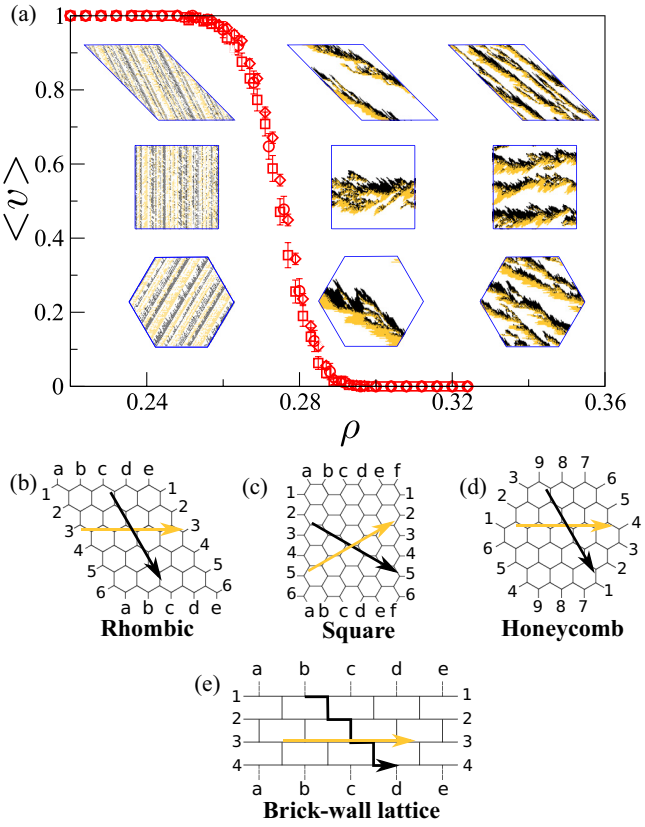


FIG. 1. Average velocity $\langle v \rangle$ vs density $\rho$ (solid red line) for the BML model on $128 \times 128$ honeycomb lattices. Here and everywhere $\langle v \rangle$ is the fraction of random initial configurations with asymptotic velocity $v = 1$. Insets show snapshots for free flow (left), one global jam (center), and random jams (right) on lattices with three boundaries: rhombic [diamonds and (b)], square [squares and (c)], and honeycomb [circles and (d)]. The flow direction is defined by just two (yellow and black arrows) of the three reflection symmetry axes. Topologically, the honeycomb lattice is equivalent to the brick-wall lattice (e).

of a car (in color direction) is currently empty, it advances; otherwise, it remains stationary. The system is implemented on a torus, i.e., with periodic boundary conditions, as in the original model. Nevertheless, there is no unique way to close a hexagonal lattice on a torus, but three [38]: square, rhombic, and honeycomb [Figs. 1(b)–1(d)]. We shall consider all these three tori in the most part of our analysis.

*Absence of anisotropy.* Starting the simulations from random configurations, the system reaches one of its limiting states after a transient period. If the system size is large enough ($L > 64$), there are only two different limiting states [Fig. 1(a)]: a free-flow phase, where all cars move freely every time step ($v = 1$) and a jammed phase, where no cars move ($v = 0$). Contrary to the original model, there are no intermediate states, and the system exhibits a sharp jamming transition between these two phases [Fig. 1(a)].

As in the original model, there is a preferred flow direction: the one bisecting the two directions for cars and, in consequence, it could be possible to find a similar anisotropy in the correlation length. Let us start by studying the isotropy of

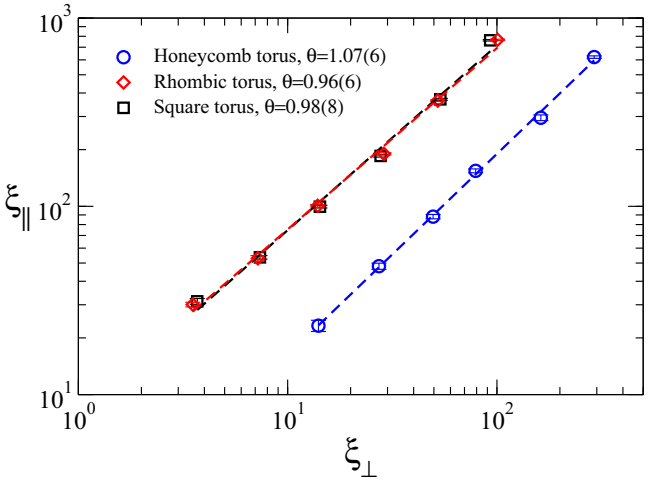


FIG. 2. Longitudinal $\xi_\parallel$ and transversal $\xi_\perp$ correlation lengths from final configurations at densities $\rho$ in the range [0.265–0.310] for honeycomb lattices of different sizes with the three boundary conditions. Each point is an average over 50 configurations. The dashed lines show the power-law fits with anisotropy exponents $\theta \approx 1.0$, i.e., the system behaves isotropic. Here and everywhere the error bars are $3\sigma$.

the system. If the density is large enough, the system reaches a jamming state after a transient period. Following the methods applied in [27], we define the parallel (perpendicular) spatial correlation function [18] as

$$G_{\parallel(\perp)}(\vec{r}') = \frac{1}{N}\left\langle \sum_{\vec{r}} \sigma(\vec{r}) \cdot \sigma(\vec{r} + \vec{r}') \right\rangle, \qquad (1)$$

where $\sigma(\vec{r}) = 1$ (0) if the site with position $\vec{r}$ is occupied (empty), $N$ is the total number of cars and $\vec{r}'$ is a vector in the direction $\parallel$ ($\perp$) you want to compute the correlation function along. The symbol $\langle\rangle$ denotes averages over final jammed configurations starting from different random initial conditions at densities slightly above the jamming transition. The correlation functions are fitted with exponentials $G_{\parallel(\perp)} \propto \exp(-r/\xi_{\parallel(\perp)})$ to estimate the correlation lengths $\xi_{\parallel(\perp)}$ in each direction. The anisotropy exponent $\theta$ can be estimated numerically from the fact that, close to the critical point, the two correlation lengths must be related by $\xi_\parallel \sim \xi_\perp^\theta$ [39,40].

Figure 2 presents the correlation lengths computed from final configurations of the BML model for the three different honeycomb tori with different sizes and at densities close to the threshold transition. A power-law fit gives values for $\theta$ very close to 1, meaning that the system can be considered isotropic, such that the standard finite-size scaling (FSS) theory is suitable for describing the phase transition. Indeed, simulations on systems with different aspect ratios (not shown here) show no difference on the transition. This surprising result is, therefore, not a consequence of the preferred flow direction alone, but also of the grid itself.

*The jamming transition.* Figure 3(a) shows the transition curves for several system's sizes, ranging from $L = 64$ to $L = 1024$. In the honeycomb-torus case, the size $L$ denotes the torus

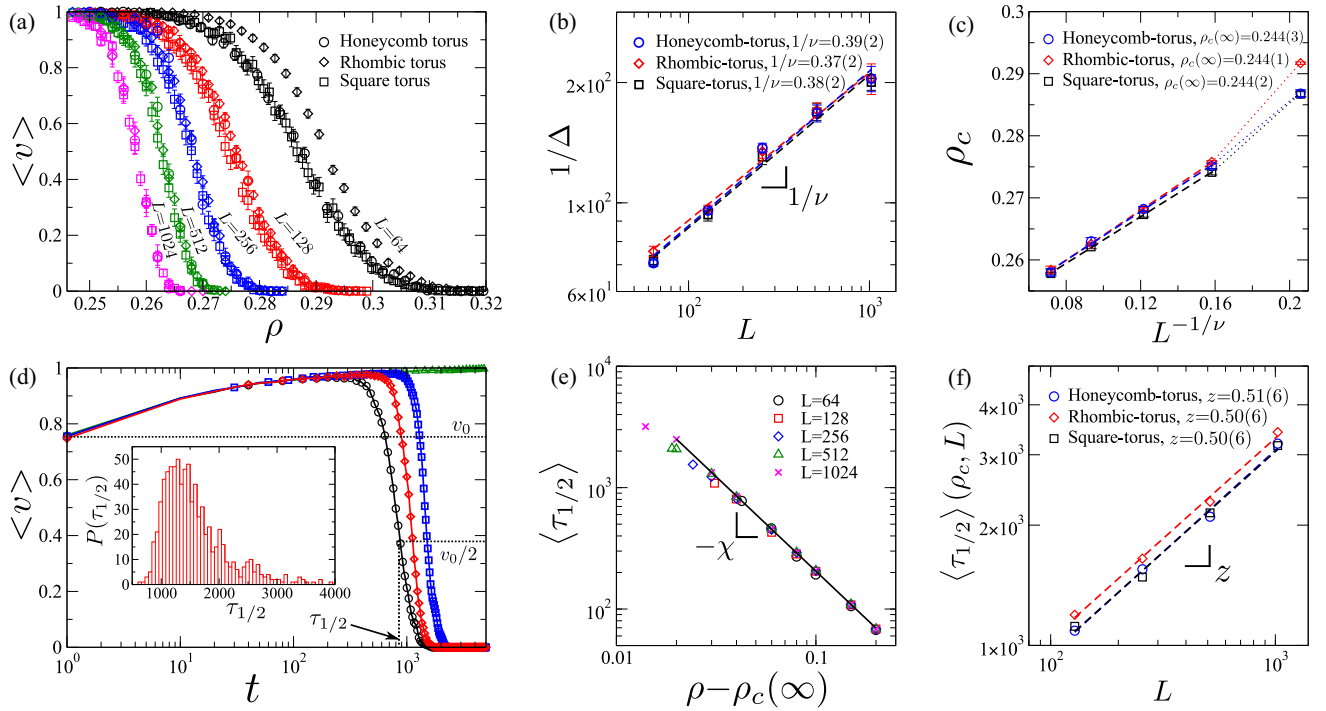


FIG. 3. Finite-size scaling analysis for the dynamical phase transition. (a) Transition curves for the three types of torus (symbols) with five different system sizes (colors), ranging from $L = 64$ to $L = 1024$. Each point is averaged over 2000 (1000) final configurations for $L \leqslant 512$ ($L = 1024$), obtained after convergence ($v = 0$ or $v = 1$) or after $2\times10^5$ time steps (whichever comes first). (b) Scaling of the transition width $\Delta(L)$. Dashed lines are power-law fits for the three tori, giving $1/\nu = 0.38(3)$ on average. (c) Scaling of the finite critical density. Because of strong finite-size effects, we neglect $L = 64$, and obtain $\rho_c(\infty) = 0.244(3)$ on average. (d) Average speed in function of time for five configurations. Dotted lines show the definition of the relaxation time $\tau_{1/2}$. The inset evidences that $\tau_{1/2}$ follows a log-normal distribution. (e) Mean relaxation time $\tau_{1/2}$ for densities above $\rho_c(\infty)$ on the honeycomb torus (results on other tori are quite similar). The slope gives on average a critical exponent $\chi = 1.55(2)$. (f) Scaling of the relaxation time at the critical point $\tau_{1/2}(\rho_c)$. On average, we obtain a dynamical critical exponent $z = 0.50(6)$. Each point on the last two figures is averaged over 100 configurations.

with the number of nodes closest to $L^2$.[1] As in many models with phase transitions in statistical physics (e.g., percolation [41]), the value of the critical density $\rho_c$ decreases with system size, reaching a critical value $\rho_c$ as the system size approaches infinity. By fitting the transition curves with an error function, Figs. 3(b) and 3(c) show that the transition width and the density threshold scale as [42]

$$\Delta(L) \sim L^{-1/\nu} \text{ and } |\rho_c - \langle\rho_c(L)\rangle| \sim L^{-1/\nu}. \qquad (2)$$

The values obtained for $\nu$ and $\rho_c(\infty)$ are very similar for the three tori. On average, we obtain $1/\nu = 0.38(3)$ and $\rho_c(\infty) = 0.244(3)$.

To investigate the dynamics of the model in the jammed state, let us define $\tau_{1/2}$ [18] as the time when the average speed is half of the initial speed [Fig. 3(d)]. This relaxation time follows a log-normal distribution and, therefore, its mean value can be estimated as $\langle\tau_{1/2}\rangle = \exp(\mu + \sigma^2/2)$, with $\mu \simeq \frac{1}{n}\sum_k \ln\tau_{1/2_k}$ and $\sigma^2 \simeq \frac{1}{n}\sum_k(\ln\tau_{1/2_k} - \mu)^2$. In the jammed phase ($\rho > \rho_c$), Fig. 3(e) shows that $\langle\tau_{1/2}\rangle$ is independent of the system size and scales as $\langle\tau_{1/2}\rangle \sim (\rho - \rho_c)^{-\chi}$ with $\chi = 1.55(2)$. In addition, the values of $\tau_{1/2}$ at the critical density $\rho_c$ scales with system size as $\langle\tau_{1/2}\rangle(\rho_c, L) \sim L^z$, with $z = 0.50(6)$ [Fig. 3(f)]. The finite size scaling theory suggests that above the transition point $\chi/\nu = z = 0.56(5)$, in fair agreement with the value above.

*A mean-field analysis.* Interestingly, the critical density can be approximated by using a *naive* mean-field analysis, inspired by [43]. Consider the mean velocity of yellow cars (by symmetry, the reasoning is also valid for black cars). A yellow car will stop either because it is blocked by a black car or by another yellow car. On honeycomb lattices, there is almost no difference between these two types of interactions. At a random initial configuration, the probability that a car is blocked is $\rho$, that is, at the beginning of the simulation the proportion of stopped cars must be equal to $\rho$. Since black (yellow) cars spend on average a time $1/v$ on a site, they will reduce the speed of yellow cars from unity by $\rho/v$. Hence, a self-consistency equation for the average speed $v$ will be

$$v = 1 - \frac{\rho}{v}, \qquad (3)$$

which gives $\rho_c$ as the critical density at which the equation ceases to give a real solution. That occurs at $\rho_c = 0.25$, very close to the value of 0.244(3) obtained from finite size scaling.

[1] A honeycomb torus of size $n$ has $6n^2$ nodes and $n$ hexagons between the center and boundary. Thus, a $L^2$ torus actually corresponds to a torus in which $n$ is the closest whole number of $L/\sqrt{6}$.

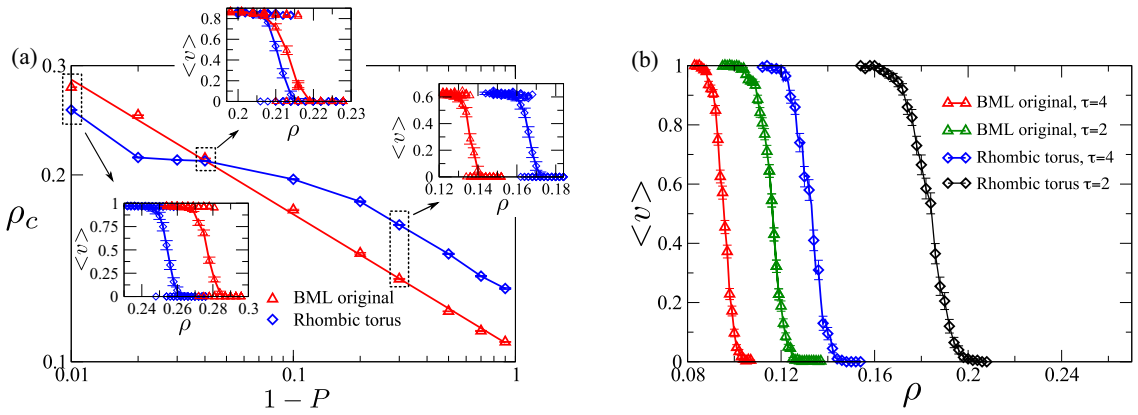


FIG. 4. Effects of two modifications of the BML model on both rhombic tori (diamonds) and square lattices (triangles). (a) Effect of including a random update, where cars move with probability $P$ if the target site is empty. The figure shows the critical density $\rho_c$ as a function of $1-P$ for lattice sizes $L=128$. Insets show the transition curves for three values of $P$. (b) Effect of increasing the traffic light period $\tau$. The figure shows transition curves for $\tau=2$ and $\tau=4$ on lattices with size $L=256$. Each point in both figures is averaged on 400 runs. Measurements are obtained after $6\times10^5$ time steps or until convergence (whichever comes first).

*A comparison with the square lattice.* Remarkably, the critical density $\rho_c=0.244(3)$ for the BML model on a honeycomb is lower than the value of 0.283(2) for the lowest transition on a square lattice [27]. However, this order is reversed in at least two cases. First, let us remove full synchrony by introducing a random update [28], where a car advances with probability $P<1$ if the target site is empty; a modification that also destroys the intermediate state in of the BML model on square lattices [25,28,29]. Figure 4(a) compares the critical density of the model as function of $1-P$ on a rhombic torus with the one on a square lattice. The BML on a square lattice follows a power law behavior, with $\rho_c \propto (1-P)^{-0.22(1)}$, and behaves better only for a narrow interval. Below $P\approx0.96$, the honeycomb lattice overcomes the square one and behaves better, that is with a higher critical density.

Second, we have also studied the effect of increasing the traffic-light periods, that is cars on each direction have the chance to advance in $\tau$ consecutive time steps ($\tau=1$ for the original model), maintaining the parallel updating scheme. This also destroys the intermediate states on the original BML model and, furthermore, produces a spatial phase separation with small global speeds at intermediate densities [30]. Again, rhombic tori show higher critical densities than square lattices, even for $\tau=2$ or $\tau=4$ [Fig. 4(b)]. These results suggest that the model on a honeycomb is more resilient against small perturbations than on a square lattice.

*Discussion.* We have shown that the BML model with two flow directions behaves isotropically on honeycomb networks. There are no intermediate states, and a sharp transition from the moving phase to the jamming phase is observed at a critical vehicle density. Despite the fact that there is a preferred flow direction, the correlation length shows to be isotropic. This surprising result may be a consequence of the symmetries of the honeycomb. Indeed, it has been shown that high-order tensors on a hexagonal lattice (the dual lattice of a honeycomb) are isotropic up to second order in the grid size [44]. Whether this is the reason for such isotropy or not will be an interesting subject of future research.

By performing a classical scaling analysis, we characterized completely the transition, measuring the critical density and three critical exponents. Although the model shows a lower critical density than on square lattices, this issue is reversed by introducing small and simple perturbations, like increasing the traffic light periods or including a random update with very low probabilities to brake. Street patterns based upon hexagonal blocks were proposed by several planners in the early 20th century [16]. Despite urban designers demonstrating the economic advantages and efficient land use of hexagonal plans, this idea never ceased to be a theoretical alternative to the rectangular grid, never implemented in urban street patterns. Furthermore, the contemporary movements of new urbanism claims that square grid layouts increase the connectivity,[2] dispersing traffic and reducing driving times, because they are assumed to be mixed use, walkable, and more pedestrian friendly. However, such assumptions are criticized by practical considerations [16]. Indeed, empirical data about safety [45,46] suggest that four-leg intersections, ubiquitous in square grids, increase both the number of crashes and injuries significantly, suggesting to reconsider urban residential layouts where T junctions and dead ends predominate (*cul de sac*, radburn, fused grid). This is why city planners use to restrict flow direction emulating T junctions, even at the cost of reducing connectivity. Although those issues are usually thought of in a highways network, they also apply to residential neighborhoods, because residential and working areas mix as cities become denser and, real-time traffic applications push cars into residential areas to avoid jams. This is the case in many Latin American cities. Thus, honeycomb grids emerge as a unifying idea, i.e., T junctions plus connectivity.

Our results suggest that the BML model on hexagons under perturbations is more robust than on squares. Since the included perturbations, i.e., traffic lights and disorder,

[2]See http://www.newurbanism.org/.

are crucial in real traffic, this work questions the real role of square gridlike designs and supports honeycombs as an interesting alternative for urban densification processes. Regarding practical applications, a honeycomb lattice can be mapped into a brick-wall lattice [see Fig. 1(e)] which, in turn, can be derived from the square lattice by eliminating bonds. Thus, instead of an improbable reconstruction of the city, we could emulate the honeycomb topology by restricting the flow in certain road segments. Of course, our model oversimplifies the city, as most previous BML models do. A real city is an open system, with cars entering and leaving the flux all the time, as described by empirical origin-destination matrices and the incoming flux as control parameter. Testing a honeycomb network against a square one in that context would be a beautiful subject of future work and a further contribution of statistical physics to the urbanism theory.

*Acknowledgments*. We thank the Complex Systems Research Center CeiBA-Complejidad and the National University of Colombia for financial support. We are indebted M. C. González for hospitality and useful discussions.

[1] E. Strano, V. Nicosia, V. Latora, S. Porta, and M. Barthelemy, Sci. Rep. **2**, 296 (2012).
[2] A. Rama, *The Lettered City* (Ediciones del Norte, Hanover, NH, 2002).
[3] D. Chowdhury, L. Santen, and A. Schadschneider, Phys. Rep. **329**, 199 (2000).
[4] A. Mazloumian, N. Geroliminis, and D. Helbing, Philos. Trans. R. Soc. A **368**, 4627 (2010).
[5] M. Li, Z.-J. Ding, R. Jiang, M.-B. Hu, and B.-H. Wang, J. Stat. Mech. (2011) P12001.
[6] J. C. M. Mombach, M. A. Z. Vasconcellos, and R. M. C. de Almeida, J. Phys. D: Appl. Phys. **23**, 600 (1990).
[7] A. B. Patel, W. T. Gibson, M. C. Gibson, and R. Nagpal, PLoS Comput. Biol. **5**, e1000412 (2009).
[8] C. W. W. Pirk, H. R. Hepburn, S. Radloff, and J.Tautz, Naturwissenschaften **91**, 350 (2004).
[9] D. Weaire, Contemp. Phys. **25**, 59 (1984).
[10] D. Weaire, *The Kelvin Problem* (Taylor and Francis, London, 1996).
[11] J. von Neumann, in *Metal Interfaces* (American Society for Metals, Cleveland, 1952), p. 108.
[12] R. Oftadeh, B. Haghpanah, D. Vella, A. Boudaoud, and A. Vaziri, Phys. Rev. Lett. **113**, 104301 (2014).
[13] L. J. Gibson and M. F. Ashby, *Cellular Solids: Structure and Properties* (Cambridge University Press, Cambridge, England, 1999).
[14] R. H. Frenkiel, US Patent No. 4,144,411, March 13, 1979.
[15] C. Jiang, J. Wang, J. Wallner, and H. Pottmann, Computer Graphics Forum **33**, 185 (2014).
[16] E. Ben-Joseph and D. Gordon, J. Urban Des. **5**, 237 (2000).
[17] O. Biham, A. A. Middleton, and D. Levine, Phys. Rev. A **46**, R6124 (1992).
[18] S. I. Tadaki and M. Kikuchi, Phys. Rev. E **50**, 4564 (1994).
[19] J. Torok and J. Kertész, Physica A **231**, 515 (1996).
[20] H. S. Gupta and R. Ramaswamy, J. Phys. A: Math. Gen. **29**, L547 (1996).
[21] J.-R. Xie, R. Jiang, Z.-J. Ding, Q.-L. Li, and B.-H. Wang, Phys. Rev. E **87**, 022812 (2013).
[22] Y. Sun and I. Timofeyev, Phys. Rev. E **89**, 052810 (2014).
[23] T. Nagatani, Rep. Prog. Phys. **65**, 1331 (2002).
[24] R. M. D'Souza, Phys. Rev. E **71**, 066112 (2005).
[25] R. M. D'Souza, Complexity **12**, 30 (2006).
[26] W. K. Yung, Master's thesis, University of Hong Kong, Department of Physics, 1998, http://hub.hku.hk/handle/10722/33474.
[27] L. E. Olmos and J. D. Muñoz, Phys. Rev. E **91**, 050801 (2015).
[28] Z.-J. Ding, R. Jiang, W. Huang, and B.-H. Wang, J. Stat. Mech. (2011) P06017.
[29] Z.-J. Ding, R. Jiang, and B.-H. Wang, Phys. Rev. E **83**, 047101 (2011).
[30] D. Sun, R. Jiang, and B.-H. Wang, Comput. Phys. Commun. **181**, 301 (2010).
[31] S. I. Tadaki, Phys. Rev. E **54**, 2409 (1996).
[32] D. Huang and W. Huang, Physica A **370**, 747 (2006).
[33] H. F. Chau and K. Y. Wan, Phys. Rev. E **60**, 5301 (1999).
[34] T. Horiguchi and T. Sakakibara, Physica A **252**, 388 (1998).
[35] T. Sakakibara, Y. Honda, and T. Horiguchi, Physica A **276**, 316 (2000).
[36] T. Nagatani, Physica A **271**, 200 (1999).
[37] J. C. García, S. Rodríguez, and F. Sancho, in *Proceedings of the European Conference on Complex Systems* (Springer International Publishing, Switzerland, 2013), pp. 943–948.
[38] I. Stojmenovic, IEEE Trans. Parallel Distrib. Syst. **8**, 1036 (1997).
[39] K. Binder and J.-S. Wang, J. Stat. Phys. **55**, 87 (1989).
[40] S. Redner and P. R. Mueller, Phys. Rev. B **26**, 5293 (1982).
[41] D. Stauffer and A. Aharony, *Introduction to Percolation Theory* (Taylor & Francis, London, 1992).
[42] M. D. Rintoul and S. Torquato, J. Phys. A: Math. Gen. **30**, L585 (1997).
[43] B. H. Wang, Y. F. Woo, and P. M. Hui, J. Phys. A **8**, 1036 (1996).
[44] S. Wolfram, J. Stat. Phys. **45**, 471 (1986).
[45] E. Dumbaugh and R. Rae, J. Am. Plann. Assoc. **75**, 309 (2009).
[46] J. Sun and G. Lovegrove, Can. J. Civil Eng. **40**, 35 (2013).

# D. Appendix D: References in the media

DAILY NEWS 28 October 2016

# Honeycomb-shaped streets would stop traffic from getting sticky

**Side effect: Hexagonal layouts can get you out of a jam**
Folco Quilici/Alinari Archives via Getty Images

By **Monica Young**

Life is sweet in the honeycomb. City planning has long depended on rectangular networks – they're simple and, urban planners say, reduce congestion. But it turns out that connecting streets to form hexagons instead of rectangles might lead to less traffic.

In a study, Luis Eduardo Olmos and José Daniel Muñoz at the National University of Colombia find that designing cities so only three streets meet at any given intersection

– as they do when they form a honeycomb shape – could help get rid of traffic jams.

The team ran a simple mathematical model allowing cars to drive diagonally in one direction, as might happen during rush hour when commuters all head home at once. For a square street network such as Manhattan, for example, the imaginary cars would run east and north to leave the city.

With only a few cars, traffic flows smoothly, and when too many vehicles appear, traffic clogs. But in between those extremes, there's an extended intermediate state, where small traffic jams clog traffic in bursts across the network.

When Olmos and Muñoz applied their model to honeycombed streets, however, they found something quite different. As the number of cars increased, the traffic transitioned suddenly, like water turning from liquid to solid: free-flowing traffic became a jam.

## Crowd-pleaser

With the addition of a few traffic lights to break up the flow, Olmos and Muñoz found that cars driving along honeycombed streets kept moving at densities that had already caused the rectangular network to clog up.

The model is a first approximation – it doesn't include pedestrians, landscapes or buildings, for example – so the authors plan to create a more-detailed simulation.

But as Eran Ben-Joseph at Massachusetts Institute of Technology quipped in a 2000 review of hexagonal city planning, "How would strangers navigate the streets of Hexagonopolis?" Even in the face of the new study, hexagonal cities remain "a concept that may work in theory but not in practice", he says.

However, even if the honeycomb model doesn't work in real cities, the same concept could be applied in other situations, the authors suggest, such as information packages travelling through the internet.

**Journal reference:** *arXiv.org*, DOI: arXiv:1610.07438v1

---

A shorter version of this article was published in *New Scientist* magazine on 5 November 2016

Semana

PUBLICADO: 26/03/2016

# "La ciudad está tan congestionada que la gente maneja por los barrios"

José Daniel Muñoz y Luis Eduardo Olmos, físicos de la Universidad Nacional, llevan más de 10 años analizando el tráfico de Bogotá.

**SEMANA: ¿Qué hace un físico estudiando trancones?**

**José Daniel Muñoz:** Es que no somos solo ecuaciones. A nosotros nos interesa el día a día, y la movilidad tiene que ver con problemas de la física. ¿O cómo explicar que el tráfico pase de un momento a otro del colapso al flujo libre?

**SEMANA: ¿Olmos y usted qué opinan de Bogotá?**

**Luis Eduardo Olmos:** El bogotano es arriesgado porque conduce muy pegado a otros carros. Esto aumenta la accidentalidad justamente en los trancones, e incide por supuesto en el tráfico porque prolonga los embotellamientos.

**SEMANA: ¿Entonces Bogotá sí es un caos de movilidad?**

**J.D.M.:** La ciudad está tan congestionada que la gente maneja por los barrios. Pero el problema de los barrios es que son manzanas cuadradas. Entonces las salidas siempre van a llevar a otro trancón.

**SEMANA: Pero no todo el mundo anda en carro.**

**L.E.O.:** Depende del estrato. El uno no se mueve, y el seis se mueve en carro o no lo necesita porque tiene todo cerca. Los demás deben atravesar la ciudad en transporte público, y aquí hay un factor: las vías no han sido planeadas teniendo en cuenta el desplazamiento al trabajo. Por eso todo colapsa.

**SEMANA: Desde la física, ¿cuáles son los puntos críticos de Bogotá?**

**J.D.M.:** Los hay entre las calles 85 y 83, y entre la 100, la carrera Séptima y la Quince. Se dan cuando llega la hora pico y la gente se mete por esos barrios y forma trancón. El centro también está afectado porque las calles están muy pegadas y hay pocas salidas.

**SEMANA: ¿Han trabajado con el Distrito?**

**L.E.O.:**En 2006 nos acercamos para simular a Bogotá, pero no hubo respuesta. Ellos trabajan con ingenieros civiles. No piensan que desde la física podamos aportar.

**SEMANA: ¿Qué podrían ustedes mejorar?**

**J.D.M.:** La Secretaría de Tránsito debería medir datos en tiempo real, e invertir en Big Data. En Colombia, con las empresas telefónicas se podrían hacer estudios para analizar la información de los GPS de los celulares de los conductores y así simular los datos en la hora pico. Esto permitiría desarrollar modelos de transporte y predecir el tráfico con anticipación.

**SEMANA: ¿Qué otras soluciones ve?**

**L.E.O.:** Que los barrios se diseñen en función de la movilidad. Para ello necesitan vías en forma hexagonal, las cuales, además, mejoran la visibilidad y reducen los accidentes.

**SEMANA: ¿Qué piensa de Waze?**

**J.D.M.:** Sirve, pero tiene un problema. Si todo el mundo lo usa en el mismo momento, pues habrá trancón.

**CIENCIA & TECNOLOGÍA**

# Hallan explicación física a trancones en los barrios

*La alternativa de serpentear entre los barrios como una manera de evadir los trancones en Bogotá podría encontrar mejores resultados en movilidad con un diseño hexagonal de las manzanas.*

**BOGOTÁ D. C.**, 11 de marzo de 2016 — *Agencia de Noticias UN-*

Así lo sugieren los estudios realizados por el magíster en Física de la Universidad Nacional, Luis Eduardo Olmos, quien a través del modelamiento de un sistema complejo (en este caso la ciudad con sus vías, número de vehículos, tiempo de los semáforos e interacciones) encontró la explicación, desde la teoría física, sobre las congestiones en las calles de los barrios.

El experto simuló el sistema, tanto con manzanas tradicionales (intersecciones de cuatro vertientes -tipo cruceta-) como con manzanas hexagonales (intersecciones de a tres -tipo panal de abejas-), y observó que hay una mayor densidad de carros (el trancón) en el primer modelo que en el segundo.

El trabajo del experto, quien hoy trabaja en un modelamiento en EE. UU. –bajo el patrocinio del Instituto Tecnológico de Massachusetts (MIT)-, se concentra en la red de calles y el colapso que se da en sus interconexiones cuando hay congestión de vehículos.

Dentro de un esquema físico, un trancón en Bogotá no es otra cosa que la concentración excesiva en tiempo y lugar de una pequeña parte de ese casi millón y medio de carros particulares que existen en la capital. Una manera de evadirlo es desplazarse a través de pequeñas calles, hecho que genera congestiones segmentadas.

Dentro del modelamiento, esas congestiones focales se manifiestan en física como pequeños parches que tienen una forma particular. Luis Eduardo Olmos encontró que esos parches surgen por lo que se denomina dirección preferencial, que combina el norte y el oriente y son más largos que anchos. “En el modelamiento, el experto analizó las pequeñas concentraciones que se formaban (los trancones entre los barrios) y observó que las relaciones entre ancho y largo de los parches cambiaba cuando el sistema se simulaba cada vez a mayor escala”, explica el docente de la U.N. y doctor en física, José Daniel Muñoz, quien coordina el trabajo del profesor Olmos.

La teoría para el modelamiento de sistemas de este tipo indica que se deben usar rectángulos ubicados en forma paralela o perpendicular a la dirección preferencial. En ese ejercicio, cuando los rectángulos son perpendiculares la densidad es de 0,28, o lo que es lo mismo, el 28 % de los sitios donde puede haber un carro están ocupados; mientras que cuando los rectángulos son paralelos, la concentración es de 0,52; es decir, más de la mitad de los sitios donde puede haber un carro están ocupados.

Así las cosas, hay una dirección preferencial constante (nororiental), pero la variación del comportamiento del sistema es la incidencia del plano en la forma de los parches; en este caso, el diseño de las manzanas.

Aunque las aplicaciones en los dispositivos (*waze* y otras) son vistas como una positiva herramienta para mejorar la movilidad, el diseño urbano es factor determinante en esas congestiones mínimas.

En ciudades como Bogotá, donde la gente se está escapando de las autopistas principales para evadir el trancón, la tendencia es usar las calles barriales como parte del sistema de descongestionamiento. Sin embargo, estas desempeñan un papel para el que no están diseñadas.

Dadas las complejidades que podrían darse para un diseño de tal naturaleza, con un parque automotor en aumento y una ciudad que demanda más transporte porque crece también el número de habitantes, “deberían contemplarse en ciertos espacios diseños hexagonales combinados con barrios con una sola vía de entrada y salida en megas manzanas”, explica el profesor Muñoz.

Un primer estudio realizado por el físico Olmos, hace casi una década, explicaba el comportamiento de la vía, por ello tabulaba los momentos en que los conductores frenaban, aceleraban o cambiaban de carril. Para entonces se estableció que, por ejemplo, una vía de dos carriles en Bogotá contenía tantos o más carros que una vía de tres carriles en una ciudad como Los Ángeles.

*(Por: Fin/HEVC/MLA/APBL)*

N.° 294

**Noticias relacionadas:**

*Explicación física de los trancones en los barrios (http://agenciadenoticias.unal.edu.co/detalle/article/explicacion-fisica-de-los-trancones-en-los-barrios.html)*

*Physics could explain Bogotá neighborhood traffic jams (http://agenciadenoticias.unal.edu.co/detalle/article/physics-could-explain-bogota-neighborhood-traffic-jams.html)*

# Dos físicos presentan estudios para disminuir trancones en Bogotá

Ambos proponen un diseño hexagonal de las manzanas para aliviar las congestiones vehiculares.

Por: CAROL MALAVER |
9:05 a.m. | 29 de marzo de 2016

Foto: Abel Cárdenas / EL TIEMPO
En ciudades como Bogotá la tendencia es usar las calles barriales como parte del sistema ...



Siempre le ha llamado la atención analizar las leyes de la física de forma digital, que el computador las pueda entender. Dice que aunque esta área del conocimiento se ha aprendido con ecuaciones, la física no son solo estas operaciones.

José Daniel Muñoz ha aplicado esto a todos sus estudios, incluso, cuando investigó la causa de los trancones de Bogotá. No lo hizo solo. De hecho, la idea surgió de uno de sus alumnos en la Universidad Nacional, Luis Eduardo Olmos. Ambos juntaron sus conocimientos para entender el porqué de las congestiones.

El primer paso fue analizar los autómatas de celdas, es decir, el espacio dividido en celdas. "Imagina que una de ellas alza la cabeza, mira cómo están las vecinas y decide cambiar de estado. Es una forma de explicar las leyes de la física", dijo José Daniel. Y ¿qué es la física? La ciencia que estudia el movimiento de las cosas y, también, por qué no se mueve". Entonces, comienza a dibujar sobre el papel. Le hace falta un tablero.

**Ellos dividieron la calle en celdas, un carro ocupa dos celdas, "aunque las busetas ocupan tres"**, precisa el dato. La idea era medir la distancia del carro de enfrente, del de atrás, las acciones de unos y otros y luego determinar cómo cambiaba la velocidad en diferentes momentos. "Eso es un autómata celular para medir tráfico".

Hace diez años, cuando eran profesor y alumno, hicieron un modelo para determinar cómo maneja la gente en Bogotá: cuándo aceleran, frenan y cambian de carril. "Todos hacen lo mismo", dice José.



MÁS LEÍDO MÁS COMPARTIDO

1 Fiscalía reiteró que joven Luis Andrés Colmenares fue asesinado
2 Por errores en la captura, presunto asesino fue dejado en libertad
3 Niña de 4 años murió, al parecer, por maltrato
4 Casa abandonada en zona histórica de Usaquén, en la mira del Distrito

de Betamax, José Daniel apuntaba la placa de los carros y los cambios en la velocidad. Luego, todos los datos se digitalizaban y se procesaba esa información.

A través de una simulación se comparaba el flujo contra la densidad, es decir, cuántos carros por minuto versus cuántos carros por kilómetro.

**"En esa época, la pendiente de la gráfica daba 70 kilómetros por hora, esa es la velocidad promedio a la que los carros aceleran al final. Eso quiere decir que la gente incumplía la norma que restringía la velocidad a 60 kilómetros por hora"**.

Mientras que en Bogotá transitaban en esa época 88 autos por minuto por carril, en Los Ángeles lo hacían 64 carros. "Eso quería decir que una calle de dos vías en Bogotá manejaba el mismo número de carros que una calle de tres vías en Los Ángeles.

Eso es porque vamos a toda, un carrito detrás del otro y eso que en esa época había la mitad del parque automotor. O sea que no era tan malo como conducían los bogotanos".

En esa ocasión revistas especializadas interpretaron estos estudios como: 'Conductores agresivos despejan las calles'. Luego de esto Luis Eduardo hizo un modelo para buses. "La diferencia básica es que las busetas van máximo hasta 50 kilómetros por hora, y los carros van a 70".

Por otro lado, **si algo afecta la movilidad son los huecos.** "Ahí la máxima velocidad va de 10 a 30 kilómetros por hora. Los buses no se ven muy afectados porque ellos bajan de 50 a 30 y vuelven a subir, es decir, no se demoran mucho tiempo en volver a acelerar, pero **los particulares sí, porque de 70 tienen que bajar a 30. Eso causa mucho trancón**".

Otra conclusión es el beneficio que trae para la ciudad que los buses de transporte público recojan personas solo en los paraderos. "Es lógico, pero eso hay que medirlo. Tenemos una calle de dos vías, 75 por ciento de carros, 25 por ciento busetas, y tenemos cinco kilómetros de calle y tenemos 10 paraderos, uno cada 500 metros y los buses tienen que parar ahí, la otra posibilidad es que cada bus pare diez veces donde le venga en gana.

Es notable que si se respeta el paradero, el flujo mejora, es más, se duplica la velocidad promedio de los carros. Eso ha mejorado mucho gracias al Sistema Integrado de Transporte Público (SITP)", dijo José Daniel. Ese fue el primer acercamiento al estudio, pero luego se interesaron por las formas de los barrios.

## Diseño de los barrios

Según Luis Eduardo, la congestión vehicular es un problema mundial, una enfermedad que sufren las grandes ciudades del mundo. **"Influyen muchos factores: la forma de la red y capacidad de las calles de la ciudad, los semáforos y la gente.** Todo determina la matriz de viajes".

que le provocó una pelea estudiantil

VER 50 MÁS LEÍDAS >

haciéndolas cada vez más densas. "Los urbanistas han optado por dividir el espacio en forma de rejilla cuadrada o rectangular, el ejemplo más claro es Manhattan; pero si uno mira en Google Maps a Bogotá y haces un zoom, la forma cuadrada predomina en el diseño en los barrios".

Eso hace que los vehículos se desborden por los barrios para evitar la congestión y por eso la funcionalidad de estas vías se hace importante, pero según los investigadores, pocas veces se analizan las formas de los barrios, cuando se estudian planes de mejora para la movilidad.

"**Lo que hicimos fue estudiar cómo es el comportamiento de red con cuadras hexagonales, cuando una gran cantidad de autos pasan por ellas y compararla con el caso rectangular**".

Luis Eduardo explicó que, dentro de un esquema físico, un trancón en Bogotá no es otra cosa que la concentración excesiva en tiempo y lugar de una pequeña parte de ese casi millón y medio de carros particulares que existen en la capital. "**Una manera de evadirlo es desplazarse a través de pequeñas calles**, hecho que genera congestiones segmentadas".

Lo que hizo el físico fue simular el sistema, tanto con manzanas tradicionales, aquellas que son de cuatro vertientes, tipo cruceta, como con manzanas hexagonales, intersecciones de a tres, tipo panal de abejas, y observó que hay una mayor densidad de carros, es decir, trancón, en el primer modelo que en el segundo.

El trabajo del experto, quien hoy trabaja en el Instituto Tecnológico de Massachusetts (MIT), concluyó que como el tráfico real está lleno de perturbaciones, errores y fallos, es decir, un comportamiento desordenado, la red hexagonal se comporta mucho mejor que la cuadrada. "Esta red es más resiliente, se adapta mejor la dinámica imperfecta", dijo Luis Eduardo.

La forma de las cuadras en una ciudad influye en el tráfico vehicular y además, aparte de la forma rectangular, hay otras formas urbanísticas que permiten una optimización en el tráfico. **"La red hexagonal es también óptima en infraestructura"**, agregó el físico.

José Daniel explica que el diseño hexagonal permite que existan calles cerradas en donde los niños puedan salir a la calle a jugar.

Así las cosas, con un parque automotor en aumento y una ciudad que demanda más transporte porque crece también el número de habitantes, "deberían contemplarse en ciertos espacios diseños hexagonales combinados con barrios con una sola vía de entrada y salida en megamanzanas. Y que de vez en cuando les pongan más cuidado a los físicos", concluyó Muñoz.

CAROL MALAVER
Redactora de EL TIEMPO

# References


[1] L. E. Olmos and J. D. Muñoz, "A simple statistical method for reproducing the highway traffic," in *Traffic and Granular Flow '13*, pp. 407–414, Springer, 2014.

[2] L. E. Olmos and J. D. Muñoz, "Unraveling the puzzling intermediate states in the Biham-Middleton-Levine traffic model," *Phys. Rev. E*, vol. 91, p. 050801, 2015.

[3] L. E. Olmos and J. D. Muñoz, "Traffic gridlock on a honeycomb city," *arXiv:1610.07438*, 2016.

[4] L. E. Olmos, S. Çolak, and M. C. González, "Non-equilibrium dynamics in urban traffic networks," *pre-print*, 2016.

[5] M. Molloy, "World's worst traffic jam? thousands of cars left stranded on motorway in china," *The Telegraph*, October 15th, 2015.

[6] J. Cortázar, "La autopista del sur," in *Todos los fuegos el fuego.*, Sudamericana, 1966.

[7] A. T. H. Chin, "Containing air pollution and traffic congestion: transport policy and the environment in singapore," *Atmospheric Environment*, 1996.

[8] M. Rosenlund, F. Forastiere, M. Stafoggia, D. Porta, M. Perucci, A. Ranzi, F. Nussio, and C. Perucci, "Comparison of regression models with land-use and emissions data to predict the spatial distribution of traffic-related air pollution in Rome," *J Expo Sci Environ Epidemiol*, vol. 18, 2008.

[9] B. Kerner, *The Physics of Traffic: Empirical Freeway Pattern Features, Engineering Applications and Theory.* Springer, first ed., 2004.

[10] B. Tilch and D. Helbing, "Evaluation of single vehicle data in dependence of the vehicle-type, lane, and site," in *Traffic and Granular Flow'99*, p. 333, Springer-Berlin, 1999.

[11] D. Chowdhury and A. Schadschneider, "Self-organization of traffic jams in cities: effects of stochastic dynamics and signal periods," *Phys. Rev. E*, vol. 59, 1998.

[12] D. Helbing, "Traffic and related self-drive many-particle systems," *Rev. Mod. Phys.*, vol. 73, pp. 1067–1141, 2001.

[13] M. Treiber and A. Kesting, *Traffic Flow Dynamics: Data, Models and Simulation.* Springer, 2013.

[14] M. Treiber, A. Kesting, and D. Helbing, "Three-phase traffic theory and two-phase models with a fundamental diagram in the light of empirical stylized facts," *Transportation Research Part B*, vol. 44, pp. 983–1000, 2010.

[15] M. Schönhof and D. Helbing, "Criticism of three-phase traffic theory," *Transportation Research Part B*, vol. 43, pp. 784–797, 2009.

[16] O.Biham, A. A. Middleton, and D. Levine, "Self-organization and a dynamical transition in traffic-flow models," *Phys. Rev. A*, vol. 46, p. R6124, 1992.

[17] H. S. Gupta and R. Ramaswamy, "Backbones of traffic jams," *J. Phys. A*, vol. 29, p. 022812, 1996.

[18] J. Torok and J. Kertész, "The green wave model of two dimensional traffic: Transitions in the flow properties and in the geometry of the traffic jam," *Physica A*, vol. 231, pp. 515–533, 1996.

[19] R. M. D'Souza, "Coexisting phases and lattice dependence of a cellular automaton model for traffic flow," *Phys. Rev. E*, vol. 71, p. 066112, 2005.

[20] R. M. D'Souza, "BML revisited: Statistical physics, computer simulation, and probability," *Complexity*, vol. 12, pp. 30–39, 2006.

[21] W. K. Yung, "Biham-Middleton-Levine traffic model in different spatial dimensions," master's thesis, University of Hong Kong, Department of Physics, Dec. 1998. http://hub.hku.hk/handle/10722/33474.

[22] S. Çolak, C. M. Schneider, and M. C. González, "On the role of spatial dynamics and topology on network flows," *New Journal of Physics*, vol. 15, p. 113037, 2013.

[23] F. Wang, D. Li, X. Xu, R. Wu, and S. Havlin, "Percolation properties in a traffic model," *EPL*, vol. 112(3), no. 38001, 2015.

[24] A. Arenas, A. Díaz-Guilera, and R. Guimerá, "Communication in networks with hierarchical branching," *Phys. Rev. Lett.*, vol. 86, no. 14, pp. 3196–3199, 2001.

[25] P. Echenique, J. Gómez-Gardeñes, and Y. Moreno, "Dynamics of jamming transitions in complex networks," *EPL*, vol. 71(2), pp. 325–331, 2005.

[26] H. S. Mahmassani, M. Saberi, and A. Zockaie, "Urban network gridlock: Theory, characteristics, and dynamics," *Transportation Research C*, vol. 36, pp. 480–497, 2013.

[27] R. Barlovic, "Traffic jams, cluster formation in low-dimensional cellular automata models for highway and city traffic," *PhD Dissertation, Universität Duisburg-Essen*, 2003.

[28] M. Li, Z.-J. Ding, R. Jiang, M.-B. Hu, and B.-H. Wang, "Traffic flow in a Manhattan-like urban system," *J. Stat. Mech. Theory Exp.*, no. P12001, 2011.

[29] S. Scellato, L. Fortuna, M. Frasca, J. Gomez-Gardenes, and V. Latora, "Traffic optimization in transport networks based on local routing," *Eur. Phys. J. B.*, vol. 73, 2010.

[30] C. F. Daganzo, V. V. Gayah, and E. J. Gonzales, "Macroscopic relations of urban traffic variables: Bifurcations, multivaluedness and instability," *Transportation Research B*, vol. 45(1), pp. 278–288, 2011.

[31] A. Mazloumian, N. Geroliminis, and D. Helbing, "The spatial variability of vehicle densities as determinant of urban network capacity," *Phil. Trans. R. Soc. A*, vol. 368, pp. 4627–4647, 2010.

[32] D. Li, B. Fu, Y. Wang, G. Lu, Y. Berezind, H. E. Stanley, and S. Havlin, "Percolation transition in dynamical traffic network with evolving critical bottlenecks," *Proc. Natl. Acad. Sci.*, vol. 112(3), p. 669–672, 2015.

[33] V. D. Blondel, A. Decuyper, and G. Krings, "A survey of results on mobile phone datasets analysis," *EPJ Data Science*, vol. 4:10, 2015.

[34] M. González, C. Hidalgo, and A. Barabási, "Understanding individual human mobility patterns," *Nature*, vol. 453, no. 7196, p. 779–782, 2008.

[35] L. Alexander, S. Jiang, M. Murga, and M. C. González, "Origin-destination trips by purpose and time of day inferred from mobile phone data," *Transport. Res. C Emerg. Technol.*, vol. 58, p. 240–250, 2015.

[36] T. Perkins and et al, "Theory and data for simulating fine-scale human movement in an urban environment," *J. R. Soc Interface*, vol. 11, no. 99, p. 20140642, 2014.

[37] S. Çolak, A. Lima, and M. C. González, "Understanding congested travel in urban areas," *Nature communications*, vol. 7, p. 10793, 2016.

[38] R. Herman and R. R. E. W. Montroll, R.B. Potts, "Traffic dynamics: analysis of stability in car following," *Operations Research*, vol. 7, no. 1, pp. 86–106, 1959.

[39] R. Herman and I. Prigogine, "A two-fluid approach to town traffic," *Science*, vol. 204, pp. 148–151, 1979.

[40] I. Prigogine and R. Herman, *Kinetic Theory of Vehicular Traffic*. New York: American Elsevier, first ed., 1971.

[41] D. Chowdhury, L. Santen, and A. Schadschneider, "Statistical physics of vehicular traffic and some related systems," *Physics Reports*, vol. 329(4), pp. 199–329, 2000.

[42] A. Schadschneider, "Traffic flow: a statistical physics point of view," *Physica A*, vol. 313, pp. 153–187, 2002.

[43] D. Helbing and M. Treiber, "Critical discussion of synchronized flow," *Coopertive Trns-*

*porttion Dynmics Internet Journal*, 2003.

[44] B. Greenshields, "An study of traffic capacity," in *Highway Research Board Proceedings*, vol. 14, p. 448, 1935.

[45] B. S. Kerner and H. Rehborn, "Experimental properties of complexity in traffic flow," *Phys. Rev. E*, vol. 53, no. 5, 1996.

[46] B. S. Kerner and H. Rehborn, "Experimental properties of phase transitions in traffic flow," *Phys. Rev. Lett.*, vol. 79, 1997.

[47] B. Kerner, "Introduction to modern traffic flow theory and control: The long road to three-phase traffic theory," *Springer, Berlin, New York*, 2009.

[48] W. Leutzbach, "Introduction to the theory of traffic flow," *Springer, Berlin*, 1988.

[49] D. Helbing, "Modeling multi-lane traffic flow with queuing effects," *Physica A*, 1997.

[50] M. Koshi, M. Iwasaki, and I. Ohkura, "I. overview on vehicular flow characteristics," *Proc. 8th International Symposium on Transportation and Traffic Theory. University of Toronto Press*, 1983.

[51] R. Kuhne and S. Immes, "Freeway speed distribution and acceleration noise-calculations from a stochastic continuum theory and comparison with measurements," *Proceedings of the 10th International Symposium on Transportation and Traffic Theory. Eds. Elsevier*, 1987.

[52] V. Knoop, S. Hoogendoorn, and van Zuylen H., "Empirical differences between time mean speed and space mean speed," in *Traffic and Granular Flow'07 Proceedings*, pp. 351–356, Springer, 2008.

[53] L. Neubert, L. Santen, A. Schadschneider, and M. Schreckenberg, "Single-vehicle data of highway traffic: a statistical analysis," *Phys. Rev. E*, vol. 60, p. 6480, 1999.

[54] J. Wardrop, "Some theoretical aspects of road traffic research," in *Proceedings of the Institution of Civil Engineers*, vol. 1, Springer-Berlin, 1952.

[55] H. van Lint, "Reliable travel time prediction for freeways," *PhD Thesis, TU Delft.*, 2004.

[56] M. Schönhof and D. Helbing, "Criticism of three-phase traffic theory," *Transportation Research Part B*, vol. 43, p. 784–797, 2009.

[57] S. Smulders, "Control of freeway traffic flow by variable speed signs," *Transp. Res., Part B: Methodol.*, vol. 24, no. 2, 1990.

[58] S. Hoogendoorn and P. H. L. Bovy, "Optimal routing control using vms's," *The Comprehensive TeX Archive Networkotorway Traffic Flow Analysis-New Methodologies and recent Empirical Findings. Delft University Press*, 1998.

[59] A. Schadschneider, D. Chowdhury, and K. Nishinari, *Stochastic Transport in Complex Systems: From molecules to vehicles.* Elsevier, first ed., 2010.

[60] Y. Sugiyama, M. Fukui, M. Kikuchi, K. Hasebe, A. Nakayama, K. Nishinari, S. i. Tadaki, and S. Yukawa, "Traffic jams without bottlenecks—experimental evidence for the physical mechanism of the formation of a jam," *New Journal of Physics*, vol. 10, p. 033001, 2008.

[61] S. i. Tadaki, M. Kikuchi, M. Fukui, A. Nakayama, K. Nishinari, A. Shibata, Y. S. T. Yosida, and S. Yukawa, "Phase transition in traffic jam experiment on a circuit," *New Journal of Physics*, vol. 15, p. 103034, 2013.

[62] K. Nagel and S. M, "A cellular automaton model for freeway traffic," *ournal de Physique I*, vol. 2, pp. 2221–2229, 1992.

[63] K. Nagel and M. Paczuski, "Emergent traffic jams," *Phys. Rev. E*, vol. 51, 1995.

[64] A. Schadschneider, "Analytical approaches to cellular automata for traffic flow: Approximations and exact solutions," *Traffic and Granular Flow '97. Springer*, 1998.

[65] A. Schadschneider, "The Nagel-Schreckenberg model revised," *Eur. Phys. J. B*, vol. 10, 1999.

[66] W. Knospe, "Synchronized traffic: Modeling and empirical observations," *Doktorarbeit, Gerhard-Mercator Universität Duisburg, Germany*, 2002.

[67] A. S. W. Knospe, L. Santen and M. Schreckenberg, "Towards a realistic microscopic description of highway traffic," *J. Phys. A*, vol. 33, 2000.

[68] L. E. Olmos and J. D. Muñoz, "A cellular automaton model for the traffic flow in Bogotá," *Int. J. Mod. Phys. C*, vol. 15, no. 10, 2005.

[69] L. Olmos, "Simulación del flujo vehicular por medio de dinámica molecular," tesis de pregrado en física, Universidad Nacional de Colombia, Departamento de Física, 2004.

[70] L. E. Olmos and J. D. Muñoz, "Traffic flow in Bogotá," in *Traffic and Granular Flow 05*, pp. 403–409, Springer-Verlag, 2005.

[71] P. Triana, "Modelamiento de tráfico vehicular mixto utilizando autómatas celulares," magister en matemática aplicada, Universidad Nacional de Colombia, Departamento de Matemáticas, 2009.

[72] A. Schadschneider, "Cellular automaton approach to highway traffic: What do we know?," in *Traffic and Granular Flow '07*, pp. 19–34, Springer, 2009.

[73] F. H. Boccara N. and Z. Q., "Car accidents and number of stopped cars due to road blockage on a one-lane highway," *J. Phys. A*, vol. 30, 1997.

[74] D. Huang and W. Tseng, "Meanfield theory for car accidents," *Phys. Rev. E*, vol. 64, p. 057106, 2001.

[75] D. Huang and Y. Wu, "Car accidents on a single-lane highway," *Phys. Rev. E*, vol. 63, p. 022301, 2001.

[76] N. Moussa, "Car accidents in cellular automata models for one-lane traffic flow," *Phys. Rev. E*, vol. 68, p. 036127, 2003.

[77] X. Yang and Y. Ma, "Car accidents determined by stopped cars and traffic flow," *J. Phys. A 35*, vol. 35, p. 10539, 2002.

[78] Y.-Q. X.-Q. Yang, "Car accidents in the deterministic and non-deterministic nagel-schreckenberg models," *Mod. Phys. Lett. B.*, vol. 16, p. 333, 2002.

[79] X. Yang, W. Zhang, K. Qiu, W. Xu, G. Tang, and L. Ren, "The relations of "go and stop" wave to car accidents in a cellular automaton with velocity-dependent randomization," *Physica A*, vol. 384, p. 589, 2007.

[80] R. Jiang, B. Jia, X.-L.Wang, and Q.-S.Wu, "Dangerous situations in a synchronized flow model," *Physica A*, vol. 377, p. 633, 2007.

[81] X.-Q. Yang, Y.-Q. Ma, and Y.-M. Zhao, "Boundary effects on car accidents in a cellular automaton model," *J. Phys. A*, vol. 37, p. 4743, 2004.

[82] R. Jiang, B. Jia, X.-L.Wang, and Q.-S.Wu, "Dangerous situations in the velocity effect model," *J. Phys. A*, vol. 37, p. 5777, 2004.

[83] X. Yang, W. Zhang, K. Qiu, and Y. Zhao, "Effects of a type of quenched randomness on car accidents in a cellular automaton model," *Phys. Rev. E*, vol. 73, p. 016126, 2006.

[84] X. Yang, Y. Ma, and Y. Zhao, "Effects of quenched randomness induced by car accidents on traffic flow in a cellular automata model," *Phys. Rev. E*, vol. 70, p. 046121, 2004.

[85] N. Moussa, "The influence of aggressive drivers on the properties of a stochastic traffic model," *Eur. Phys. J. B*, vol. 41, p. 421–431, 2004.

[86] R. Kuhne and N. H. Gartner, *75 Years of the Fundamental Diagram for Traffic Flow Theory: Greenshields Symposium*. Transportation Research Board, first ed., Washington, DC, 2011.

[87] D. Stauffer and A. Aharony, *Introduction to Percolation Theory*. Taylor and Francis, London, 1992.

[88] M. Sahimi, *Applications of Percolation Theory*. Taylor and Francis eds., 1994.

[89] J. Marro and R. Dickman, *Nonequilibrium Phase Transitions in Lattice Models*, vol. 1. Cambridge University Press, 2005.

[90] K. Christensen and N. R. Moloney, *Complexity and Criticality*, vol. 1. Imperial College Press Advanced Physics Texts, 2005.

[91] M. Henkel, H. Hinrichsen, and S. Lübeck, *Non-Equilibrium Phase Transitions: Absorbing phase transitions.*, vol. 1. Springer, 2008.

[92] S. Broadbent and J. Hammersley, "Percolation processes I. crystals and mazes," *Proceedings of the Cambridge Philosophical Society*, vol. 53, 1957.

[93] P. Grassberger, "On the critical behavior of the general epidemic process and dynamical percolation," *Mathematical Biosciences*, vol. 63, no. 2, pp. 157–172, 1982.

[94] R. Dickman, "Nonequilibrium critical poisoning in a single-species model," *Physics Letters A*, vol. 127, no. 3, pp. 132–137, 1988.

[95] U. Alon, M. E. H. Hinrichsen, and D. Mukamel, "Smooth phases, roughening transitions, and novel exponents in one-dimensional growth models," *Phys. Rev. E*, vol. 57, p. 4997?5012, 1998.

[96] S. Redner and A. Coniglio, "Flory theory for directed lattice animals and directed percolation," *J. Phys. A*, vol. 15, p. L273, 1982.

[97] K. A. Takeuchi, M. Kuroda, H. Chaté, and M. Sano, "Directed percolation criticality in turbulent liquid crystals," *Physical Review Letters*, vol. 99, p. 234503, 2007.

[98] P. Grassberger, "Directed percolation: results and open problems," in *Nonlinearities in complex systems*, 1997.

[99] S. Lubeck, "Universal scaling behavior of non-equilibrium phase transitions," *International Journal of Modern Physics B*, vol. 18, no. 31, pp. 3977–4118, 2004.

[100] S. Lämmer, B. Gehlsen, and D. Helbing, "Scaling laws in the spatial structure of urban road networks," *Physica A*, pp. 89–95, 2006.

[101] C. F. Daganzo and N. Geroliminis, "Macroscopic modeling of traffic in cities," in *86th Annu. Meeting of the Transportation Research Board, Washington, DC.*, vol. 1, 2007. Paper no 07-0413.

[102] M. Li, Z.-J. Ding, R. Jiang, M.-B. Hu, and B.-H. Wang, "Traffic flow in a Manhattan-like urban system," *J. Stat. Mech. Theory Exp.*, no. P12001, 2011.

[103] H. B. Higgins, *The grid book*. The MIT Press, first ed., 2009.

[104] A. Rama, *The lettered city*. Ediciones del Norte, 2002.

[105] WikipediaContributors, "Radburn design housing," april 2017. Online.

[106] DHATODAY, "10 best examples of cul-de-sac style communities," jan 2013. Online.

[107] C. Thorpe, "Experimental radburn town planning disappearing from canberra," jun 2014. Online.

[108] S. Marshall, *Street & Patterns*. Spon Press, first ed., 2005.

[109] E. Ben-Joseph and D. Gordon, "Hexagonal planning in theory and practice," *Journal of Urban Design*, vol. 5, no. 3, pp. 237–265, 2000.

[110] N. Cauchon, "Hexagonal blocks for residential districts," in *The American City*, vol. 17, pp. 145–146, 1925.

[111] I. Triggs, *Town Planning Past Present and Possible*. London, Methuen, first ed., 1909.

[112] N. Cauchon, "Hexagonal planning, traffic intercepter, and orbit," in *the meeting of the City Planning Division, American Society of Civil Engineers, New York City*, 1926.

[113] N. Cauchon, "Hexagonal planning: health properties," in *The National Health*, 1926.

[114] J. Brody, "The neighbourhood unit concept and the shaping of land planning in the united states 1912-1968," *Journal of Urban Design*, no. 3, pp. 340–362, 2013.

[115] S. I. Tadaki and M. Kikuchi, "Jam phases in a two-dimensional cellular-automaton model of traffic flow," *Phys. Rev. E*, vol. 50, p. 4564, 1994.

[116] S. Wolfram, "Computation theory of cellular automata," *Commun. Math. Phys.*, vol. 96, pp. 15–57, 1984.

[117] S. Wolfram, *A new kind of Science*. London: Wolfram Media, Inc., first ed., 2002.

[118] N. J. Linesch and R. M. D'Souza, "Periodic states, local effects and coexistence in the bml traffic jam model," *Physica A*, vol. 387, pp. 6170–6176, 2008.

[119] S. I. Tadaki, "Two-dimensional cellular automaton model of traffic flow with open boundaries," *Phys. Rev. E*, vol. 54, pp. 2409–2413, 1996.

[120] D. Huang and W. Huang, "Biham-Middleton-Levine model with four-directional traffic," *Physica A*, vol. 370, pp. 747–755, 2006.

[121] J. M. J.A. Cuesta, F.C. Martínez and A. Sánchez, "Phase transition in two-dimensional traffic-flow models," *Phys. Rev. E*, vol. 48, 1993.

[122] T. Nagatani, "Effect of jam-avoiding turn on jamming transition in two dimensional traffic flow model," *J. Phys. Soc. Jpn.*, vol. 63, 1994.

[123] T. Nagatani, "Self-organization in 2d traffic flow model with, jam-avoiding drive," *J. Phys. Soc. Jpn.*, vol. 64, 1995.

[124] K. H. Chung, P. M. Hui, and G. Q. Gu, "Two-dimensional traffic flow problems with faulty traffic lights," *Phys. Rev. E*, vol. 51, 1995.

[125] T. Nagatani, "Jamming transition induced by a stagnant street in a traffic-flow model.," *Physica A*, vol. 198, 1993.

[126] C. HF and W. KY, "Phase diagram of the Biham-Middleton-Levine traffic model in three dimensions," *Phys. Rev. E*, vol. 60, pp. 5301–5304, 1999.

[127] Z.-J. Ding, R. Jiang, W. Huang, and B.-H. Wang, "Traffic flow in a Manhattan-like urban system," *J. Stat. Mech. Theory Exp.*, vol. 06, p. P06017, 2011.

[128] Z.-J. Ding, R. Jiang, and B.-H. Wang, "Traffic flow in the Biham-Middleton-Levine model with random update rule," *Phys. Rev. E*, vol. 83, p. 047101, 2011.

[129] D. Sun, R. Jiang, and B.-H. Wang, "Timing of traffic lights and phase separation in two-dimensional traffic flow," *Computer Physics Communications*, vol. 181, no. 2, pp. 301–304, 2010.

[130] T. Horiguchi and T. Sakakibara, "Numerical simulations for traffic-flow models on a decorated square lattice," *Physica A*, vol. 252, p. 388, 1998.

[131] T. Horiguchi and T. Sakakibara, "Numerical simulations for two-dimensional traffic-flow problem," *Interdisc. Inf. Sci.*, vol. 4, p. 39, 1998.

[132] T. Nagatani, "Jamming transition in traffic flow on triangular lattice," *Physica A*, vol. 271, pp. 200–221, 1999.

[133] J. C. Garía, S. Rodríguez, and F. Sancho, "Biham-Middleton-Levine traffic model in two dimensional hexagonal lattice," in *Interdisc. Inf. Sci.*, vol. 4, p. 39, 2013.

[134] D. Chowdhury, L. Santen, and A. Schadschneider, "Statistical physics of vehicular traffic and some related systems," *Phys. Rep.*, vol. 329, p. 199, 2000.

[135] H. Yue, H. Hao, X. Chen, and C. Shao, "Simulation of pedestrian flow on square lattice based on cellular automata model," *Physica A*, vol. 384, pp. 567–588, 2007.

[136] J. Cividini, H. J. Hilhorst, and C. Alpert-Rolland, "Exact domain wall theory for deterministic tasep with parallel update," *J. Phys. A*, vol. 46, p. 345002, 2013.

[137] T. Ohira and R. Sawatari, "Phase transition in a computer network traffic model," *Phys. Rev. E*, vol. 58, p. 193, 1998.

[138] M. Rickert, "Simulationen zweispurigen autobahnverkehrs mit zellularautomaten.," *Diplomarbeit, Universitat zu Koln.*, 1994.

[139] K. Nagel, "TRANSIMS: Transportation analysis and simulation system," *Los Alamos National Laboratory, Los Alamos.*, 2004.

[140] I. Triggs, "Physics of transport and traffic, University Duisburg-Essen," jan 2013. Online.

[141] S. Ostojic, T. J. H. Viugt, and B. Nienhuis, "Universal anisotropy in force networks under shear," *Phys. Rev. E 75*, p. 030301, 2007.

[142] D. Bi, J. Zhang, B. Chakrabortty, and R. P. Behinger, "Jamming by shear," *Nature*, vol. 480, pp. 355–358, 2011.

[143] T. Vicsek and A. Zafeiris, "Collective motion," *Physics Reports*, vol. 517, pp. 71–140, 2012.

[144] M. Pleimling and M. Henkel, "Anisotropic scaling and generalized conformal invariance at Lifshitz points," *Phys. Rev. Lett*, vol. 87, no. 12, p. 125702, 2001.

[145] B. Schmittmann and R. P. Zia, *Statistical mechanics of driven diffusive system*, vol. 17 of *Phase transitions and Critical Phenomena*. London: Academic Press, first ed., 1995.

[146] H. Hinrichsen, "Non-equilibrium critical phenomena and phase transitions into absorbing states," *Adv. Phys.*, vol. 49, pp. 815–958, 2001.

[147] M. Henkel, H. Hinrichsen, and S. Lubeck, *Non-Equilibrium Phase Transitions*, vol. 14 of *Theoretical and Mathematical Physics*. Springer, first ed., 2008.

[148] K. Binder and J.-S. Wang, "Finite-size effects at critical points with anisotropic correlations: Phenomenological scaling theory and monte carlo simulations," *J. Stat. Phys.*, vol. 55, p. 87, 1989.

[149] S. Redner and P. R. Mueller, "Conductivity of a random directed-diode network near the percolation threshold," *Phys. Rev. B*, vol. 26, p. 5293, 1982.

[150] J. K. Williams and N. D. Mackenzie, "Directed percolation: a Monte Carlo approach," *J. Phys. A*, vol. 17, pp. 3343–3351, 1984.

[151] B. H. Wang, Y. F. Woo, and P. M. Hui, "Improved mean-field theory of two-dimensional traffic flow models," *J. Phys. A*, vol. 8, no. 10, pp. 1036–104, 1996.

[152] T. Nagatani, "Spreading of traffic jam in a traffic flow model," *J. Phys. Soc. Japan*, vol. 62, p. 2656, 1993.

[153] E. Strano, V. Nicosia, V. Latora, S. Porta, and M. Barthelemy, "Elementary processes governing the evolution of road networks," *Scientific Reports*, vol. 2:296, 2012.

[154] J. Mombach, M. Vasconcellos, and R. D. Almeida, "Arrangement of cells in vegetable tissues," *J. Phys. D: Applied Physics*, vol. 23(5), pp. 600–606, 1990.

[155] A. B. Patel, W. T. Gibson, M. C. Gibson, and R. Nagpal, "Modeling and inferring cleavage patterns in proliferating epithelia," *PLoS Computational Biology*, vol. 5(6), p. e1000412, 2009.

[156] C. W. W. Pirk, H. R. Hepburn, S. Radloff, and J.Tautz, "Honeybee combs: construction through a liquid equilibrium process," *Naturwissenschaften*, vol. 91, pp. 350–353, 2004.

[157] D. Weaire, "Soap, cells and statistics: Random patterns in two dimensions," *Contemp. Phys.*, vol. 25, pp. 59–99, 1984.

[158] D. Weaire, *The Kelvin Problem.* Taylor and Francis, London, 1996.

[159] J. von Neumann, "Discussion to grain shapes and other metallurgical," in *Metal Interfaces*, p. 108, American Society for Metals, Cleveland, 1952.

[160] R. Oftadeh, B. Haghpanah, D. Vella, A. Boudaoud, and A. Vaziri, "Optimal fractal-like hierarchical honeycombs," *Phys. Rev. Lett.*, vol. 113, p. 104301, 2014.

[161] L. J. Gibson and M. F. Ashby, *Cellular solids: Structure and properties.* Cambridge University Press, Cambridge, England, 1999.

[162] R. H. Frenkiel, *, U.S. Patent 4,144,411 Cellular Radiotelephone System for Different Cell Sizes.* Bell Laboratories, 1979.

[163] C. Jiang, J. Wang, J. Wallner, and H. Pottmann, "Freeform honeycomb structures," *Computer Graphics forum*, vol. 33(5), pp. 185–194, 2000.

[164] I. Stojmenovic, "Honeycomb networks: Topological properties and communication algorithms," *IEEE Transactions on Parallel and Distributed System*, vol. 8, no. 10, pp. 1036–1042, 1997.

[165] M. D. Rintoul and S. Torquato, "Precise determination of the critical threshold and exponents in a three-dimensional continuum percolation model," *J. Phys. A: Math. Gen.*, vol. 30, pp. L585–L592, 1997.

[166] S. Wolfram, "Cellular automata fluids 1: Basic theory," *J. Stat. Phys.*, vol. 45, no. 3, pp. 471–526, 1986.

[167] E. Dumbaugh and R. Rae, "Safe urban form: revisiting the relationship between community design and traffic safety," *Journal of the American Planning Association*, vol. 75(3), pp. 309–329, 2009.

[168] J. Sun and G. Lovegrove, "Comparing the road safety of neighbourhood development patterns: traditional versus sustainable communities," *Canadian Journal of Civil Engineering*, vol. 40(1), pp. 35–45, 2013.

[169] A. Barrat, M. Bartheémy, and A. Vespignani, *Dynamical Processes on Complex Networks*. Cambridge, first ed., 2008.

[170] C. F. Daganzo, "Existence of urban-scale macroscopic fundamental diagrams: some experimental findings," *Transportation Research B*, vol. 42, pp. 759–770, 2008.

[171] H. Mahmassani, Williams, J.C., and R. Herman, "Investigation of network-level traffic flow relationships: some simulation results," *Transportation Research Record: Journal of the Transportation Research Board*, vol. 971, pp. 121–130, 1984.

[172] H. Mahmassani, Williams, and R. J.C., Herman, "Performance of urban traffic networks," in *Proceedings of the 10th International Symposium on Transportation and Traffic Theory.*, pp. 1–20, 1987.

[173] J. Williams, H. Mahmassani, and R. Herman, "Urban traffic network flow models," *Transportation Research Record: Journal of the Transportation Research Board*, vol. 1112, pp. 78–88, 1987.

[174] J. Williams, H. Mahmassani, and R. Herman, "Sampling strategies for two-fluid model parameter estimation in urban networks," *Transportation Research Part A*, vol. 29(3), p. 229?244, 1995.

[175] H. Mahmassani and S. Peeta, "Network performance under system optimal and user equilibrium dynamic assignments: implications for ATIS," *Transportation Research Record: Journal of the Transportation Research Board*, vol. 1408, pp. 83–93, 1993.

[176] C. F. Daganzo and N. Geroliminis, "An analytical approximation for the macroscopic fundamental diagram of urban traffic," *Transport. Res. B*, vol. 42, pp. 771–781, 2008.

[177] D. Helbing, "Derivation of a fundamental diagram for urban traffic flow," *Eur. Phys. J. B*, vol. 70, pp. 229–241, 2009.

[178] V. Knoop, J. Van Lint, and S. Hoogendoorn, "Data requirements for traffic control on a macroscopic level," in *2nd International Workshop on Traffic Data Collection and its Standardisation*, 2011.

[179] C. Buisson and C. Ladier, "Exploring the impact of homogeneity of traffic measurements on the existence of macroscopic fundamental diagrams," *Transport. Res. Rec*, vol. 2124, pp. 127–136, 2009.

[180] V. Gayah and C. Daganzo, "Clockwise hysteresis loops in the macroscopic fundamental diagram: an effect of network instability," *Transportation Research Part B*, vol. 45(4), pp. 643–655, 2011.

[181] N. Geroliminis and S. J., "Properties of a well-defined macroscopic fundamental diagram for urban traffic," *Transportation Research Part B*, vol. 45(3), pp. 605–617, 2011.

[182] M. Saberi and H. Mahmassani, "Exploring the properties of network-wide flow-density relations in freeway networks," in *Transportation Research Record: Journal of the Transportation Research Board*, pp. 153–163, 2012.

[183] M. Saberi and H. Mahmassani, "Empirical characterization and interpretation of hysteresis and capacity drop phenomena in freeway networks," in *Transportation Research Record: Journal of the Transportation Research Board*, 2012.

[184] R. Jayakrishnan, W. T. Tsai, J. N. Prashker, and S. Rajadhyaksha, "A faster path-based algorithm for traffic assignment," *University of California Transportation Center*, vol. UCTC 191, 1994.

[185] B. N. Janson, "Dynamic traffic assignment for urban road networks," *Transportation Research Part B*, vol. 25(2), pp. 143–161, 1991.

[186] E. J. Manley, J. Addison, and T. Cheng, "Shortest path or anchor-based route choice: a large-scale empirical analysis of minicab routing in london," *Journal of Transport Geography*, vol. 43, pp. 123–139, 2015.

[187] R. Oftadeh, B. Haghpanah, D. Vella, A. Boudaoud, and A. Vaziri, "Understanding individual routing behaviour," *Interface*, vol. 13, 2016.

[188] U. D. Transportation, "2015 traffic fatalities data has just been released: A call to action to download and analyze," jan 2015. Online.